



**NEAR EAST UNIVERSITY  
INSTITUTE OF GRADUATE STUDIES  
DEPARTMENT OF MECHANICAL ENGINEERING**

**AN INVESTIGATION OF THE HARDNESS AND FATIGUE  
BEHAVIOURS OF A HIGH TEMPERATURE Cu-BASED  
SHAPE MEMORY ALLOY WITH GRAPHENE ADDITIONS**

**PhD THESIS**

**Wasiu Ayinde ISSA**

**Nicosia**

**December, 2024**

**WASIU-ISSA**

**AN INVESTIGATION OF THE HARDNESS AND  
FATIGUE BEHAVIOURS OF A HIGH  
TEMPERATURE Cu-BASED SHAPE MEMORY  
ALLOY WITH GRAPHENE ADDITIONS**

**PhD THESIS**

**2024**

**NEAR EAST UNIVERSITY  
INSTITUTE OF GRADUATE STUDIES  
DEPARTMENT OF MECHANICAL ENGINEERING**

**AN INVESTIGATION OF THE HARDNESS AND FATIGUE  
BEHAVIOURS OF A HIGH TEMPERATURE Cu-BASED SHAPE  
MEMORY ALLOY WITH GRAPHENE ADDITIONS**

**PhD THESIS**

**Wasiu Ayinde ISSA**

**Supervisors**

**Prof. Dr. Hüseyin ÇAMUR  
Prof. Mahmut Ahsen SAVAŞ**

**Nicosia**

**Dcember, 2024**

### Approval

We certify that we have read the thesis submitted by Wasiu Ayinde ISSA titled “**An investigation of the Hardness and Fatigue Behaviours of a High Temperature Cu-based Shape Memory Alloy with graphene additions**” and that in our combined opinion it is fully adequate, in scope and in quality, as a thesis for the degree of Doctor of Philosophy in Mechanical Engineering.

Examining Committee	Name-Surname	Signature
---------------------	--------------	-----------

Head of the Committee:	Prof. Dr. Hasan Hacışefki (EMU)	.....
------------------------	---------------------------------	-------

Committee Member*:	Assist. Prof. Dr. Ali Şefik (CIU)	.....
--------------------	-----------------------------------	-------

Committee Member*:	Assoc. Prof. Dr. Youssef Kassem	.....
--------------------	---------------------------------	-------

Committee Member*:	Assist. Prof. Dr. Metin Bilin	.....
--------------------	-------------------------------	-------

Committee Member*:	Assist. Prof. Dr. Elbrus Imanov	.....
--------------------	---------------------------------	-------

Supervisor:	Prof. Dr. Hüseyin Çamur	.....
-------------	-------------------------	-------

Co-Supervisor:	Prof. Dr. Mahmut Ahsen Savaş	.....
----------------	------------------------------	-------

Approved by the Head of the Department

09/12/2024  
  
 Prof. Dr. Hüseyin Çamur

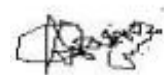
Head of Department

Approved by the Institute of Graduate Studies

...../...../20...  
  
 Prof. Dr. Kemal Hüsnü Can Başer  
 Head of the Institute

**Declaration of Ethical Principles**

I hereby declare that all information, documents, analysis and results in this thesis have been collected and presented according to the academic rules and ethical guidelines of Institute of Graduate Studies, Near East University. I also declare that as required by these rules and conduct, I have fully cited and referenced information and data that are not original to this study.

**Wasiu Ayinde ISSA****9/12/2024**

**Acknowledgments**

I appreciate my supervisors, Prof. Dr. Hüseyin ÇAMUR and Prof. Mahmut Ahsen SAVAŞ for their support for the success of this research. I appreciate Prof. M. O. Durowoju, Engr. M. O. Ajetunmobi, Dr. K. O. Oladosu, Dr. S. A. Bello, Engr. Wale, Engr. Rasheed, and Mr. Adamu, for their assistance in providing support in material sourcing among others. I thank my family for their patience and prayers.

**Wasiu Ayinde ISSA**

## Abstract

### **An investigation of the hardness and fatigue behaviours of a high temperature Cu-based shape memory alloy with graphene additions**

**Issa, Wasiu Ayinde**

**PhD, Department of Mechanical Engineering**

**December, 2024, 129 pages**

CuAlNi shape memory alloys (SMA) find usefulness in high temperature engineering applications. They have ease of production and are cheap in comparison with Nickel - Titanium alloys. The alloy is usually under cyclic load/stress but lacks excellent fatigue properties. In this study, the effects of graphene (C), i.e. a polymorph of carbon, on the fatigue life and hardness of CuNiAl SMA were investigated. The resulting S-N curves revealed that as the number of stress cycles increases, the magnitude of stress leading to fatigue failure reduces. Design Expert Software version 13.0 was deployed to predict the interaction between fatigue life, percentage compositions of Cu and graphene (C). The parameters were significant model terms at  $p < 0.05$ , indicating that they have significant effects on the fatigue life of SMA. The model obtained indicates a good fit with  $R^2$  of 94.87%. The developed model can be employed in fatigue life study of shape memory alloys containing a fourth addition such as graphene.

**Key Words:** mechanical properties, shape memory alloy, fatigue life CuAlNi and CuAlNiC

## Özet

### **Yüksek sıcaklıktaki mekanik ve yorulma performansının incelenmesi Grafen ilaveli Cu tabanlı şekil hafızalı alaşım**

**Issa, Wasiu Ayinde**

**Doktora, Makine Mühendisliği Bölümü**

**Aralık, 2024, 129 pages**

CuAlNi şekil hafızalı alaşımları (SMA), yüksek sıcaklık mühendislik uygulamalarında kullanışlıdır. Üretimleri kolaydır ve Nikel - Titanyum alaşımlarına kıyasla ucuzdur. Alaşım genellikle döngüsel yük/gerilim altındadır ancak mükemmel yorulma özelliklerinden yoksundur. Bu çalışmada, grafenin (C) CuNiAl SMA'nın yorulma ömrü ve mekanik özelliği (Sertlik) üzerindeki etkisi incelenmiştir. Elde edilen S-N eğrileri, stres döngülerinin sayısı arttıkça yorulma arızasına yol açan stresin büyüklüğünün azaldığını ortaya koymuştur. Yorulma ömrü, Cu ve grafenin (C) yüzdelik bileşimleri arasındaki etkileşimi tahmin etmek için Design Expert Yazılım sürüm 13.0 kullanılmıştır. ANOVA testinden elde edilen p-parametre değeri  $< 0,05$  bulundu. Bu ise SMA'nın yorulma ömrü üzerinde anlamlı bir etkiye sahip olduklarını ve matematiksel modelin %94,87'lik R2 ile iyi bir uyum gösterdiğini göstermektedir. Geliştirilen model, grafen gibi dördüncü bir katkı içeren şekil hafızalı alaşımın yorulma ömrü çalışmasında kullanılabilir.

**Anahtar kelimeler:** anahtar kelime, mekanik özellikler, şekil hafızalı alaşım, yorulma ömrü CuAlNi ve CuAlNiC

## Table of Contents

Approval .....	I
Declaration .....	II
Acknowledgements .....	III
Abstract .....	IV
Summary .....	V
Table of Contents . .....	VI
List of Appendices .....	IX
List of Tables.....	X
List of Figures .....	XI
List of Abbreviations.....	XIV

## CHAPTER I

Introduction.....	1
Engineering Applications of SMA.....	3
Review of Classes of Engineering Materials.....	5
Mechanical Characteristics/Behaviour of Metallic Materials.....	23
Statement of the Problem .....	37
Purpose of the Study .....	38
Research Questions .....	39
Significance of the Study .....	39
Definition of Terms.....	39

## CHAPTER II

Literature Review.....	40
------------------------	----

Theoretical Framework.....	40
Review of Previous Researches.....	41
Impact of Quaternary Element Addition to CuAlNi SMA.....	42
Fatigue behaviour of Shape Memory Alloy.....	44
Empirical Modelling.....	46
Related Research .....	48

### CHAPTER III

Methodology.....	50
Determination of Mass Constituent of the Elements.....	51
Methods of making SMA.....	52
Mechanical Testing of Samples.....	55
Fatigue Testing of Samples.....	63
Microstructural Investigation.....	65
Use of Computer Software to Analyse Fatigue of SMA.....	66
Method used to Analyse Results.....	66

### CHAPTER IV

Findings and Comments .....	67
Findings for Crystal Orientation of the Samples.....	67
Findings for Samples' Elemental Composition and Surface Structure.....	69
Findings for Mass Composition of Samples.....	71

Findings for Characterization of SMA.....	72
Findings for Mechanical Testing of SMA.....	79
Findings for Fatigue Testing of SMA.....	80
Findings for the Use of Computer Software to Analyse Fatigue of SMA.....	86

## CHAPTER V

Discussion.....	92
Crystal Orientation of Samples.....	92
SMA Composition/Production.....	93
Effect of Graphene on the Alloy Characterization.....	94
Effect of Graphene on the Mechanical Property of CuAlNi SMA.....	94
Effect of Graphene on the Fatigue Property.....	95
D-Optimal Model Formulation.....	96

## CHAPTER VI

Conclusion And Recommendations .....	97
Recommendations.....	98
Recommendations According to Findings.....	98
Recommendations for Further Research .....	99
REFERENCES .....	100
APPENDICES .....	111

**List of Appendices**

	<b>Page</b>
<b>Appendice X:</b> Turnitin Similarity Report	111
<b>Appendice:</b> Curriculum Vitae	112

**List of Tables**

	<b>Page</b>
<b>Table 1.</b> Shear and elastic Moduli at room-temperature	27
<b>Table 2.</b> Different techniques for hardness test	30
<b>Table 3.</b> Different Rockwell scales	30
<b>Table 4.</b> Different superficial scales	31
<b>Table 5.</b> Rockwell test descriptions with symbols.	56
<b>Table 6.</b> Rockwell Hardness C scale.	57
<b>Table 7.</b> Schematic Diagram of Overall Dimensions used in rockwell test	57
<b>Table 8</b> Percentage Composition of Samples	71
<b>Table 9.</b> Rockwell test, C-scale results with diamond indenter of Kgf 150.	79
<b>Table 10.</b> Results of Fatigue testing of specimen A, B, C and D.	81
<b>Table 11.</b> Experimental runs (input) and responses (output)	86
<b>Table 12.</b> Fatigue life in terms of coded factors	87
<b>Table 13.</b> ANOVA (Analysis of Variance) for Fatigue Life.	88
<b>Table 14.</b> Summary of the model.	89
<b>Table 15.</b> SMA Percentage Composition of Samples.	93
<b>Table 16.</b> SMA Percentage Composition derived from literary works .	93

**List of Figures**

	<b>Page</b>
<b>Figure 1.</b> Transformation between low and high temperature phases.	1
<b>Figure 2.</b> Metal fabrication techniques.	9
<b>Figure 3.</b> Metal deformation during (a) forging, (b) rolling, (c) extrusion, and (d) drawing.	10
<b>Figure 4.</b> Typical sand mould (a) Mould Section and casting nomenclature (b) pattern attached with gating and risering system.	14
<b>Figure 5.</b> Mould Section and casting nomenclature, (a) top view, (b) front view.	15
<b>Figure 6.</b> Making a simple sand mould.	17
<b>Figure 7.</b> Making a simple sand mould.	18
<b>Figure 8.</b> Making a simple sand mould.	19
<b>Figure 9.</b> Schematic cross sectional representation showing the zones in the vicinity of a typical fusion weld.	23
<b>Figure 10.</b> Three ways to apply load: shear, tension, and compression.	25
<b>Figure 11.</b> Torsional load.	25
<b>Figure 12.</b> Stress-Strain Curve.	26
<b>Figure 13.</b> Stress- Strain Curve for a material undergoing Elongation which is elastic.	27
<b>Figure 14.</b> Fatigue failure of a shaft showing the Fracture surface..	33
<b>Figure 15.</b> Typical curve for fatigue failure.	33
<b>Figure 16.</b> Curve for Low-cycle fatigue failure.	34
<b>Figure 17.</b> Influence of mean stress, $m$ on stress-number of cycles (S–N), Fatigue behaviour.	34
<b>Figure 18.</b> S–N curves showing how shot peening affects steel's fatigue behaviour.	36
<b>Figure 19.</b> Example of how engineering design can reduce stress concentration. (a) sharp edges thus Poor design. (b) Good engineering design: fatigue life is improved through the addition of rounded fillet to a shaft as the point of change in cross section.	37

<b>Figure 20.</b> Ni-Ti SMA stress-Fatigue life curve.	46
<b>Figure 21.</b> Materials used (a) Graphene (b) Copper (c) Aluminium (d)Nickel	50
<b>Figure 22.</b> Schematic of sand molding.	54
<b>Figure 23.</b> Alloy casting (a) Pit Furnace (b) Crucible Pot containing metal to be melted (c) Mould .(d ) Casted Alloy.	55
<b>Figure 24.</b> Rockwell hardness Test Principle.	56
<b>Figure 25.</b> Schematic parts diagram.	58
<b>Figure 26.</b> Indication dial gauge schematic diagram.	59
<b>Figure 27.</b> Handles of Loading and unloading.	60
<b>Figure 28.</b> Selection of test force.	60
<b>Figure 29.</b> Oil needle Regulation.	61
<b>Figure 30.</b> Indenter Installation.	61
<b>Figure 31.</b> Rockwell Hardness Testing.	61
<b>Figure 32.</b> (a) Machine Specimen specifications (b) Avery Denison Fatigue Testing Machine.	63
<b>Figure 33.</b> Pattern obtained for copper via use of XRD (X-Ray Diffraction).	67
<b>Figure 34.</b> Pattern obtained for Aluminium via use of XRD (X-Ray Diffraction).	67
<b>Figure 35.</b> Pattern obtained for Nickel using X-Ray Diffraction (XRD).	68
<b>Figure 36.</b> Pattern obtained for Graphene via use of XRD (X-Ray Diffraction).	69
<b>Figure 37.</b> Surface morphology and elemental compositions of Copper (Cu) sample.	69
<b>Figure 38.</b> Surface morphology and elemental compositions of Aluminium (Al) sample.	70
<b>Figure 39.</b> Surface morphology and elemental compositions of Nickel (Ni) sample.	70
<b>Figure 40.</b> Surface morphology and specification of Graphene used.	71
<b>Figure 41.</b> Pattern obtained for Sample A, B, C and D via use of	

XRD ( X-Ray Diffraction)	72
<b>Figure 42</b> The composition of elements and surface morphology of Alloy specimen A (a) SEM micrograph (b) EDX result.	73
<b>Figure 43.</b> The composition of elements and surface morphology of Alloy specimen B (a) SEM micrograph (b) EDX result.	74
<b>Figure 44.</b> The composition of elements and surface morphology of Alloy specimen C (a) SEM micrograph (b) EDX result.	76
<b>Figure 45.</b> The composition of elements and surface morphology of Alloy specimen D (a) SEM micrograph (b) EDX result.	77
<b>Figure 46.</b> Impact of graphene on SMA as determined by the hardness test findings.	80
<b>Figure 47.</b> Fatigue Life (S-N) graph for specimens A.	82
<b>Figure 48.</b> Fatigue Life (S-N) graph for specimens B.	82
<b>Figure 49.</b> Fatigue Life (S-N) graph for specimens C	83
<b>Figure 50.</b> Fatigue Life (S-N) graph for specimens D.	83
<b>Figure 51.</b> Fatigue Life (S-N) graph for the combined graph.	84
<b>Figure 52.</b> Further Comparison of the Fatigue Life of the four specimens A, B, C and D.	85
<b>Figure 53.</b> For fatigue life, a three-dimensional response surface plot A.	89
<b>Figure 54.</b> For fatigue life, a three-dimensional response surface plot B.	89
<b>Figure 55.</b> For fatigue life, a three-dimensional response surface plot C.	89.

**List of Abbreviations**

<b>ANOVA:</b>	Analysis of Variance
<b>CNTs:</b>	Carbon Nanotubes
<b>CuAlNi:</b>	Copper Aluminium Nickel
<b>EDS:</b>	Energy Dispersive x-ray Spectroscopy
<b>EM</b>	Empirical Model
<b>MNE:</b>	Ministry of National Education
<b>SMA:</b>	Shape Memory Alloy
<b>SMP:</b>	Shape Memory Polymer
<b>SEM:</b>	Scanning Electron Microscope
<b>TRNC:</b>	Turkish Republic of North Cyprus
<b>XRD:</b>	X-Ray Diffraction

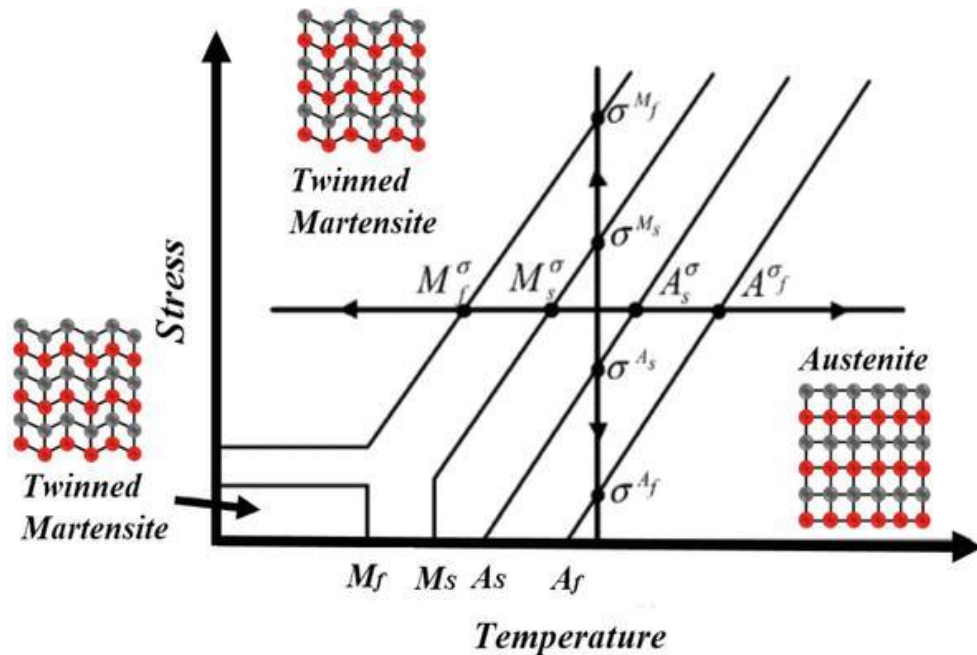
## CHAPTER I

### Introduction

Materials with the phenomenon of remembering and reversing to their former shape after being deformed are said to possess shape memory effects. Alloys that show this kind of behaviour are termed as Shape Memory Alloys (SMA) (Callister, & Rethwisch, 2018). Some external stimuli, such mechanical or electrical ones, can cause the deformed shape to return to its original state (Petrini & Migliavacca, 2011, Cho et al., 2005), chemical (Lendlein, 2005), thermal (Ji, et al., 2006), and electro-magnetic (Lendlein, 2005). The material shape memory usually occurs when the material is heated while the deformation occurs at low temperature (Callister, & Rethwisch, 2018). This is as a result of a twin boundary transformation, i.e. between a martensite, which is a phase at a reduced temperature and austenite, which is a phase at an increased temperature (Saud, et al., 2019). This process is reversible, see Figure 1 below.

Figure 1.

*Transformation between low and high temperature phases (Saud, et al., 2019).*



The martensitic phase transition is a phase transformation which is diffusionless and shear-dominant solid-state that arises from the growth and nucleation of the martensitic phase from a parent phase, austenitic. This is the main source of this behaviour. It changes from a high-symmetry, often cubic, austenitic phase to a low-symmetry martensitic phase when a martensitic phase transformation takes place in a SMA. The phase transition occurs while the parent and product phases coexist. The same parent phase crystal can yield a variety of martensite variations due to the martensitic phase's crystal structure having less symmetry than that of the parent austenitic phase. When the free energies of the two phases are equal, the martensitic transformation takes place when austenite's free energy is higher than martensite's at a temperature lower than the critical temperature. When stress is present, the transformation starts at  $M_s$  (martensite start) temperature, and it's lower than, rather than at that precise moment. As the temperature is decreased, the transformation keeps changing until it reaches a temperature known as  $M_f$  (martensite completion). Likewise, when the material is completely austenite, the opposite change (martensite - austenite) starts at  $A_s$  temperature (austenite start) which at  $A_f$  (austenite finish) during the heating cycle (Dagusta, 2014, Saud, et al., 2019).

The property of the material to experience an extensive plastic deformation called pseudoelasticity and also 'recollect' its previous geometry called Shape Memory Effect are the important material properties mostly used (Callister, & Rethwisch, 2018). Temperature variation is responsible for the reversible martensitic transformation for shape memory effect while change in stress is responsible for pseudoelasticity (superelasticity) (Petrini & Migliavacca, 2011; Ma, et al., 2010; Tsuchiya, 2011).

copper-zinc-silicon (Cu-Zn-Si), iron-palladium (Fe-Pd), Copper-aluminum-nickel (Cu-Al-Ni), indium-titanium (In-Ti), copper-zinc-aluminum (Cu-Zn-Al), nickel-aluminum (Ni-Al), copper-zinc-gallium (Cu-Zn-Ga), nickel-titanium (Ni-Ti), copper-aluminum-manganese (Cu-Al-Mn), iron-platinum (Fe-Pt), copper-tin (Cu-Sn), copper-zinc-tin (Cu-Zn-Sn), etc are

among twenty elements in the actual periodic table region that exhibit shape memory (dagusta, 2014). Nonetheless, research and development has mostly focused on three alloy systems that are widely recognized to display the SM phenomenon. They are copper-based alloys (Cu), nickel-titanium (Ni-Ti), and iron-based alloys (Callister, & Rethwisch, 2018, Dagusta, 2014). CuAlNi SMA has advantage of high temperature suitability in applications (Prasad, 2017). SMA finds applications in engineering and many areas due to their unique characteristics (Issa, et. al, 2021; Cisse, et al., 2016). These include their usage in oil and gas, biomedical, automotive, aerospace, and robotics (Barbarino, et al., 2014).

SMA is usually under cyclic loads and thus, the fatigue failure is an important study in shape memory alloys modelling (Vanderson, et al., 2020). Fatigue failure is the reduction in material resistance to fluctuating stresses (Bhandari , 2016; Ugural & Fenster, 2012). Fatigue test is the process of fracturing a machined material through the application of reversed known stresses (Obiukwu, 2015). This helps us to know the fatigue life of a material i.e. the stress the material can sustain before service failure (Callister, & Rethwisch, 2018).

Some polymer materials also show shape memory behaviour. Materials of this nature are termed SMP stands for shape memory polymers. Two materials that are extensively researched are SMA and SMP (Hornbogen, 2016; Gunes & Jana, 2016; El Feninat, 2002).

Ni-Ti based alloys with superior biological compatibility are mostly utilized in biomedical applications among the three alloy systems previously discussed, which are typically economically exploited for their SM features. Because they are less expensive, Cu-based SMAs is preferable to Ni-Ti ones in other applications. Cu-based SMAs have been at the forefront of research and development for many years, although they are not widely available commercially (Callister, & Rethwisch, 2018, Rupa, 2014).

### ***Engineering Applications of SMA***

The reversible phase change behaviour of SMA finds useful applications in engineering such as in aerospace, biomedical, civil, electrical and mechanical engineering (Melton, 1999).

### **Aerospace Engineering**

SMA usage in aircraft has benefits which include operating cost reduction and overall weight reduction (Saurabh, et al., 2018). The shape change helps to lower the aerodynamic load (Barbarino, 2004). SMA finds usefulness in morphing aircraft (Girolamo & Maria, 2020; Saurabh, et al., 2018; Bashir, et al., 2018). Researches utilizing shape memory technology has increased since its first usage on F-14 till the present time in the aerospace industry (Kwon, et al., 2015; Hartl, 2007).

### **Biomedical Engineering**

A ternary Ti-Ni-Cu SMA used on medical implants helps to prevent bacterial infections (Li, 2016). SMA is used in quick recovery of broken bones (Mantovani, 2000). It also used in brain treatment, teeth treatment, and in circulatory system (Li, 2016; Daniela, et. al., 2009; Petrini & Migliavacca, 2001).

### **Chemical Engineering**

SMA is use to prevent leakage and corrosion in oil field, underground water and in chemical plants (Liu, 1995).

### **Civil Engineering**

SMA installed in structures, buildings and bridges help to prevent extensive deformation and eventual collapse (Sarth & Zunubia, 2017; Wen-Shao & Yoshikazu, 2016; Indirli & Castellano, 2008; Yachuan & Jinping, 2008; Corbi, 2003; Dolce, et al., 2001; Wilde, et al., 2000).

### **Electrical Engineering**

SMA finds application in electrical fuse safety system (Han, et al., 2021), electronics (Zhang, 2021), telecommunication system (Saurabh, et al., 2018; Otsuka & Wayman, 1998; Otsuka & Xiaobing, 1999), micromanipulator (Liu, 2021) and electric motor (José Marques, et al., 2020).

### **Mechanical Engineering**

SMA used as actuators in cars help to improve safety and comfort of driver (Saurabh, et al., 2018). SMA is used in heat engines (Churchill, et al., 2016; Saurabh, et al., 2018; Jaronie, et al., 2014), water ways, naval operations (Angilella, et al., 2015; Saurabh, et al., 2018), and in common household appliances like rice cooker, among others (Wang, et al., 2016).

### ***Review of Classes of Engineering Materials***

The importance of materials in our everyday life cannot be overemphasized. Overtime, man has discovered ways of producing materials like metals and pottery with better properties than naturally occurring ones like stone, wood etc. The knowledge of the relationship between properties and structural elements of materials over a long period of time has helped scientist evolved lots of materials with much specialized characteristics. The applicability of materials are determined by six different property classification: Electrical, deteriorative, mechanical, thermal, magnetic and optical. Four factors should also be taken into account when designing, producing, and using materials. Processing, Structure, Properties, and Performance are these. The qualities of a material, which are also determined by its structure or structures, determine its performance. Furthermore, the structure is determined by the processing of the components. Finally, the cost of the manufactured item, any deterioration of the material's qualities during operation, and the service condition to which the material will be subjected are the three key factors that determine the choice of material.. (Callister, & Rethwisch, 2018; Ashby Jones, & 2005; Jacobs, & Kilduff, 2005).

#### **Classification of Materials**

Three broad categories are used to classify materials based on their atomic structures and chemistry. These include ceramics, metals, and polymers. Composites are materials made up of two or more different types of materials. Semiconductors, biomaterials, smart materials, and nanomaterials are examples of advanced materials used in high-tech (high-tech) applications. (McMahon, 2004; Callister, & Rethwisch, 2018).

#### **Metals**

Examples of metals are iron and aluminium. They consist of one or more metallic elements, and occasionally trace amounts of carbon, nitrogen, and oxygen are present. In contrast to ceramics and polymers, metals and their alloys have atoms that are grouped in an orderly fashion and are quite dense. Although metals are strong and rigid, they are also ductile and fracture-resistant. Their widespread use in structural applications can be attributed to this. Non-localized electrons in metallic

materials give them a variety of characteristics, including their ability to transport heat and electricity well and their glossy look.

lustrous appearance among others. (Van, 1989; Callister, & Rethwisch, 2018; white, 1999)

### **Ceramics**

Common ceramic materials include composites between metallic and nonmetallic elements, such as silica (SiO<sub>2</sub>) and alumina (Al<sub>2</sub>O<sub>2</sub>). Others include what are known as classic ceramics, which include cement, glass, and clay minerals. Ceramic materials are usually highly hard and somewhat stiff. They have a significant risk of breaking and are quite brittle. New materials for automotive engine parts, etc., exhibit improved fracture resistance. In addition to being opaque, translucent, and transparent, ceramics also have certain oxides that exhibit magnetic properties. Compared to metals and polymers, ceramic materials are better insulators and are more resilient to harsh environments and high temperatures.

### **Polymers**

Many Polymers are organic compounds with very large molecular structures and have carbon background; others contain hydrogen and other non-metallic element (i.e. O, N, Si). Examples include; Polyethylene (PE), nylon, silicon rubber, etc. Polymers have low densities. They are neither stiff nor strong as metals and ceramic materials, but on per mass basis, many times their strengths and stiffness's can be compared with those of ceramic and metals due to their low densities. (Callister, & Rethwisch, 2018).

### **Composites**

These consist of at least two different material types of metals; ceramic and polymers, with a goal to achieve better properties than that of their individual component materials. It can be naturally occurring like wood and bone, or synthetic (human made) like fiberglass. For example, embedding glass fibres within polyester will result in a glass fibre that is relatively stiff, strong and flexible with a low density. Similarly, embedding carbon fibres within a polymer will yield carbon-fiber-reinforced polymer (CFRP) which is useful in aircraft and aerospace applications. The CFRP is stiffer and stronger than glass fiber-reinforced material but more expensive. (Callister, & Rethwisch, 2018).

### **Advanced Materials**

These are materials that fracture or operates using relatively intricate and sophisticated principles; such as computers, fibre-optic systems among others. They are traditional materials with enhanced properties. They may be metals, ceramics, polymers, semiconductors, biomaterials, or smart materials and nano-engineered materials and are usually expensive. (Callister, & Rethwisch, 2018; Schaffer et al., 1999; Jacobs, & Kilduff, 2005; Smith, & Hashemi, 2010).

### **Semiconductors**

They possess electrical properties between those of electrical conductors and insulators. The presence of minute amount of impurity atoms in them, affects their electrical characteristics through which over very small spatial regions, the concentration may be controlled. It is very useful in electronic and computer industries. (Callister, & Rethwisch, 2018).

### **Biomaterials**

These are materials compatible with and implanted into the human body to replace diseased or damaged body parts. They may be metals, ceramics, polymers, composites and semiconductors. (Callister, & Rethwisch, 2018).

### **Smart Materials**

These materials react to environmental changes by exhibiting characteristics similar to those of humans. These answers are provided in a preset format. Some sort of sensors and actuators are included in the component. Shape memory alloys, piezoelectric ceramics, magnetostrictive materials, and electrorheological/magnetorheological fluids are the four possible materials for the actuators. When the temperature is adjusted, metals known as "shaped-memory alloys" regain their previous shape after deformation. In reaction to an applied electric field, piezoelectric ceramics expand and contract, producing an electric field when their dimensions are changed. While magnetostrictive and piezoelectrics behave similarly, magnetostrictive is more sensitive to magnetic fields. Finally, the magnetorheological and electrorheological liquids are those that undergo significant viscosity changes when an electric or magnetic field is applied, respectively.

(Callister, & Rethwisch, 2018)

Devices or materials used as sensors include optical fibers, piezoelectric

materials and microelectromechanical systems. For example, noise created by the rotating rotor blade of an helicopter, is reduced using a type of smart system. The blade stresses and deformation is monitored by piezoelectric sensors; a computer controlled adaptive device, received feedback signals from the sensors which generates noise-cancelling antinoise. (Callister, & Rethwisch, 2018).

### **Nanomaterials**

These are materials having sizes in the nanoscale ( $10^{-9}\text{m}$ ). They may be metals, ceramics, polymers and composites. The development of the scanning probe microscope has made it easier to analyze individual atoms and material molecules. One atom or molecule at a time, this has aided in the creation and development of novel structures from their atomic constituents. Opportunities to develop mechanical, electrical, magnetic, and other qualities that would not typically be attainable have been made possible by this. Nanotechnology is the study of these materials' characteristics. Carbon nanotubes and nanocomposites in tennis balls are a couple of the uses. A small nanoparticle's surface area to volume ratio is incredibly high. The toxicity and toxicological interactions of these materials with humans and animals in newly produced materials must be taken into consideration because they can result in significant chemical reactivity. There are fears over the harm these materials may cause if absorbed into the body as their safety is relatively unexplored. (Callister, & Rethwisch, 2018).

### **Modern Materials' Needs**

As was already established, the necessity of materials in today's world cannot be overstated. Fuel efficiency can be increased, for example, by raising engine operating temperatures and lowering the weight of transportation vehicles. Many energy-related issues will be resolved by materials like fuels, facilities for disposing of leftover trash, and contaminated constructions. (Callister, & Rethwisch, 2018).

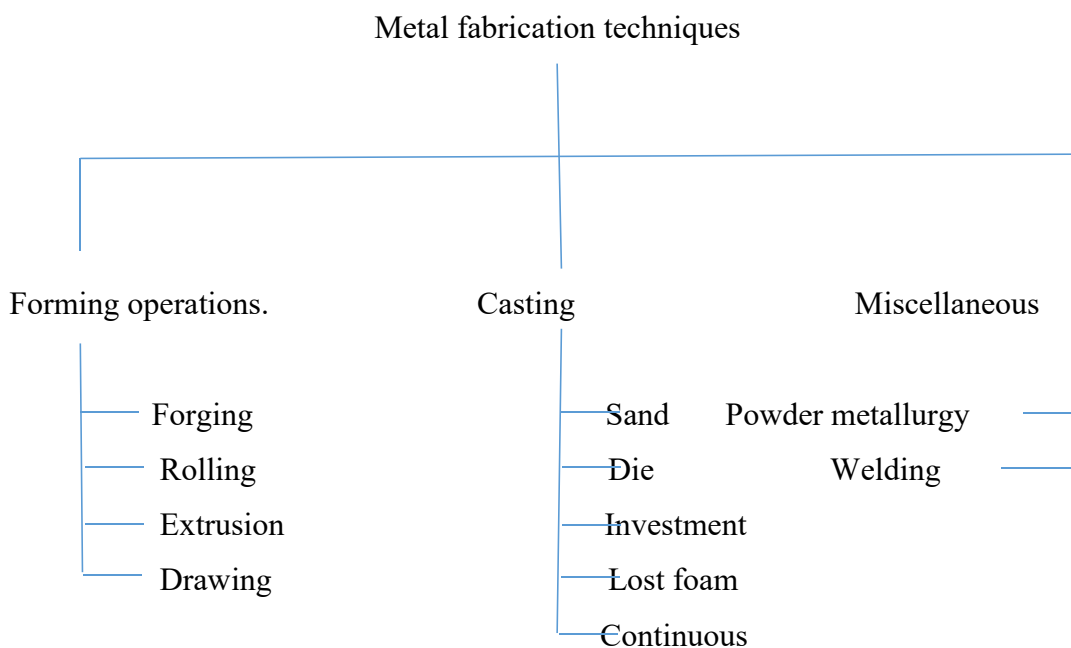
### ***Fabrication of Metals***

Refinement, alloying, and frequently heat-treating procedures that yield alloys with the required properties typically come before metal fabrication techniques. Various metal-forming processes, casting, powder metallurgy, welding,

and machining are among the categories of fabrication techniques; frequently, two or more of them must be utilized before a piece is completed. The most significant determinants of the techniques selected are the metal's characteristics, the final product's dimensions and form, and, of course, the price. The methodology shown in Figure 2 is used to categorize the metal manufacturing techniques. (Callister, & Rethwisch, 2018).

Figure 2.

*Metal fabrication techniques. (Callister, & Rethwisch, 2018).*



### **Forming Operations**

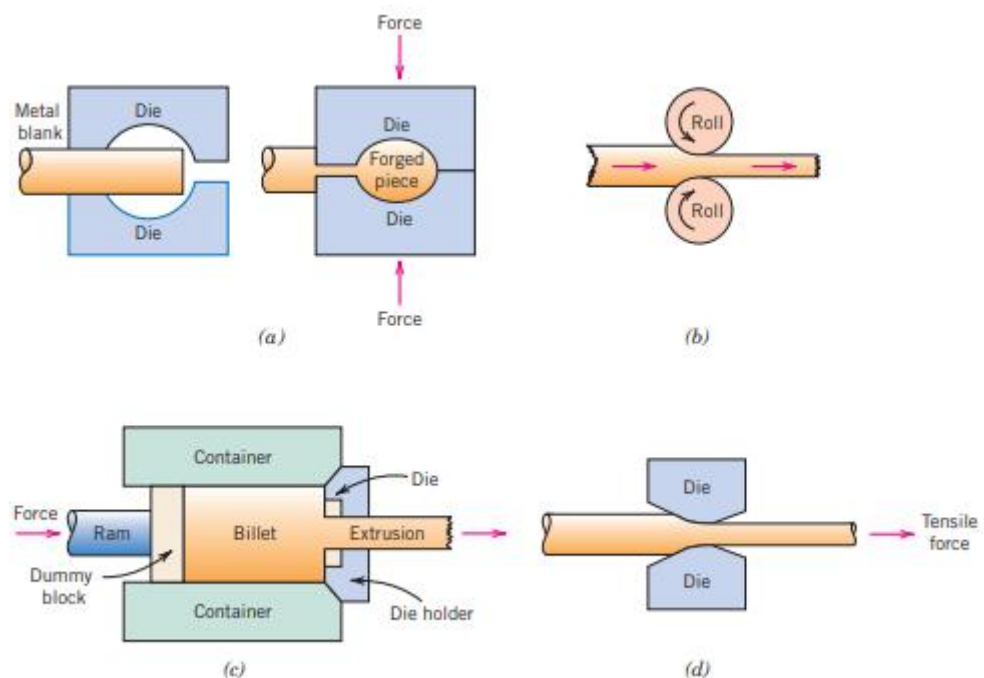
Forging, rolling, extrusion, and drawing are examples of common forming processes. Forming operations are those in which plastic deformation changes the shape of a metal component. Naturally, an external force or stress that is greater than the material's yield strength must cause the deformation. Since most metallic materials are at least somewhat ductile and can undergo some permanent deformation without breaking or cracking, they are well suited to these processes. (Pandey & Singh 2003; Callister, & Rethwisch, 2018).

The procedure is known as "hot working" when deformation is accomplished at a temperature higher than that at which recrystallization takes place; otherwise, it is known as "cold working." Both hot- and cold-working processes are feasible with

the majority of forming techniques. Large deformations are conceivable for hot-working techniques, in which, as the metal is still pliable and malleable, can be performed repeatedly. Additionally, less deformation energy is needed than with cold working. Nevertheless, surface oxidation occurs in most metals to some extent, leading to material loss and a subpar ultimate surface polish. Because the metal strain hardens, cold working increases strength while decreasing ductility. The benefits of cold working over hot working include a better surface finish, more mechanical properties and a wider range of them, and more precise dimensional control of the final product. Occasionally, the piece is cold worked a little bit at a time before being process annealed to get the desired total distortion; nevertheless, this is a costly and inconvenient operation. The forming operations to be discussed are illustrated schematically in Figure 3. (Pandey & Singh 2003; Callister, & Rethwisch, 2018).

Figure 3.

*Metal deformation during (a) forging, (b) rolling, (c) extrusion, and (d) drawing. (Callister, & Rethwisch, 2018).*



### Forging

A single piece of usually hot metal is mechanically worked or deformed during forging; this can be done by applying successive blows or by continuously squeezing. There are two types of forgings: closed die and open die. In a closed die,

two or more die halves with the final shape are subjected to a force that deforms the metal in the space between them. See Figure 3a. Two dies with basic geometric shapes, such as parallel; flat, or semicircular, are used for open die, typically on big workpieces. The best combination of mechanical characteristics and exceptional grain structures are found in forged products. Common products made with this method include piston connecting rods, automotive crankshafts, and wrenches. (Kalpakjian, & Schmid, 2009; Callister, & Rethwisch, 2018).

### **Rolling**

A piece of metal is passed between two rolls during rolling, the most common deformation technique; the compressive pressures the rolls apply cause the metal to thin. Sheet, strip, and foil with a superior surface polish can be produced by cold rolling. See Figure 3b. Grooved rolls are used to create railroad rails, I-beams, and circular shapes. (Callister, & Rethwisch, 2018)

### **Extrusion**

A compressive force supplied to a ram forces a bar of metal through a die hole during extrusion; the resulting extruded piece has the required form and a smaller cross-sectional area. Rods and tubing with intricate cross-sectional geometries are examples of extrusion products; seamless tubing can also be extruded. Example is shown in Figure 3c. (Kalpakjian, & Schmid, 2009; Callister, & Rethwisch, 2018).

### **Drawing**

A tensile force exerted on the exit side pulls a metal item through a die with a tapered bore. This process is known as drawing. This leads to a decrease in cross section and an increase in length. There may be a series of dies used in the entire drawing operation. This method is frequently used to create rod, wire, and tubing products. See example in Figure 3d. (Callister, & Rethwisch, 2018).

### **Casting**

In the casting process, a completely molten metal is poured into a mold cavity with the required shape; as the metal solidifies, it takes on the mold's shape but also shrinks slightly. When:

(1) the final shape is so big or complex that any other way would be unfeasible,

(2) a certain alloy has such low ductility that it would be challenging to form by either hot or cold working, and

(3) Casting is the most cost-effective method of manufacture when compared to other methods. Moreover, casting may be used as the last stage in the refinement of even ductile metals. Numerous casting methods, including sand, die, investment, lost foam, and continuous casting, are frequently used. (Kalpakjian, & Schmid, 2009; Prashant, 2010; Callister, & Rethwisch, 2018).

### **Die Casting**

Die casting involves forcing liquid metal into a mold at a relatively fast speed and under pressure, then allowing the metal to solidify while the pressure is maintained. The two components of a permanent steel mold or die are fastened together to generate the required shape. The cast piece is released from the die parts once the metal has fully solidified. Moreover, a single set of dies can be used for thousands of castings, making this a cost-effective technique that allows for rapid casting rates. However, only very small pieces and low-melting-temperature alloys of magnesium, aluminum, and zinc can be used with this process. (Kalpakjian, & Schmid, 2009; Prashant, 2010; Callister, & Rethwisch, 2018).

### **Investment Casting**

A wax or plastic with a low melting temperature is used to create the pattern for investment casting, also known as lost-wax casting. Plaster of Paris is typically utilized. A fluid slurry is poured around the pattern, setting to create a solid mold or investment. After that, the mold is heated to the point where the pattern melts and burns out, leaving behind a mold cavity with the appropriate shape. This method is used, for instance, in jewelry and dental crowns and inlays, where great dimensional precision, exquisite detail reproduction and a superior polish are necessary. Additionally, investment cast is used to make gas turbine blades and jet engine impellers. (Kalpakjian, & Schmid, 2009; Prashant, 2010; Callister, & Rethwisch, 2018).

### **Lost Foam Casting**

Lost foam casting is a type of investment casting. Polystyrene beads can be compressed into the required shape and then heated to form foam, which serves as the disposable pattern in this case. Alternatively, you can cut out pattern shapes from sheets and glue them together. The mold is then created by packing sand around the

design. The pattern vaporizes and is replaced by the molten metal as it is poured into the mold. The compressed sand stays in place, and the metal takes on the mold's shape as it solidifies. (Kalpakjian, & Schmid, 2009; Prashant, 2010; Callister, & Rethwisch, 2018).

Tight tolerances and intricate geometries are achievable using lost foam casting. Additionally, lost foam is a less complicated, faster, and more cost-effective process than sand casting, and it produces fewer environmental wastes. Cast iron and aluminum alloys are the metal alloys that employ this process the most frequently; other applications include electric motor frames, crankshafts, cylinder heads, car engine blocks, and marine engine blocks. (Kalpakjian, & Schmid, 2009; Prashant, 2010; Callister, & Rethwisch, 2018).

### **Continuous Casting**

Many molten metals are cast into enormous ingot molds to solidify them at the end of extraction processes. Ingots often undergo a primary hot-rolling process that results in a flat sheet or slab, which are more practical shapes to use as starting points for secondary metal-forming processes including forging, extrusion, and drawing. A continuous casting technique, sometimes known as strand casting, may combine these rolling and casting phases. This happens in a water-cooled die containing the desired cross-sectional geometry. Compared to ingot-cast products, continuous castings have more consistent mechanical characteristics and chemical composition across the cross sections. Continuous casting is also more effective and more mechanized. (Kalpakjian, & Schmid, 2009; Prashant, 2010; Callister, & Rethwisch, 2018; Ganesh, 2020).

### **Sand Casting**

Ordinary sand is used as the mold material in sand casting, which is arguably the most popular technique (see Figure 4). Sand is packed around a pattern with the desired casting's shape to create a two-piece mold. Additionally, a gating mechanism is typically built into the mold to reduce internal casting flaws and speed the flow of molten metal into the cavity. Large pipe fittings, fire hydrants, and automobile cylinder blocks are examples of sand-cast components. (Kalpakjian, & Schmid, 2009; Prashant, 2010; Ganesh, 2020; Callister & Rethwisch, 2018).

Figure 4.

Typical sand mould (a) Mould Section and casting nomenclature (b) pattern attached with gating and risering system. (Ghosh, & Mallik,1986, Callister, & Rethwisch, 2018; Ganesh, 2020)

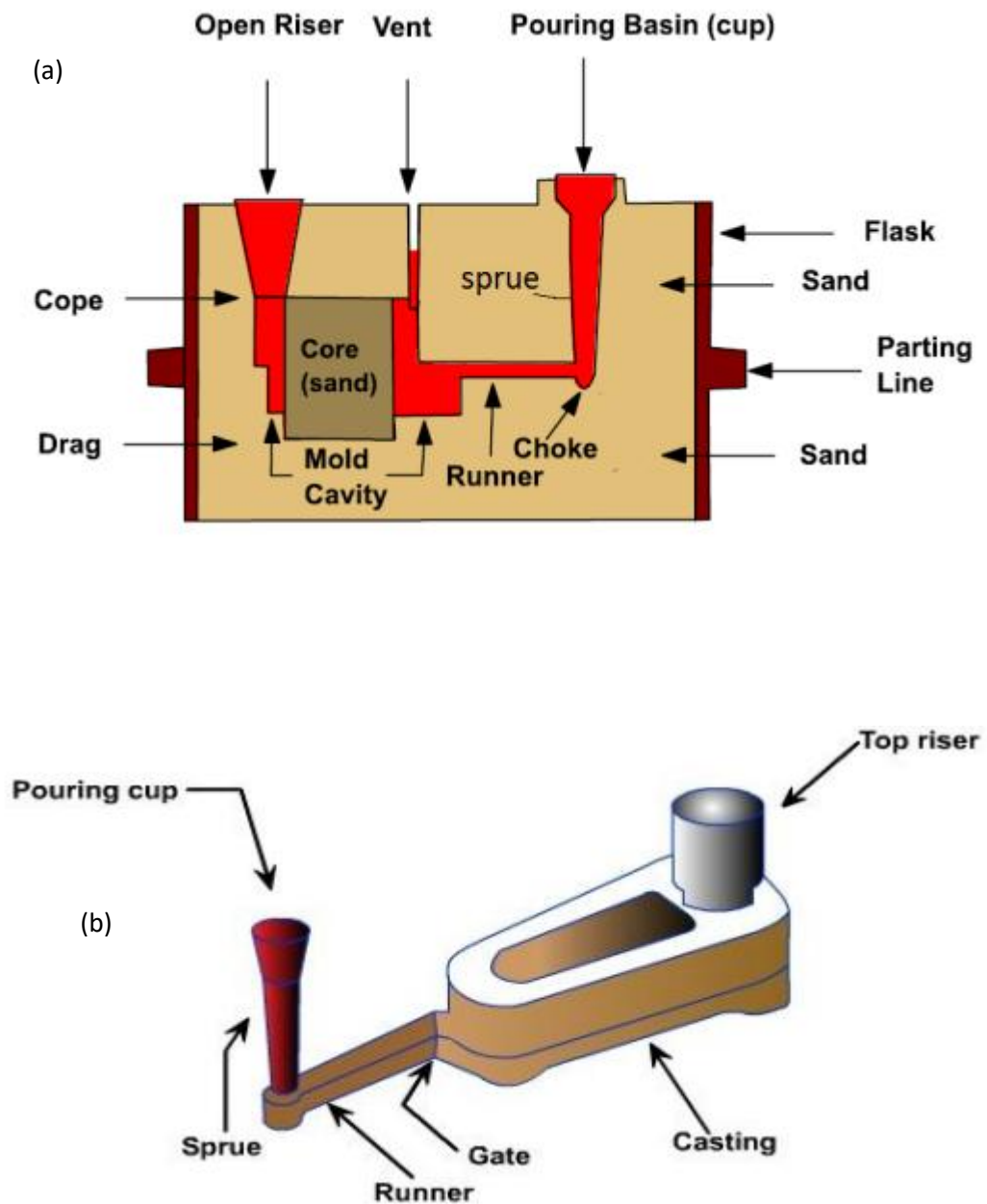
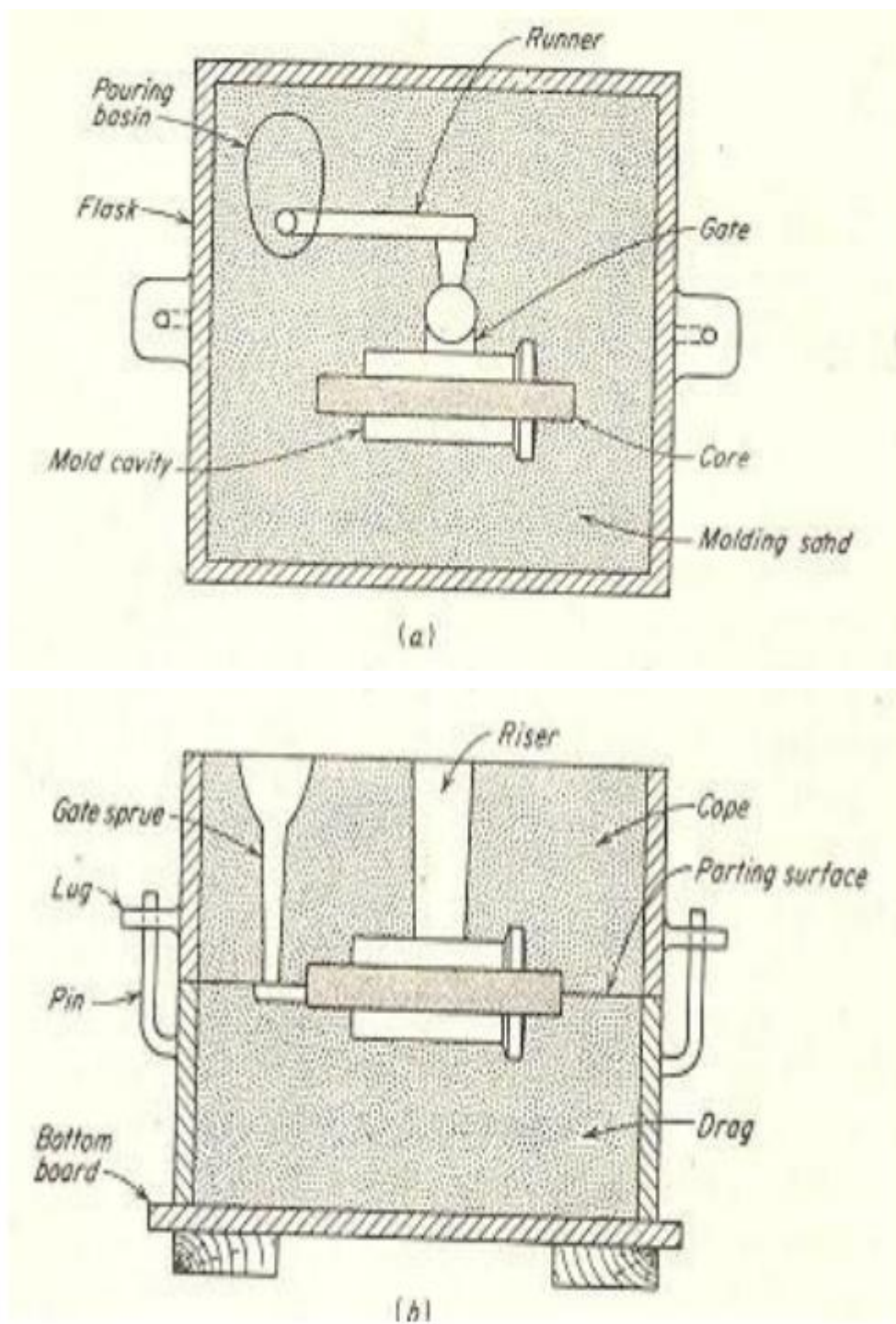


Figure 5.

*Mould Section and casting nomenclature, (a) top view, (b) front view (Ganesh, 2020)*



**Important casting terms (Ganesh, 2020)**

**Flask:** The mold is formed in a frame made of wood or metal that has no fixed top or bottom. There are several names for the flask depending on where it is in the moulding structure, including cheek, which is an intermediate moulding flask used in three piece moulding, cope, which is an upper moulding flask, and drag, which is a lower moulding flask.

**Pattern:** It is a duplicate of the finished product. The design is used to create the mold cavity.

**Parting line:** The two molding flasks that comprise the mold are separated by this line.

**Moulding sand:** Sand, which retains its permeability to gasses and air while binding firmly. It is a blend of clay, silica sand, and moisture in the right amounts.

**Facing sand:** To improve the castings' surface smoothness, a tiny bit of carbonaceous material was dusted on the inner surface of the mold chamber.

**Core:** A distinct component of the mold, usually baked and composed of sand, that is used to make holes and different-shaped cavities in the castings.

**Pouring basin:** A tiny, funnel-shaped opening at the top of the mold that is filled with molten metal.

**Sprue:** The opening through which the pouring basin's molten metal enters the mold cavity. In many instances, it regulates the metal's flow into the mold.

**Runner:** The path that the molten metal takes as it moves from the sprue to the gate.

**Gate:** The molten metal enters the mold cavity through this channel.

**Chaplets:** In order for the cores inside the mold cavity to support themselves and overcome the metallostatic force, chaplets are utilized.

**Riser:** A column of molten metal is inserted into the mold to feed the solidifying and shrinking castings. Another name for it is "feed head."

**Vent:** A tiny hole in the mold that allows gasses and air to escape.

**Steps in producing a simple sand mould (Ganesh, 2020):**

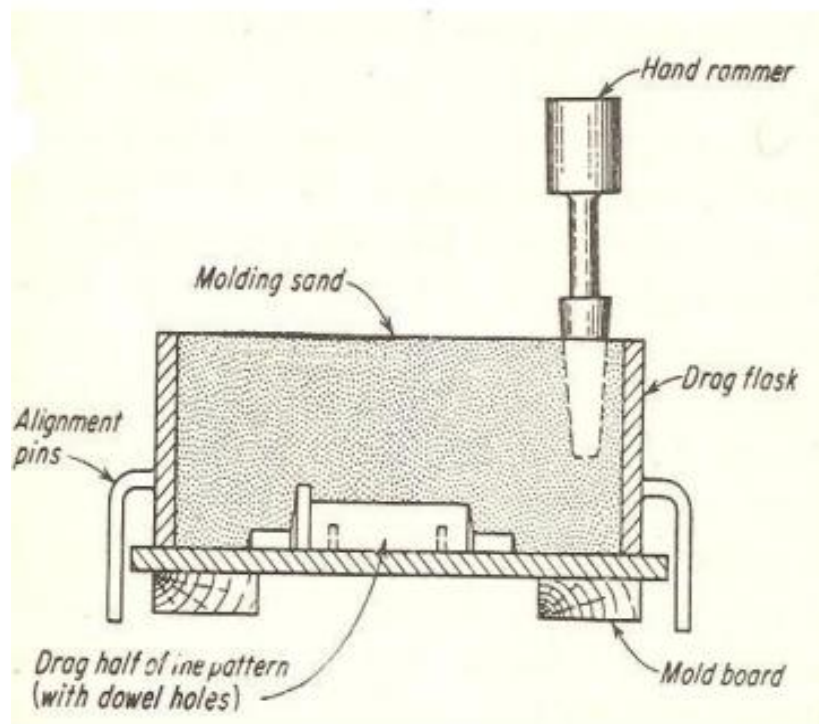
- 1) The drag flask is positioned on the board
- 2) then a dry facing sand is spread over it, the board
- 3) half of the drag pattern is positioned on the mould board. The dry facing sand will help to produce a non-sticky medium/layer.

4) then the molding sand is poured upon. This help to cover the pattern with the aid of the fingers. The drag is then filled totallly.

5) Hand rammers is used to pack the sand in the drag tightly. Surface ramming is done with butt hammer while for drag pattern, peen hammers are used.

Figure 6.

*Making a simple sand mould (Ganesh, 2020):*



6) The ramming needs to be appropriate, meaning it shouldn't be excessively soft or harsh. A weak mold and a poor pattern imprint will result from overly soft ramming. Excessive ramming prevents gasses and air from escaping, which causes bubbles to form in the casting and produce flaws known as "blows." Additionally, it will be challenging to make runners and gates.

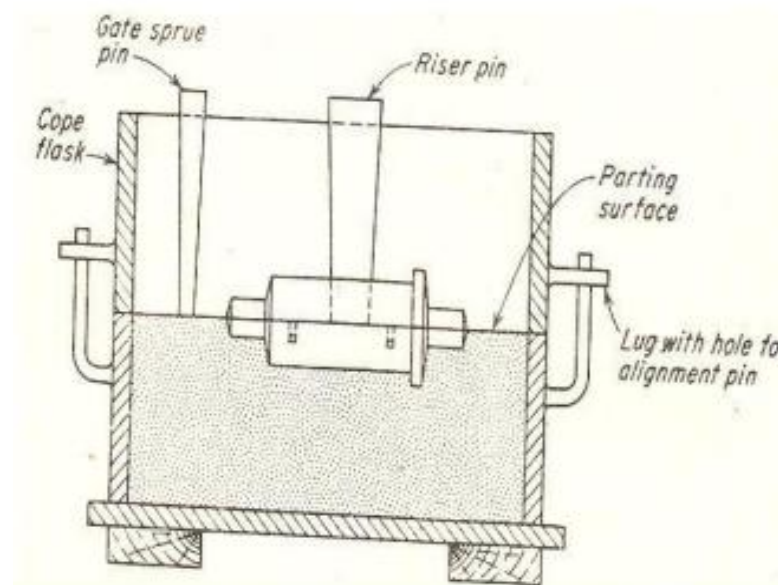
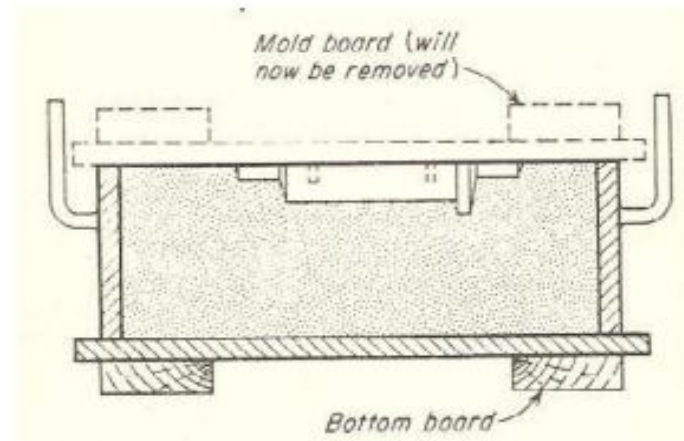
7) A straight bar called a strike rod is used to level or remove extra sand once the ramming is complete.

8) To make it easier to remove gasses during pouring and solidification, vent holes are cut in the drag to the entire depth of the flask as well as to the pattern. The vent rod was used.

9) To reveal the pattern, the completed drag flask is now turned upside down.

Figure 7.

*Making a simple sand mould (Ganesh, 2020)*



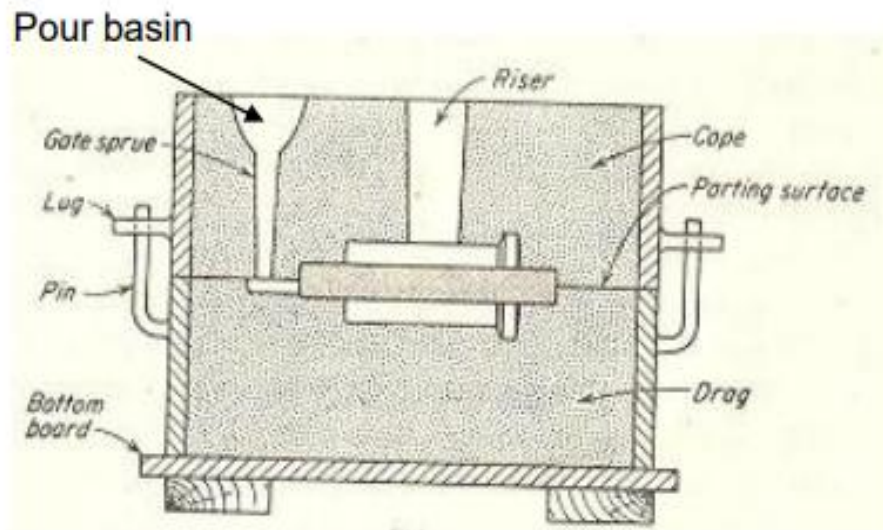
10) Next, using locating pins, place the other half of the design on the drag pattern. Pins are also used to locate the cope flask. The pattern and the drag surface are both dusted with the dry parting sand.

11) At a certain distance from the pattern edge is a sprue pin that is used to create the sprue channel. The riser pin is positioned correctly.

12) The cope is filled, rammed, and vented in the same way.

Figure 8.

*Making a simple sand mould*



13) The riser and sprue are taken out, and the liquid metal is poured into a pouring basin that is created on top.

14) Remove the cope and drag pattern.

15) A gate cutter is utilized to cut the separating surface in order to create runners and gates. Sheets of metal bent to the required radius are called gate cutters.

16) The drag's mold chamber is now filled with the core needed to create a central hole. stays in core printing.

17) The mold has now been put together and is prepared to pour.

### **Moulding Sand Composition**

The main components of any moulding sand are: (Callister, & Rethwisch, 2018; Ganesh, 2020).

(a) Silica sand ( $\text{SiO}_2$ ) 80.8%

(b) Alumina ( $\text{Al}_2\text{O}_3$ ) 14.9%

(c) Iron oxide ( $\text{Fe}_2\text{O}_3$ ) 1.3%

(d) Combined water 2.5%

(e) Other inert materials 1.5%

### **Properties of Moulding Sand.**

The following qualities should be present in the molding sand (Callister, & Rethwisch, 2018; Ganesh, 2020)::

1. **Plasticity:** Sand's ability to flow to all areas of the molding box and take on a certain shape when subjected to hammering pressure and maintain that shape when the pressure is released makes it crucial to create a mold. For the sand to form a good mold, it must be sufficiently malleable. Adding clay and water to sand increases its flexibility.
2. **Cohesiveness:** During ramming, the sand grains adhere to one another because of this characteristic. It can be characterized as the molding sand's strength. There are three different kinds of it:
  - (a) **Green strength:** After water has been added, the green sand needs to be sufficiently strong and malleable to form molds. Grain size and form, clay type and quantity, and moisture level all affect green strength.
  - (b) **Dry strength:** The sand next to the hot metal rapidly loses water content as steam when the molten metal is poured. In order to prevent the mold from growing, the dry sand needs to be strong enough to withstand erosion and the pressure of the molten metal.
  - (c) **Hot strength:** The sand may need to be strong at temperatures above 100°C once the moisture has evaporated. The pressure of the liquid metal bearing against the mold walls may cause the mold to enlarge if the sand lacks hot strength, or it may produce erosion, fissures, or breaking if the metal is still flowing.
3. **Flowability:** Sand's ability to behave like a fluid allows it to flow to all areas of a mold when slammed, distributing the ramming pressure uniformly. Sand particles typically do not move around corners. Generally speaking, flowability rises as grain size and green strength decline. Additionally, the moisture content affects it.
4. **Sand's permeability, also known as porosity, is what allows gases like steam to flow through the sand mold. A lot of additional gasses are released when hot molten metal is put into the sand mold and comes into contact with the wet sand. The casting will have gas holes and pores if these gasses do not entirely escape through the mold. Therefore, the sand used to make the mold needs to be permeable or porous. Grain size and form, as well as the amount of moisture and clay in the molding sand, all affect the porosity of the**

material. The porosity of the mold is directly impacted by the quality of the sand.

5. Adhesiveness: Sand sticks to the molding box's sides because of this characteristic. For big sand masses to be properly held in a moulding box without the risk of falling out when the box is removed, good sand needs to be sufficiently sticky , when removing the board.
6. Refractoriness: Sand's ability to withstand high temperatures from molten metal without breaking or fusing is known as its refractoriness. Sand that has a high refractoriness is necessary for higher pouring temperatures, like those for ferrous alloys. The amount of quartz presents as well as the size and shape of the particles determine the degree of refractoriness.

## **Other Techniques**

### **Powder Metallurgy**

Compaction of metal powder, followed by heat treatment to create a denser piece, is yet another production method. The procedure is commonly referred to as P/M and is appropriately named powder metallurgy. A almost nonporous component with characteristics nearly identical to the fully dense parent material can be produced via powder metallurgy. The formation of these qualities is mostly dependent on diffusional processes that take place during the heat treatment. Because just a slight plastic deformation of the powder particles is required, this process works particularly well with metals that have low ductilities. P/M speeds up fabrication since it is challenging to melt and cast metals with high melting temperatures. Furthermore, parts that require very close dimensional tolerances (e.g., bushings and gears) may be economically produced using this technique. (Callister, & Rethwisch, 2018).

### **Welding**

Welding can be thought of as a fabrication method in a way. When one-part fabrication is costly or inconvenient, welding joins two or more metal components to create a single piece. It is possible to weld both different and similar metals. Unlike riveting and bolting, which are purely mechanical, the connecting connection is metallurgical (including some diffusion). There are numerous welding techniques, such as brazing, soldering, and arc and gas welding. The filler material (i.e., welding

rod) and the workpieces to be connected are heated to a high enough temperature to melt them both during arc and gas welding; once solidified, the filler material creates a fusion joint between the workpieces. As a result, the area next to the weld that may have undergone microstructural and property changes is known as the heat-affected zone (abbreviated HAZ). The following changes are possible: (Callister, & Rethwisch, 2018).

1. A reduction in strength, hardness, and toughness may have resulted from recrystallization and grain growth in this heat-affected zone if the workpiece material had previously undergone cold working. In this case, Figure 11.9 shows a schematic representation of the HAZ.
2. Remaining tensions that weaken the joint may develop in this area after cooling.
3. The steel in this area might have been heated to high enough temperatures to produce austenite. The microstructural products that occur as the alloy cools to room temperature are determined by the alloy composition and cooling rate. Typically, simple carbon steels will have a proeutectoid phase and pearlite. However, because of its high brittleness, martensite—a microstructural result of alloy steels—may be undesirable.
4. Intergranular corrosion can occur because certain stainless steels might become "sensitized" during welding. Laser beam welding is a more recent joining method that uses a highly concentrated and powerful laser beam being utilized as the heat source.

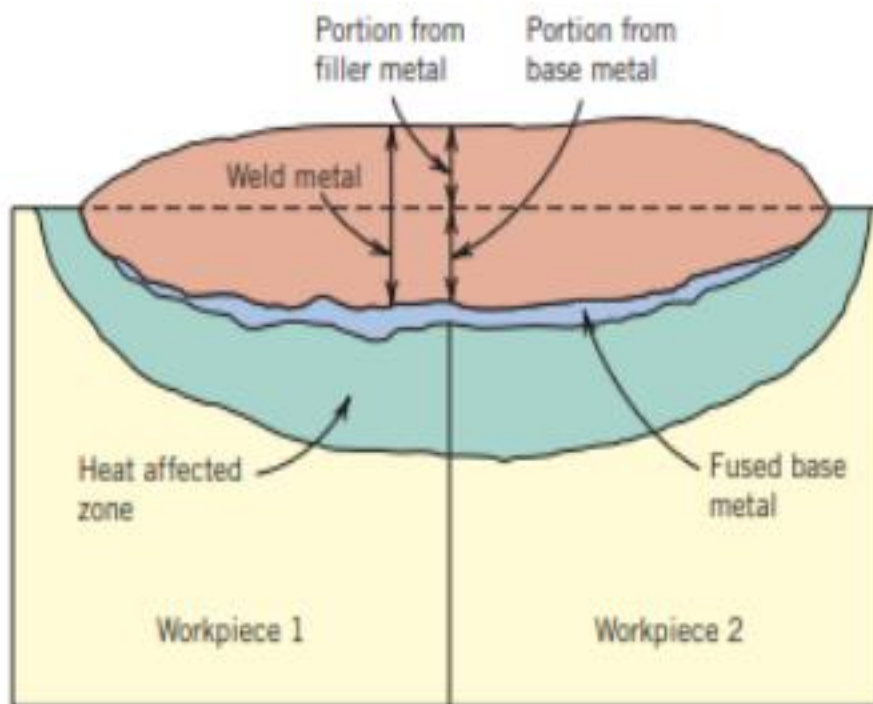
A fusion junction is created when the parent metal is melted by the laser beam and solidifies; frequently, no filler material is required. The following are a few benefits of this method: (Callister, & Rethwisch, 2018).

- (1) It may be quick and highly automated;
- (2) It is a noncontact method, which removes mechanical deformation of the workpieces;
- (3) a wide range of metals and alloys can be joined using this technique;
- (4) welds can be small and extremely precise;
- (5) a low energy input to the work piece means that the heat-affected zone size is minimal; and

(6) porosity-free welds with strengths equal to or greater than the base metal are possible. The automotive and electronic sectors make substantial use of laser beam welding, where high quality and rapid welding rates are required.

Figure 9.

*Schematic cross sectional representation showing the zones in the vicinity of a typical fusion weld. (Walton, & Opar, 1981).*



### ***Mechanical Characteristics/Behaviour of Metallic Materials***

Engineers may be required to design buildings or components using pre-set materials in order to prevent unacceptable levels of deformation and/or failure. It is their responsibility to comprehend how the various mechanical properties are measured and what these qualities signify.

The steel in an automotive axle and the aluminium alloy used to make aviation wings are two examples of materials that are subjected to stresses or forces while in use. Through meticulously planned laboratory experiments that as closely resemble the service circumstances as feasible, the mechanical characteristics of materials are determined. The type of applied load, how long it lasts, and the surrounding circumstances are all factors to take into account. (Callister, & Rethwisch, 2018).

Many parties with varying interests are concerned about mechanical qualities, including government bodies, research groups, and material producers and consumers. As such, it is essential that the way tests are performed and the interpretation of their findings be somewhat consistent. Standardized testing methods are used to achieve this consistency. Professional associations frequently coordinate the creation and dissemination of these standards. The American Society for Testing and Materials (ASTM) is the busiest organization in the US. Many of the standards in the Annual Book of ASTM Standards, which is published and revised annually, are related to mechanical testing methods. In this and later chapters, a number of these are cited in footnotes. (Callister, & Rethwisch, 2018).

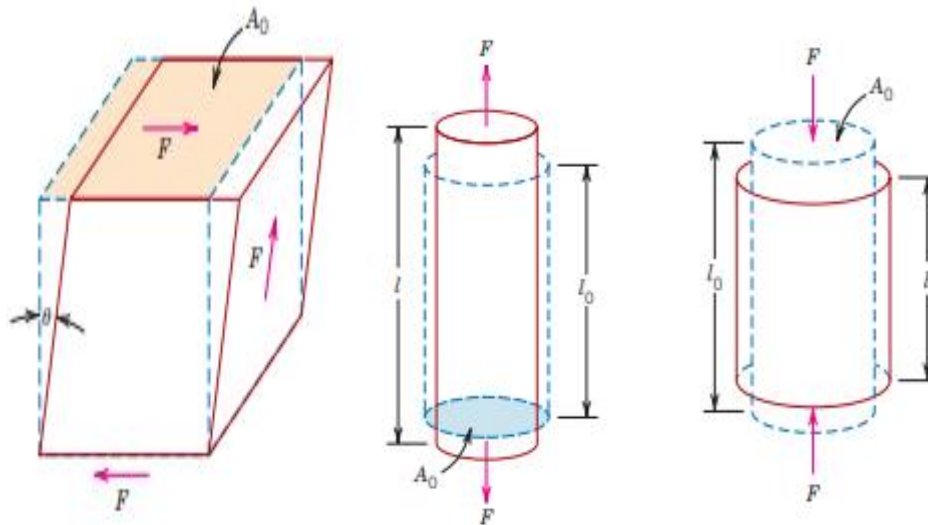
Metallurgical and materials engineers, on the other hand, are focused on creating and manufacturing materials that satisfy the service requirements that these stress studies anticipate. Understanding the connections between a material's mechanical properties and its microstructure, or interior features, is a prerequisite for this. Because of their desirable mechanical property combinations, materials are commonly selected for structural applications. The current research is limited to metals' mechanical properties. (Callister, & Rethwisch, 2018).

### **Concepts of Elongation/Strain and Stress**

If a load is uniformly distributed throughout a part's surface or cross section and is either static or changes very slowly over time, the mechanical behavior of the part can be ascertained using a simple stress-strain test. Metals at room temperature are the most common subjects of these experiments. Shear, tension, and compression are the three methods of applying load, Figure 10. (Callister, & Rethwisch, 2018).

Figure 10.

*Three ways to apply load: shear, tension, and compression.*



Where:

$F$  = Applied Force;

$\Theta$  = Shear Angle

$A_0$  = Initial Area

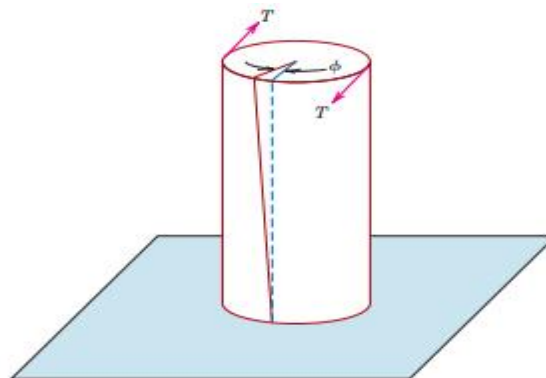
$l$  = Final Length

$l_0$  = Initial Length

Many of the daily stresses used in engineering practice are torsional rather than pure shear, as may be shown in Figure 11.

Figure 11.

*Torsional load*



### **Stress-Strain behaviour**

For elastic deformation (compression and tension), Hooke's law provides the relationship between stress and strain. The law states thus; The level to which a

material deforms is a function or depends on the amount of the applied stress. This means that stress is proportional to strain. It is expressed in the equation (1) below:

$$\sigma \propto \epsilon E \dots\dots\dots(1)$$

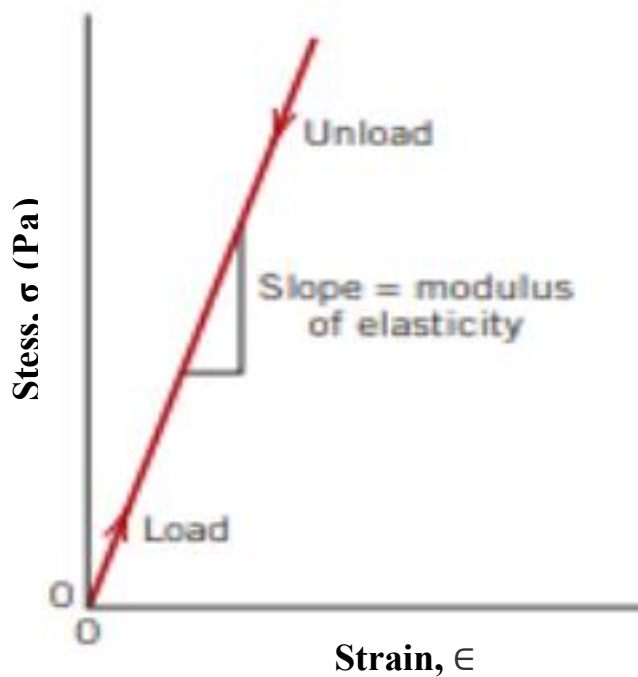
$$\sigma = \epsilon E$$

$\sigma$  = stress ;

$\epsilon$  = strain

The equation above is referred to as Hooke's law. It is also shown graphically below; Figure 12.

*Stress-Strain Curve*



The Young's modulus, often known as the modulus of elasticity, is the proportionality constant E (GPa or psi) as shown in Figure 12. It has a magnitude of around 45 GPa (6.5 X 10<sup>6</sup> psi) for magnesium and 407 GPa (59 X 10<sup>6</sup> psi) for tungsten. Its value varies depending on the metal. For certain metals, the values of the modulus of elasticity at room temperature are shown in the Table 1.

Table 1.

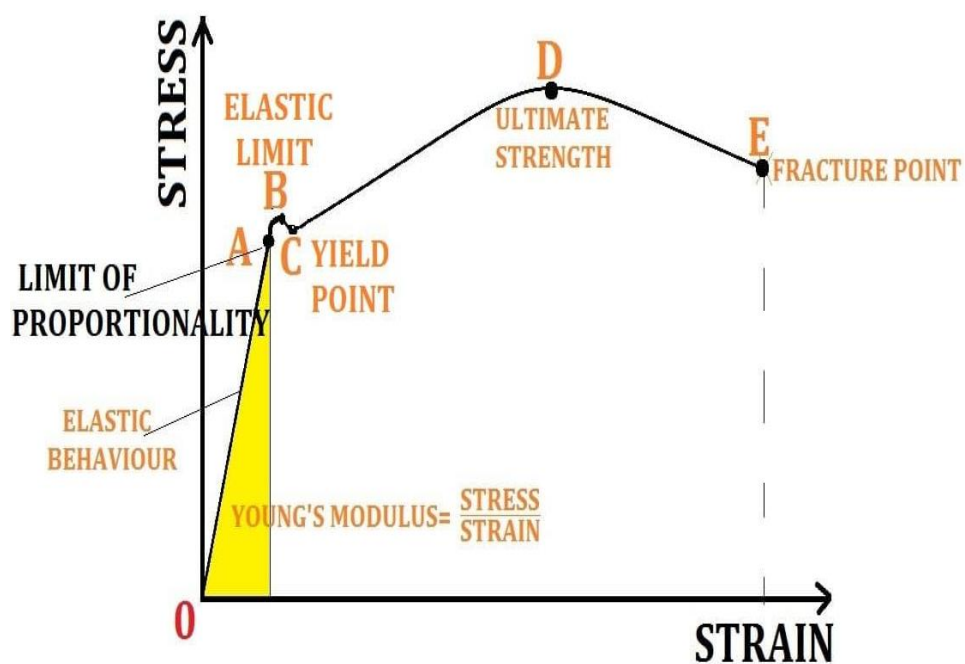
*Shear and elastic Moduli at room-temperature, including Poisson's Ratio for different Metal Alloys(Callister, & Rethwisch, 2018).*

Metal Alloy	Modulus of Elasticity		Shear Modulus		Poisson's Ratio
	GPa	10 <sup>6</sup> psi	GPa	10 <sup>6</sup> psi	
Aluminum	69	10	25	3.6	0.33
Brass	97	14	37	5.4	0.34
Copper	110	16	46	6.7	0.34
Magnesium	45	6.5	17	2.5	0.29
Nickel	207	30	76	11.0	0.31
Steel	207	30	83	12.0	0.30
Titanium	107	15.5	45	6.5	0.34
Tungsten	407	59	160	23.2	0.28

For an elastic material, the stress strain relation is depicted on the graph in Figure 13. Stress and strain for an elastic material (Amrit, 2021):

Figure 13.

*Stress- Strain Curve for a material undergoing elongation which is elastic (Amrit, 2021).*



There are several points on the graph above. These points can be described as follows (Amrit, 2021):

**The Elastic Behaviour Region (O-A):**

Here, the Hooke's law is obeyed. It is called the proportionality region where stress is proportional to strain. A spring material will always return to its original size and shape when stress in this region.

**The Region A-B**

In this region, the material deviates from the Hooke's law, meaning that, stress is not proportional to strain. Point B is the elastic limit of the material. This is the largest amount of stress a material can sustain.

**The Region B-C**

Increasing the stress/load above the elastic limit of the material, a point is reached, C, at which a noticeable extension is seen. The point C is referred to as the yield point. This means that the material shows a plastic behaviour between point B and C. By plastic behaviour means that a material in this region will not regain its original shape and size.

**The Region C-D**

Increasing the applied stress beyond point C, the material in question elongates rapidly until it reaches point D as seen on the curve. This is referred to as the breaking point or breaking stress or the ultimate stress.

**The Region/Point E**

This is the destruction or fracture point of the material.

***Hardness***

This is the resistance of a body or an engineering material to plastic deformation, abrasion, indentation, among others. It is a necessary material property not to be neglected for consideration. The primitive way hardness test was carried out was based on the ability of a material to scratch another. The Mohr's scale was a further qualitative method developed for hardness test. Quantitative hardness techniques have been developed. This included the use of indenter which is forced onto the surface of the test piece or material whose hardness is to be determined. This is carried out under controlled conditions of applied load and rate of application.

The indentation depth achieved in the test material is measured. This is further compared or related with the hardness number. More indentation depth is achieved with a softer material, thus lower the material index number. The results are only relative values, not absolute. This implies that much care should be observed while comparing values obtain from different techniques. (Callister, & Rethwisch, 2018; Savaş, 2021).

Hardness test are more common as compared to other test for the following reasons;

1. Material being tested is not destroyed. Its a non-destructive test
2. It's inexpensive and easy to carryout. You don't prepare any special specimen to carryout hardness test.

You can determine other mechanical properties like tensile strength from the result of the hardness test. (Callister, & Rethwisch, 2018).

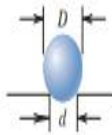
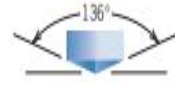
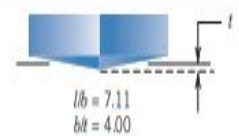
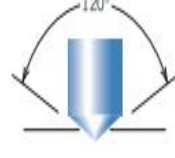
### **Rockwell Hardness Tests**

This test method is easy to carryout thus constitute a common hardness test method. Different scales may be used resulting from combination of indenters and different weights/loads. This makes it possible to possibly test all metals or alloys, including polymers. The kind of indenters used include hardened steel balls and spherical indenters. These have different diameters of 6.350mm, 1.588mm, 12.70mm and 3.175mm. indenter in conical shape is used for extremely hard materials. The indentation gives a measure of the hardness number. This results from an application of a small load followed by a major load. The use of a small load increases the accuracy of the test being carriedout. (Callister, & Rethwisch, 2018).

As a result of application of small or major load, there are two test types. These are the rockwell and the superficial rockwell test. The Rockwell test has a small load of 10 kg, while the major loads includes 60 kg, 100 kg, and 150 kg. A letter of the alphabet represents each scale as seen in the Table 3.

Table 2.

*Different techniques for hardness test. (Callister, & Rethwisch, 2018).*

Test	Indenter	Shape of Indentation		Load	Formula for Hardness Number <sup>a</sup>
		Side View	Top View		
Brinell	10-mm sphere of steel or tungsten carbide			P	$HB = \frac{2P}{\pi D [D - \sqrt{D^2 - d^2}]}$
Vickers microhardness	Diamond pyramid			P	$HV = 1.854P/d_1^2$
Knoop microhardness	Diamond pyramid			P	$HK = 14.2P/l^2$
Rockwell and superficial Rockwell	{ Diamond cone; $\frac{1}{16}$ , $\frac{1}{8}$ , $\frac{1}{4}$ , $\frac{1}{2}$ -in.-diameter steel spheres			60 kg } Rockwell 100 kg } 150 kg } 15 kg } Superficial Rockwell 30 kg } 45 kg }	

For the hardness formulas given, P (the applied load) is in kg, whereas D, d, and l are all in mm. (Callister, & Rethwisch, 2018).

Table 3.

*Different Rockwell scales*

Scale Symbol	Indenter	Major Load (kg)
A	Diamond	60
B	$\frac{1}{16}$ -in. ball	100
C	Diamond	150
D	Diamond	100
E	$\frac{1}{8}$ -in. ball	100
F	$\frac{1}{16}$ -in. ball	60
G	$\frac{1}{16}$ -in. ball	150
H	$\frac{1}{8}$ -in. ball	60
K	$\frac{1}{8}$ -in. ball	150

The superficial tests has 3 kg as it's small load while the possible majour loads are 15 kg, 30 kg, and 45 kg. The scales are known by 15, 30, or 45 (with respect to load), and this is followed by N, T, W, X, or Y, based on the indenter. Superficial tests are carried out often on thin samples/materials. Table 4 shows different superficial scales. (Callister, & Rethwisch, 2018).

Table 4.

*Different superficial scales.*

<i>Scale Symbol</i>	<i>Indenter</i>	<i>Major Load (kg)</i>
15N	Diamond	15
30N	Diamond	30
45N	Diamond	45
15T	$\frac{1}{16}$ -in. ball	15
30T	$\frac{1}{16}$ -in. ball	30
45T	$\frac{1}{16}$ -in. ball	45
15W	$\frac{1}{8}$ -in. ball	15
30W	$\frac{1}{8}$ -in. ball	30
45W	$\frac{1}{8}$ -in. ball	45

When specifying Rockwell and superficial hardnesses, it is required to provide both the hardness number and the scale symbol. The scale is identified by the HR symbol, which is followed by the appropriate scale identification. For example, on the 30W scale, 60 HR30W indicates a surface hardness of 60, and on the B scale, 80 HRB indicates a Rockwell hardness of 80. The hardness numbers on each scale are imprecise when they increase over 100 or fall below 20, even though they can fluctuate up to 130. In these situations, it is best to use the next tougher or softer scale because the scales overlap. Inaccuracies may also result from an indentation placed too near a specimen edge, from the test specimen being too thin, or from two indentations placed too near to each other. The specimen thickness should be at least ten times the indentation depth, and the distance between the center of one indentation and the specimen edge, or the center of a second indentation, should not exceed three indentation diameters. Additionally, testing specimens that are stacked on top of one another is not advised. Additionally, in order to attain accuracy, the indentation needs to be made into a smooth, flat surface. (Callister, & Rethwisch, 2018).

## **Failure**

For a number of reasons, including the potential loss of human life, financial damage, and disruption of the supply of goods and services, engineered material failure is nearly always an unwanted occurrence. It might be challenging to provide failure prevention even when the reasons for failure and the behaviour of materials are recognized. Poor component design, improper material selection and processing, and component misuse are the most frequent causes. Furthermore, regular inspection, repair, or replacement of structural components is necessary for safe design because they may experience damage while being used. Engineers are in charge of anticipating any problems, identifying the cause of them, and, if required, putting preventive measures in place. (Callister, & Rethwisch, 2018).

There are three failure modes are these are; fatigue, fracture and creep.

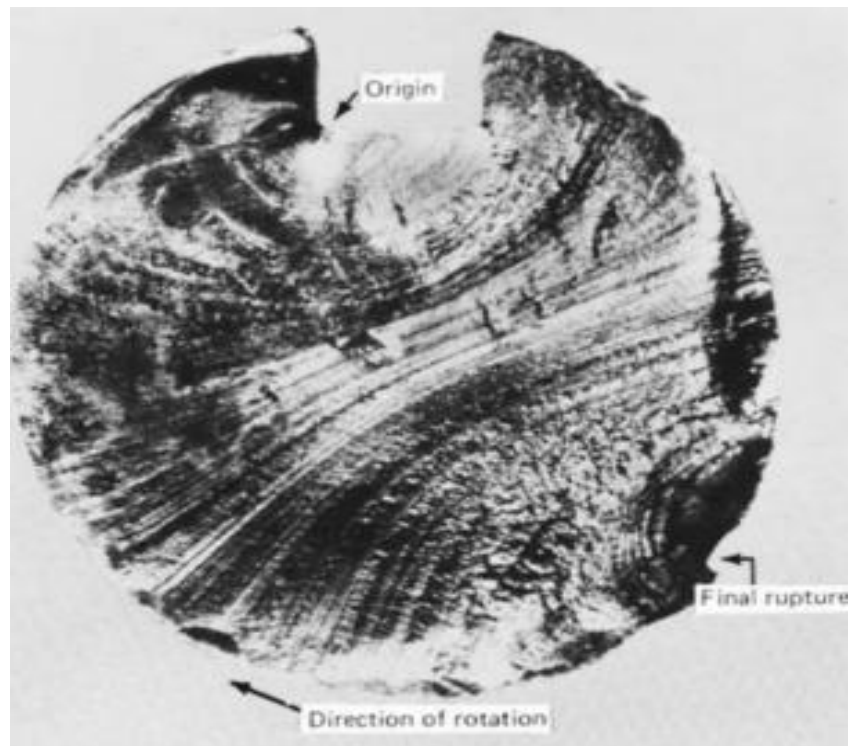
### **Fatigue Failure**

When structures like bridges, aeroplanes, and machine parts are exposed to dynamic and fluctuating loads, a type of failure known as fatigue takes place. Failure may occur in these circumstances at a stress level significantly below the yield or tensile strength for a static load. The term fatigue is used because this type of breakdown usually occurs after a lengthy period of repeated stress or strain cycling. Fatigue is considered to be the primary cause of failure in metals, accounting for around 90% of all metallic failures. Aside from glasses, polymers and ceramics are also susceptible to this type of failure. Furthermore, fatigue strikes suddenly and unexpectedly, and it is destructive and cunning. (Callister, & Rethwisch, 2018).

This failure mode has a brittle like failure in nature. Also it may be in ductile metals. This means that there there may not be plastic deformation in this type of fatigue. The fatigue occurs with vrack initiation, then crack propagation, and the fracture surface is at normal to the applied tensile stress direction. (Callister, & Rethwisch, 2018).

Figure 14.

*Fatigue failure of a shaft showing the Fracture surface.*

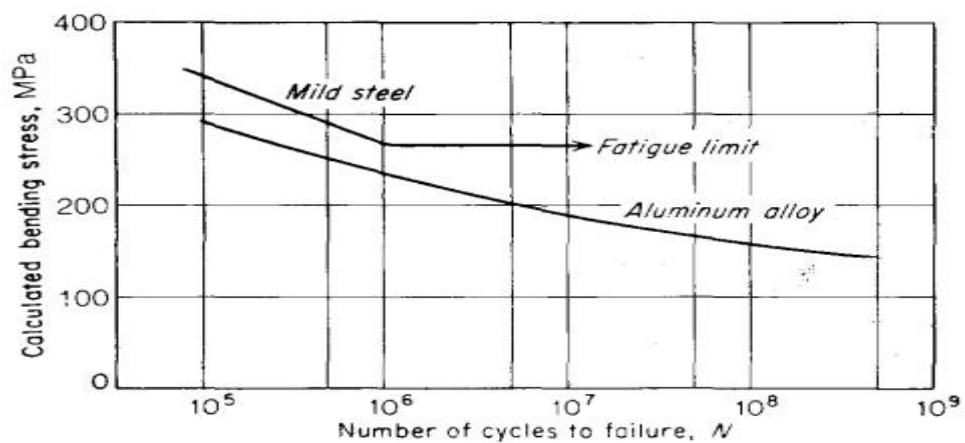


### S-N Curves

This is the basic means of showing fatigue results. This is called the stress-number of cycles curve. It is a plot of stress  $S$ , values with respect to the number of cycles to failure  $N$ . The scale used for  $N$  is usually a logarithmic scale. The figure 15 is a sample S-N resulting from a rotating-beam experiments. (Callister, & Rethwisch, 2018).

Figure 15.

*Typical curve for fatigue failure (Callister, & Rethwisch, 2018).*

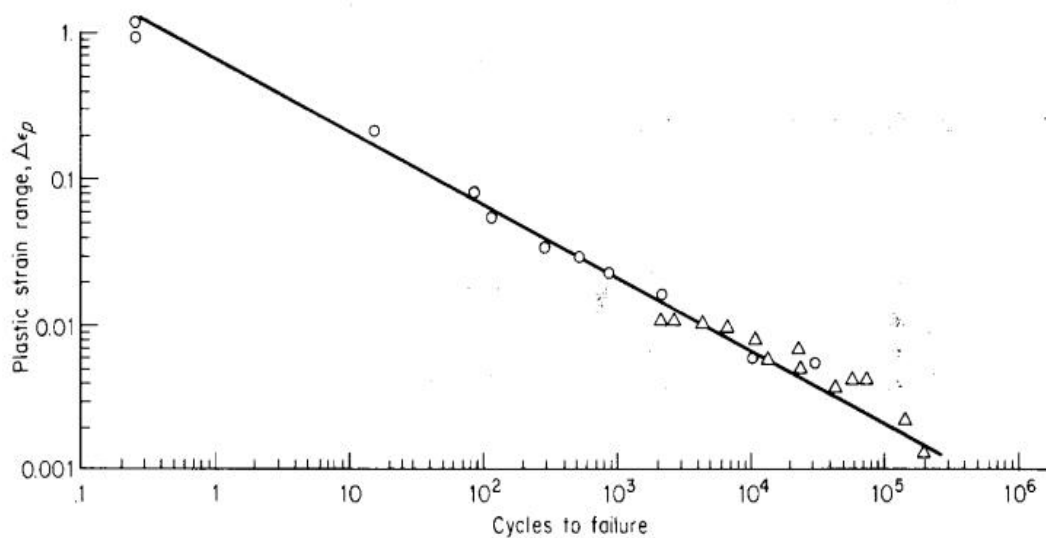


### ***Low-Cycle Fatigue***

Most fatigue research has been towards those of failure cycles of over  $10^4$  cycles of stress. The fatigue type where is called a low cycle fatigue, has a fatigue failure which occurs at high stress and low cycles, less than  $10^4$ . Fatigue failure of this nature is considered in steam turbines, nuclear pressure vessels and many power machinery. (Callister, & Rethwisch, 2018).

Figure 16.

*Curve for Low-cycle fatigue failure (George, 1988).*



### **Factors that influence Fatigue Life**

The number of cycles to failure of engineering materials is sensitive or influenced by different kinds of factors. Among these factors are geometrical design, level of the mean stress, metallurgical variables and the surface effects, including the environmental factors. A material fatigue resistance can be improved through proper considerations of the following factors;

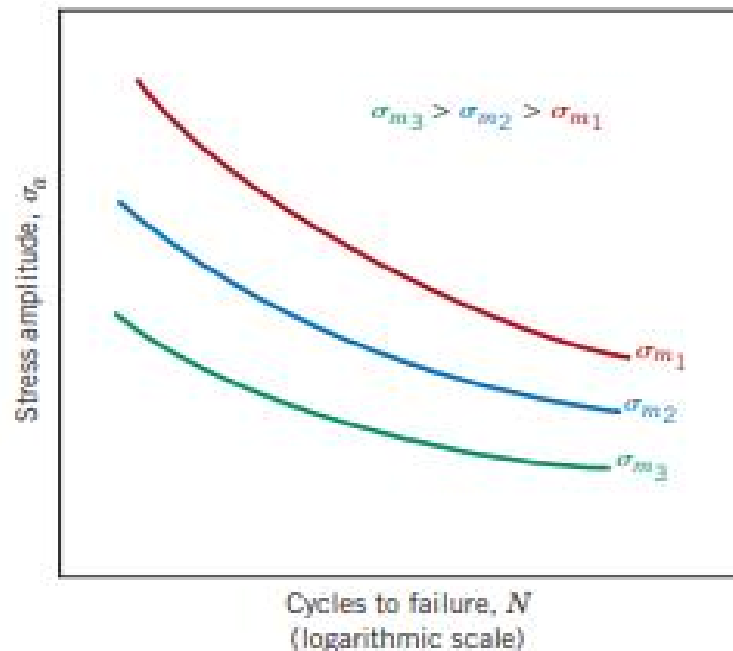
#### **Mean Stress**

The S-N curve shows the dependence of number of cycles to failure on stress amplitude. This is applicable when the mean stress is constant but the mean stress is zero for a reverse cycle. This is represented in the diagram in Figure 17;

Figure 17.

*Influence of mean stress,  $m$  on stress-number of cycles ( $S-N$ ), fatigue behavior.*

(Callister, & Rethwisch, 2018).



From the graphs, by raising the level of the mean stress results to a decrease in the fatigue life.

### **Surface Effects**

Most force related applications within a structure or component have their stress concentrations at the surface of the component or structure. This also explain while failure due to fatigue due to cracks also emanates from the material surface, especially at the point of stress concentration. As a result of this, observation reveal that material configuration and condition affects fatigue life. Appropriate management of factors which affects fatigue life will result to reducing failure by fatigue. These factors include but not limited to surface treatment and design criteria. (Callister, & Rethwisch, 2018).

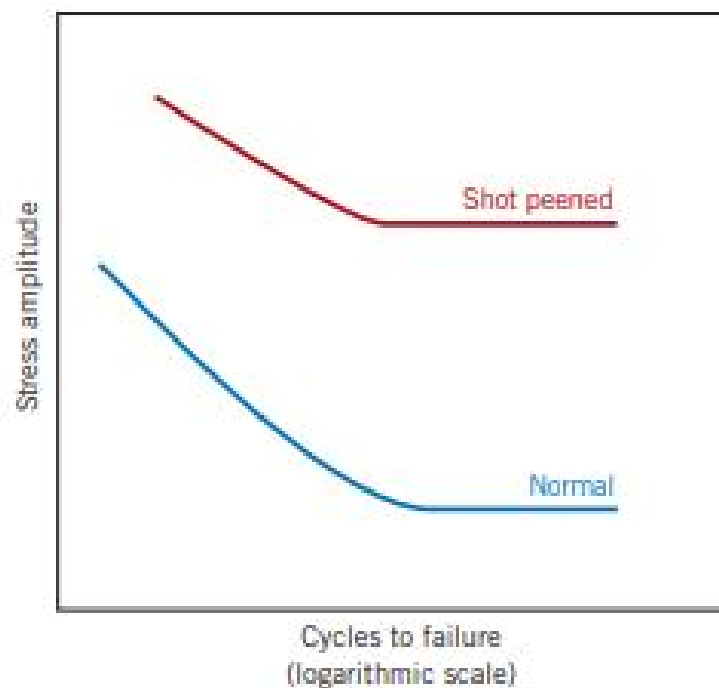
### **Surface Treatments:**

Small scratches and grooves are always created in the workpiece surface by the action of the cutting tool during machining processes. These surface characteristics may restrict the fatigue life. Enhancing the surface finish through polishing has been shown to greatly increase fatigue life. By applying residual compressive stresses within a thin outer surface layer, fatigue performance can be

increased in one of the most efficient ways. Consequently, the residual compressive stress will partially negate and diminish the amplitude of an externally sourced surface tensile stress. Overall, the chance of crack formation and, thus, fatigue failure is decreased. Localized plastic deformation on the outer surface region of ductile metals is a frequent mechanical mechanism for introducing residual compressive stresses. In the commercial world, shot peening is a common method used to do this. The surface to be treated is exposed to high-velocity projections of small, hard particles (shot) with sizes between 0.1 and 1.0 mm. Compressive stresses are induced by the ensuing deformation to a depth of one-half to one-quarter of the shot diameter. The following Figure 18 schematically illustrates how shot peening affects steel's fatigue behaviour. (Callister, & Rethwisch, 2018).

Figure 18.

*S-N curves showing how shot peening affects steel's fatigue behaviour.*



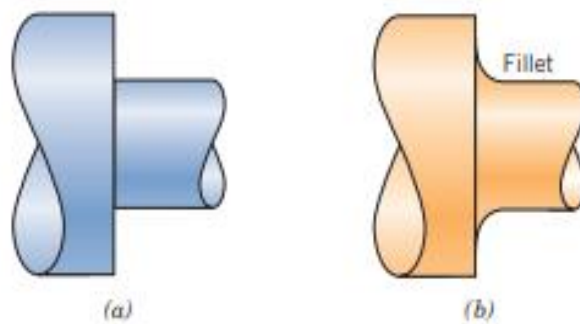
### **Design Factors:**

An important factor affecting a component's fatigue characteristics is its design. Any geometrical discontinuity, including keyways, threads, grooves, holes, and so on, can elevate stress and act as the starting point for fatigue fractures. As the discontinuity becomes more abrupt, the stress concentration rises. It is possible to reduce the risk of fatigue failure by avoiding such structural imperfections or by

altering the design to remove sudden contour changes that produce sharp corners. At the place where the diameter varies, for example, a rotating shaft would need rounded fillets with considerable radii of curvature. (Callister, & Rethwisch, 2018).

Figure 19.

*Example of how engineering design can reduce stress concentration. (a) sharp edges thus Poor design. (b) Good engineering design: fatigue life is improved through the addition of rounded fillet to a shaft as the point of change in cross section.*



### **Microstructure**

Mostly, engineering materials mechanical behavior and atimes, their physical properties are dependent on their microstructure. This is subjecting the material to microscopic study/observation, with the aid of an electron or optical microscopes. In alloys, microstructure is dependent/ characterized by the amount of phases available, the way they are arranged or distributed and thie proportions. Alloy heat treatment, alloying elements and concentrations are the determining variables to ascertain the microstructure of an alloy. (Callister, & Rethwisch, 2018).

### **Statement of the Problem**

Industries (aerospace, automotive, control, machine vitality, warming, ventilation, safety and security) have long recognized the need to enhance shape memory alloys' characteristics. CuAlNi SMA is stable at increased temperatures which make them relevant for applications with high temperatures over 100<sup>0</sup>C (Prasad, 2017). The alloys are cheap compared with NiTi alloys. They have ease of production (Lojen, 2005). They have little hysteresis and increased transformation

temperature as compared with other SMA (Saud, 2019), but CuAlNi SMA are brittle (Edwards, et al., 2019), fragile (Sellitto & Riccio, 2019), possess low exhaustion quality (Leal & Savi, 2018), are unsteady (Kaya, 2019) and are not suitable for numerous cyclic activities (Strittmatter, et al., 2019). The demerits of CuAlNi SMA have reduced their usage (Oliveira, et al., 2019; Yang, et al., 2019; Tian, et al., 2019). By refining the grains in the microstructure of CuAlNi SMA with the addition of fourth elements like Boron, Manganese etc. will help reduce the shortcomings associated with the alloy thereby making the commercial application increased (Vajpai, et al., 2011). An improvement was observed in the properties of CuAlNi SMA (Guniputi & Murigendrappa, 2018; Hussain, et al. 2019) due to grain growth and grain refinement by the alloying element (Zhu, et al., 2009). This research will focus on the improvement of fatigue and hardness properties of CuAlNi SMA through addition of graphene, due to its many advantages. In addition, Design Expert Software version 13.0, will be used to obtain multilinear model in terms of the coded factors for the accurate prediction of the fatigue life.

### **Purpose of the Study**

The aim of this investigation is to ascertain the impact of the inclusion of graphene as a fourth component to the Mechanical and Fatigue Properties of CuAlNi SMA. The specific objectives include:

1. The mechanical parameters, such as the CuAlNi SMA's hardness, to be determined.
2. Using graphene, the fourth element, to produce CuAlNiC and enhance the mechanical characteristics of the CuAlNi SMA.
3. To characterize the microstructure of CuAlNiC SMA produced with quaternary and CuAlNiC SMA without fourth element.
4. Examining the SMA fatigue behaviour of CuAlNi and CuAlNiC.
5. Evaluation of SMA fatigue behaviour of CuAlNi and CuAlNiC.
6. Application of Design Expert Software version 13.0, to predicting Factigue Life (FL) using MultiLinear Regression (MLR) model.

### **Research Questions**

1. Is the property of shape memory alloy affected by an alloying element?
2. Is there any failure problem associated with the cyclic operation of shape memory alloy?
3. Is there ways to solve failure problems affecting shape memory alloy?
4. Is there any way to make a type of shape memory alloy commercially available?

### **Significance of the Study**

CuAlNi SMA has ease of manufacture, are compatible with applications involving high temperatures and are cheaper compared with NiTi alloys. They are applicable in aerospace, automotive industries to mention few. CuAlNi SMA lack excellent mechanical properties and fatigue behaviours. In view to raising the mechanical properties and reduce the fatigue behaviours, alloying elements are added into the shape memory alloys (Williams, et al., 2011). Graphene possess high strength. It is very light and tough. The interesting properties of graphene if properly utilized as additive with CuAlNi shape memory alloys, is expected to increase alloy mechanical and fatigue properties.

This makes the findings extremely significant for the engineering field. It shows how the hardness and fatigue characteristics of CuAlNi SMA are affected by the inclusion of graphene. Using a quaternary element such as graphene, a model was created that can be used to investigate the fatigue life of Shape Memory Alloy. One advantage of the mathematical model generated for fatigue life is its equation's accessibility. This facilitates the perception of the influence of every input parameter on the alloy's fatigue life.

### **Definition of Terms**

EM – Empirical Modelling

FL – Fatigue Life

MLR - MultiLinear Regression

SMA - Shape Memory Alloy

SMP – Shape Memory Polymer

## CHAPTER II

### Literature Review

#### Theoretical Framework

SMA is polymorphic. This means that shape memory alloy may have two crystal structures/ phase while the phase transformations between them is the shape-memory effect. The austenite phase being one of the phases, has structure that exist at elevated temperatures as a body-centered cubic structure. This austenite phase transforms to a martensite phase upon cooling. This phase transformation is similar to those of iron-carbon system, i.e. it involves a shift of atom in an orderly manner, it's diffusionless, and "Ms" and "Mf", which are the start and finish transformation temperature. Also, the martensite twinned heavily. Migration of twin boundaries is responsible for martensite deformation, under an applied stress influence. Also, the deformed shape is retained at this temperature when the applied stress is removed. Lastly the material returns to its previous shape when heated. The described deformation-transformation cycle can be repeated for the material with a shape memory behaviour. The initial shape (i.e. shape designated to be remembered) is produced through heating to a temperature higher than  $A_f$  temperature (this makes austenite transformation to be completed). The material is then restrained, for a time sufficient enough, to the preferred memory shape. (Callister, & Rethwisch, 2018).

The deformation experienced by shape memory alloy is not completely plastic i.e. it's semipermanent, nor completely elastic, it is referred to as thermoelastic. This is as a result of nonpermanent nature of the deformation, when the deformed material is later heat-treated. The material highest recoverable deformation strains is around 8%. This makes it possible to vary the transformation temperature of different temperatures for shape memory alloys, adding other elements or altering the composition ratio of the shape memory alloy. (Callister, & Rethwisch, 2018).

#### Review of Previous Researches

In shape memory alloy systems, numerous additive alloying metal elements have been added to improve or change their functional and characteristic properties, such as achieving higher or lower martensitic transformation temperatures, improving ductility or strength, or improving shape recovery or superelasticity capabilities.

Shape memory alloys (SMAs), being among famous smart materials, are the subject of research. In SMA systems, additional materials can be added, even though metals are frequently the additive constituents. The most promising substitute for the better but more costly Ni-Ti SMAs is thought to be Cu-based SMAs.

Thus, researchers working in this field are also extremely interested in increasing the SMA properties of the Cu-based SMAs through various techniques (e.g., adding additional components, manufacturing them through other production processes, etc.).

It can be drawn from various literatures that the grains in the microstructure of CuAlNi SMA can be refined to reduce the demerits of the alloy and increase the commercial demand. This can be achieved by adding a quaternary element such as Manganese, Boron, Titanium, among others as alloying element (Hussain, et al., 2019; Guniputi & Murigendrappa, 2018; Zhu, et al. 2009; Vajpai, et al., 2001).

Miyakai et al. (1982) varied the different percentage constituents of Ni and Al in CuAlNi Shape Memory Alloys and observed changes both in the crack formation and propagation. They observed that with an increment of Ni and Al amount from 3.9 and 14% by weight to 4 and 14.2% by weight, this will result to formation of clear crack (Saud 2019; Miyazaki, et al., 1982). Wayman and Lee (1986) observed that stress concentration nucleated at boundaries of the grain is relieved due to addition of borride particle. Morris (1991) observed that the ductility of the CuAlNi Shape Memory Alloys is increased with boron addition. It was reported that the presence of boride particles to CuAlNi SMA changes the material failure mode from brittle to transgranular and intergranular (Saud, 2019). Xu et al. (2008) examined how beryllium affected CuAlNi SMA and observed that it improved the material's fatigue life. (Xu, et al. 2008; Xu, et al., 2011). From literatures reviewed, fourth element addition to CuAlNi SMA helps to improve the fatigue and mechanical properties. (Saud, 2019). Lastly, graphene has been used widely to increase the properties of metal matrix nanocomposites for many purposes, with respect to their superior electrical, mechanical and thermal usefulness. A study of the impact of reinforcing aluminium 7075 matrix with graphene (C) and beryllium (Be) through a stir casting method with fixed volume of beryl and different volume fractions of

graphene. They observed that the composite increases in strength with an increment in the volume fraction of the reinforcement as compared with that without reinforcement (Shanawaz, et al., 2019).

### ***Impact of Quaternary Element Addition to CuAlNi SMA***

Cu-Al-Ni SMAs are highly susceptible to the impacts of alloying elements, particularly the phase transformation temperature behaviour, which can alter the alloys' crystallographic characteristics and other factors. Cu-Al-Ni SMAs' shape memory effects hold promise as clever and intelligent engineering materials. In addition, compared to other shape memory alloys like NiTi SMAs, the low cost and ease of production have garnered a lot of interest. Here are some of the scientists' and researchers' studies of the domain and grain size changes in terms of microstructure effects, as well as the mechanical properties of Cu-Al-Ni SMAs on certain transformation parameters (due to the effects of alloying element additions).

The impacts of adding a fourth element to CuAlNi SMA from literatures reviewed are as follows:

#### **Impact of Beryllium (Be) Addition on CuAlNi SMA as a Fourth Element**

Beryllium helps to improve the fatigue life of CuAlNi SMA when added to the ternary (Xu, et al., 2011). Zhu (2009) reported an enhancement in the percentage elongation, bending rate and tensile strength of CuAlNi SMA with the inclusion of Beryllium.

#### **Impact of Boron (B) Addition on CuAlNi SMA as a Fourth Element**

Boron addition to CuAlNi SMA helps to reduce the stress concentration and improve the grains (Wayman & Lee 1986). The addition of boron to CuAlNi SMA changes the material failure mode from brittle to transgranular and intergranular (Saud, 2019). The tensile strength, hardness and yield strength were observed to improve by boron addition (MAaSG, 1992). Saud (2013) observed that the boride particles limited the interface movement thus ensuring the martensitic re-ordering stress to be rise.

#### **Impact of Carbon Nanotubes (CNTs) Addition on CuAlNi SMA as a Fourth Element**

The effects of introducing carbon nanotubes to CuAlNi SMA with (Cu–11.5 wt-%Al–4.5 wt-%Ni) were studied by Saud et al. (2004). They found that the addition increased shape recovery and improved fracture stress and strain.

#### **Impact of Chromium (Cr) Addition on CuAlNi SMA as a Fourth Element**

Zare and Ketabchi (2017) in their research observed that adding Cr to CuAlNi SMA embrittles the alloy and it reduces the SMA's hardness to fracture and tensile strength.

#### **Impact of Cobalt (Co) Addition on CuAlNi SMA as a Fourth Element**

Saud et al. (2015) carried out research on the impact of Cobalt (Co) as a quaternary on CuAlNi SMA. They concluded that adding 1.14% to CuAlNi SMA yielded an improvement in ductility, alloy transformation temperature including the shape memory recovery.

#### **Impact of Manganese (Mn) Addition on CuAlNi SMA as a Fourth Element**

Saud et al. (2014) carried out research on effect of manganese (Mn) on the mechanical properties of CuAlNi SMA as a quaternary. Varying Mn addition results in fluctuation in grain size. Other properties being influenced includes a decrease in corrosion rate, increase in stress-strain behaviour and improvement in shape memory effect when optimum amount of 0.7 wt.% Mn is added to CuAlNi SMA (Saud, et al., 2014).

#### **Impact of Niobium (Nb) Addition on CuAlNi SMA as a Fourth Element**

Gomes et al. (2008) investigated the impact of (Nb) on mechanical characteristics of CuAlNi SMA as a quaternary and concluded that it increased to rupture strain of the CuAlNi.

#### **Impact of Silver Nanoparticles (Ag) Addition on CuAlNi SMA as a Fourth Element**

The addition of silver nanoparticles to CuAlNi SMA increased the strain and stress due to fracture, including the alloy shape recovery (Saud, et al., 2014).

#### **Impact of Tantalum (Ta) Addition on CuAlNi SMA as a Fourth Element**

A study by Saud et al. (2017) investigated how the properties of CuAlNi SMA were affected by tantalum (Ta), as a quaternary. They noticed that the internal friction is

doubled with an increase in phase transformation and shape recovery (Saud, et al., 2017).

#### **Impact of Titanium (Ti) Addition on CuAlNi SMA as a Fourth Element**

Research on effect of adding Ti on the characteristics of CuAlNi SMA show an improvement in shape and strain recovery, including a rise in phase transformation temperature and grain refinement (YingCi, et al., 2017; Saud, et al., 2014).

#### **Impact of Vanadium (Va) Addition on CuAlNi SMA as a Fourth Element**

Vanadium addition to CuAlNi SMA helps to increase the rupture strain (Gomes, et al., 2008).

#### ***Fatigue behaviour of Shape Memory Alloy***

Understanding fatigue behaviour is crucial since many SMA applications call for the material to go through multiple cycles of deformation. Three distinct forms of failures/weariness that are significant for SMAs were found by Van Humbeeck.<sup>9</sup> The first is the typical fracture failure brought on by cycling under strains or stresses at a steady temperature. The second is modifications to the material's characteristics, like transformation hysteresis and transformation temperatures brought on by thermal cycling during the transformation. The third is the SME's deterioration as a result of thermal or mechanical cycling.

Rachinger's work seems to be the first to be published on fatigue in SMAs. (Van Humbeeck, 1991). He discovered a fatigue life of 53,000 cycles after conducting a single test on a single crystal of Cu-Al-Ni alloy in plane bending with surface strain limits of  $\pm 2\%$ . Most materials would break in 50 cycles or less under such circumstances, he said. Then, according to Buehler and Wang, "a specimen [of Ni-Ti] could be loaded up to about four times its yield strength, with significant specimen deflection during testing, and still run 107 cycles without failure." (Rachinger, 1957). Since then, a lot of research has been done on alloys based on copper and Ni-Ti.

The behaviour of Ni-Ti alloys is examined first since they are the most commercially significant SMAs. Cu-Zn-Al alloys based on SMAs have been utilized commercially, while Cu-Al-Ni alloys have been developed but not yet put on the market. Numerous studies have been conducted on the fatigue behaviour of single

crystals, especially for copper alloys, even though the focus of this article is on polycrystalline materials. (Sade, & Ahlers, 1985).

### **Fatigue Failure of Nitinol-Titanium (Ni-Ti) Shape Memory Alloy**

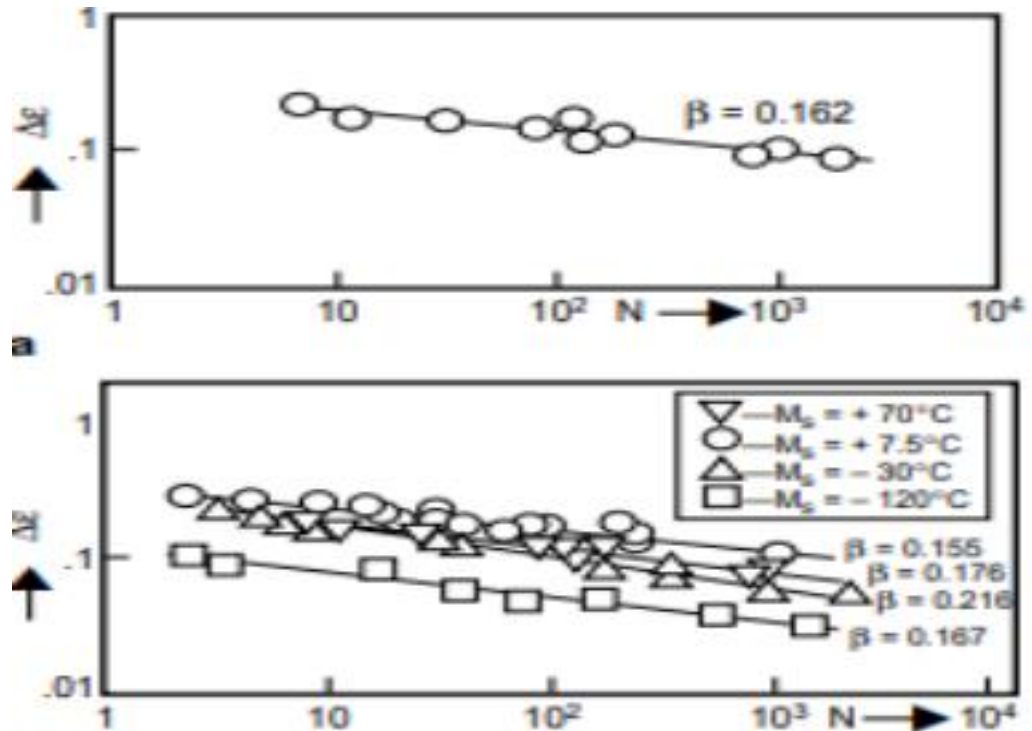
The fatigue behaviour of Ni-Ti was further studied by Melton and Mercier, (Melton, & Mercier, 1979). McNichols et al., (1981), Tobushi et al., (1981), Miyazaki et al., (1999) and Tablani et al., (1999) in addition to Buehler and Wang's early work. In their studies, Melton and Mercier utilized rods that ranged in diameter from 3 to 8 mm; Tablani et al. employed tubes that had an internal diameter of 1 mm and an outside diameter of 1.3 mm.

By making small compositional adjustments, Melton and Mercier produced specimens with  $M_s$  temperatures ranging from  $-120^{\circ}\text{C}$  to  $70^{\circ}\text{C}$ . Each experiment was conducted at ambient temperature. Tensile stress-strain curves for temperatures ranging from  $-30^{\circ}\text{C}$  to  $70^{\circ}\text{C}$  were obtained for  $M_s$ . Due to the development of the stress-induced martensite, the stress-strain curves for the originally austenitic specimens with  $M_s = -30^{\circ}\text{C}$  and  $10^{\circ}\text{C}$  displayed plateaus of 4% to 6%. The stress required to form martensite increases with the distance between the test temperature and  $M_s$  (if the test temperature is greater than  $M_s$ ). With  $M_s = 70^{\circ}\text{C}$ , the initially martensitic material experiences considerable pressures due to reorientations of the thermally formed martensite platelets.

Using a minimum to maximum stress ratio (R) of -1, Figure 10 displays a stress-fatigue life curve (S-N) for the same three alloys under controlled-stress amplitudes. The Figure 20 displays the results of fatigue testing conducted at constant strain amplitudes.

Figure 20.

*Ni-Ti SMA stress-Fatigue life curve (Melton, & Mercier, 1979).*



### Fatigue Failure of Cu-Zn-Al Shape Memory Alloy

Several studies have investigated the fatigue behaviour of polycrystalline Cu-Zn-Al alloys, including Melton and Mercier (Melton, & Mercier, 1979), Delaey et al. (1978), Janssen et al. (1982), Oshima, & Yoshida, (Oshima, & Yoshida), and Thumann and Hornbogen, (Thumann, & Hornbogen, 1988). In addition to Brown's study on polycrystalline Cu-Zn-Sn (Brown, 1982), Sade et al. research on Cu-Zn-Al single crystals. (Sade, & Ahlers, 1985), and Brown's study of single crystal Cu-Zn-Sn alloy has also been conducted.

The strain obtained for Nitinol-Titanium (Ni-Ti) were larger compare with those obtained for Cu-Zn-Al. The differences between Ni-Ti and Cu-Zn-Al alloys were as a result of the platelet size and grain size. Cu alloys possess grain size about ten times larger than Ni-Ti alloys. The martensite platelet sizes of Cu alloys are about 100 times lager than those of Ni-Ti alloys.

## **Use of Computer Software to Analyse Fatigue of SMA**

### **Empirical Modelling**

This approach is a situated computer-based modelling. Empirical Modelling (EM) is dependent upon an unconventional method to describing a phenomena that based on observation rather than those based on object in nature. This method is intended at accounting for phenomena with respect to agents activities based on state-change. Activities of agents and interrelations among agents are described as observables changes. The interactions among observables in which changes in one observable affects the other in a way that is indivisible, conceptually is modelled as a dependency. (Yih, 2001)

The idea of agent, dependency and observable are rudiment to Empirical Modelling. To certain extent, these ideas are used in computing practices of today, An example is the 'spreadsheets', 'agent-based systems', and 'the java package observers java.util'. The special nature of interationship among the referent, the computer model(artefact) and the modeller differentiates Empirical Modelling from the use of ideas relating to dependency, agency, and observation. The modeller's knowledge of the referent with respect to experimentation and observation is specifically, the artefact. (Yih, 2001).

The concept of agents, dependency and observable is used in Empirical Method. Although they may involve agency, observation, and dependency in some way, it will be appropriate in this thesis to refer to modelling techniques other than EM as "conventional modelling methods" and to view them as fundamentally framed in a "classical" ontological framework. Since typical modelling methodologies for software system development do not result in the identification and embodiment of agency and dependency in the way that EM does, this classification is uncontroversial. (Yih, 2001).

The word 'empirical' means that the Empirical Model has a principles dependent upon experimentation and observation. The approach used here is modelling the world based on experiences, i.e. modelling from experiences of others (i.e. the computer model). In reality, 'empirical modelling' emanate as a result of making distinction between experiential models we obtained based on definitive scripts and conventional mathematical modelling. (Yih, 2001).

An overview of our modeling process is provided below: Due to EM's state-based and observation-oriented nature, all of the variables are assumed to represent the observed referent's current state. To illustrate the observables of the real-world subject, EM also provides a visual metaphor that the modeller can directly edit. Stated differently, the model is constructed as a metaphorical representation of the subject that is consistent with the modeller's opinion. Traditional confined modeling cannot convey the dependency between observables through spreadsheet-like definitions, which EM does in addition to being definition-based. (Yih, 2001).

In an area where the user may not fully comprehend the subject, EM focuses on creating artifacts (computer-based representations) for experimentation and engagement. It is based on observation and experience since we can analyze the subject and the domain by figuring out how our experiences in that area are structured. Additionally, Empirical Modeling's analysis and modeling are experiential rather than preconceived, which puts computer modeling closer to users and maintains the openness of the artifacts that represent our real-world experiences (Yih, 2001).

### **Empirical Modelling Concepts and Principles (Yih, 2001).**

Observables, dependencies between observables, and agents operating by adding or altering observables and dependencies are the three main ideas of EM. The following is a summary of these concepts' definitions and traits:

- An observable is a perceptible and identifiable component of the domain whose present value in the model reflects the referent's state. There are two types of observables: physical and abstract. Only when referring to an agent's perception and interaction with a subject or model feature can the observable be meaningful.
- A relationship between observables that might be interpreted differently by various agents is called dependence. Other observables, also known as the dependents of that observable, will also vary in value in a predictable manner once the value of one observable changes. The observable and its dependents undergo indivisible changes. In this context, an agent is a state-changing entity, which is a family of observables with the ability to alter the states of dependencies and observables. The term "agent" in empirical modelling can refer to any part of the topic that is thought to be in

charge of state changes, not just humans. For the state change, the agency stands in for the agent's privilege or responsibility.

### **Related Research**

It has been established that metals' thermomechanical and structural qualities can be enhanced by nanoparticles without compromising their malleability (saud, 2015). Thermal stability, strength, stiffness, plasticity, corrosion resistance, and durability at high temperatures can all be altered or enhanced by adding nanoparticles to metals and alloys (lester, 2015; chen, 2015). Reports on using carbon and carbon nanoparticles to improve SMAs are scarce in the literature. The shape recovery ratio, martensitic microstructure, phase transformation temperatures, and associated thermodynamic parameters were all significantly impacted by the addition of carbon nanotubes (CNTs), according to Saud et al. (2014) improvement of a CuAlNi SMA with a little amount of CNTs (Prendota, 2018).

Research on graphene's effect on CuAlNi Shape Memory Alloy's fatigue life is lacking. A close work from literatures is that of Karaduman and Canbay (2021) where they added small amount of 5nm graphene nanoplatelets to CuAlNi SMA through arc melting method. They observed that the alloy transformation temperature and other mechanical properties can be controlled however with no report on the failure of the alloy.

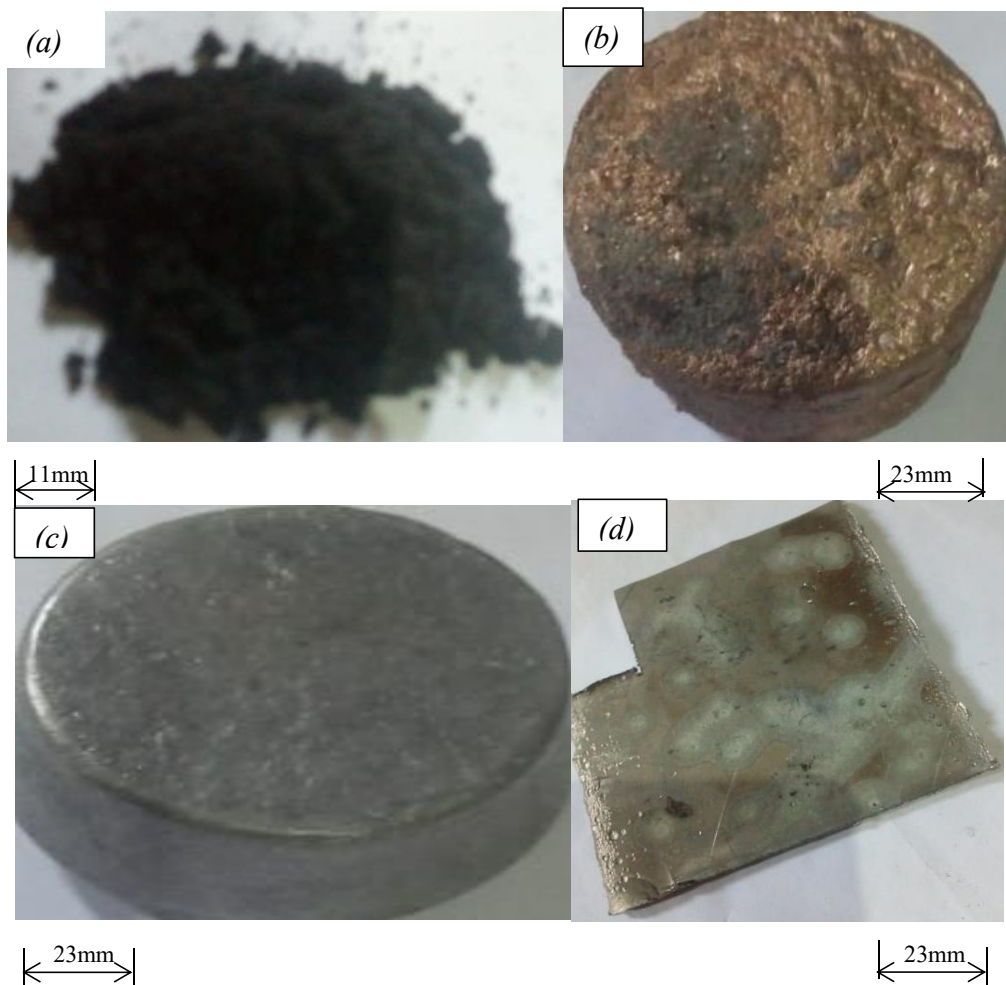
## CHAPTER III

### Methodology

The graphene (C) enhanced CuAlNiC shape memory alloy was created using graphene nanoplatelets and powders of 99.9% pure Cu, Al, and Ni metal components. It has an unparalleled composition of copper, aluminium, and nickel. Copper (Cu), Nickel (Ni) and Aluminium (Al) of good quality, in commercial amount respectively, were purchased from Oshogbo, South West Nigeria. 5nm size graphene nanoplatelet of high purity with  $170 \text{ m}^2 / \text{g}$  specific weight,  $30\mu\text{m}$  diameter was purchased from Turkey (Nanografi Nanotechnology Company). After combining and balancing each powder according to the alloy composition, the powder mixture was compressed and palletized.

Figure 21.

*Materials used (a) Graphene (b) Copper (c) Aluminium (d) Nickel.*



### ***Determination of Mass Constituent of the Elements***

From Literatures, the mass fraction of each element for a SMA includes: Cu= 0.843; Al= 0.119; Ni= 0.038. And Densities of Cu=8.96g/cm<sup>3</sup>; Al=2.7g/cm<sup>3</sup>; Ni= 8.9 g/cm<sup>3</sup>. The samples were prepared using the principle of rule of mixtures.

$$\frac{1}{\rho(\text{Cu-Al-Ni})} = \frac{\% \text{Cu}}{\rho \text{Cu}} + \frac{\% \text{Al}}{\rho \text{Al}} + \frac{\% \text{Ni}}{\rho \text{Ni}} \quad (2)$$

Using equation (2),

$$\rho(\text{Cu - Al - Ni}) = 7.022 \text{ g/cm}^3$$

$$\text{Volume of rod to form from mould} = A = \pi r^2 h. r= 1\text{cm}; h=25\text{cm}; \text{Vol.} = 78.55 \text{ cm}^3$$

**SAMPLE A** (Control Sample).

$$\text{Mass of alloy} = \text{Density} \times \text{Volume} = 551.507 \text{ g}$$

$$\text{Mass of element in alloy} = \% \text{ of element} \times \text{Mass of SMA.}$$

$$\text{Cu} = 464.92 \text{ g}; \text{Al} = 65.63 \text{ g}$$

$$\text{Ni} = 20.957 \text{ g}$$

Graphene was used in SAMPLES B, C, and D at 0.15%, 0.3%, and 0.45%, respectively, by the following formulas (3) and (4).

$$\frac{1}{\rho(\text{SMA-Gr})} = \frac{\% \text{SMA}}{\rho \text{SMA}} + \frac{\% \text{Gr}}{\rho \text{Gr}} \quad (3)$$

$$\text{Mass of element in alloy} = \% \text{ of element} \times \text{Mass of SMA} \quad (4)$$

**SAMPLE B**

$$\rho(\text{SMA - Gr}) = 7.0947 \text{ g/cm}^3$$

$$\text{Mass of (SMA - Gr)} = \rho \times V = 557.2887 \text{ g}$$

$$\text{Mass of Gr} = 0.0015 \times 557.2887 = 0.8359\text{g};$$

$$\text{Mass of SMA} = 557.2887 - 0.8359 = 556.4528\text{g}$$

$$\text{Mass of Element} = \% \text{Element} \times \text{Mass of SMA}; \text{Cu}=469.0897\text{g}; \text{Al}=66.218\text{g};$$

$$\text{Ni}=21.145\text{g}$$

**SAMPLE C**

$$\rho(\text{SMA - Gr}) = 6.977 \text{ g/cm}^3$$

$$\text{Mass of (SMA - Gr)} = \rho \times V = 548.0594 \text{ g}$$

$$\text{Mass of Gr} = 0.003 \times 548.0594 = 1.644\text{g}$$

$$\text{Mass of SMA} = 548.0594 - 1.644 = 546.415\text{g}$$

$$\text{Mass of Element} = \% \text{Element} \times \text{Mass of SMA}; \text{Cu}=460.629\text{g}; \text{Al}=65.023\text{g};$$

$$\text{Ni}=20.764\text{g}$$

## **SAMPLE D**

$$\rho(SMA - Gr) = 6.955 \text{ g/cm}^3$$

$$\text{Mass of } (SMA - Gr) = \rho \times V = 564.35 \text{ g}$$

$$\text{Mass of Gr} = 0.0045 \times 564.35 = 2.46 \text{ g}$$

$$\text{Mass of SMA} = 564.35 - 2.46 = 543.89 \text{ g}$$

$$\text{Mass of Element} = \% \text{Element} \times \text{Mass of SMA}; \text{Cu}=458.5 \text{ g}; \text{Al}=64.72 \text{ g}; \text{Ni}=20.67 \text{ g}$$

### ***Methods of making SMA***

The majority of studies have created Cu-based SMAs using either liquid or powder metallurgical methods, unless single crystals have been generated. When growing single crystals, the Bridgeman approach was applied. An induction furnace is typically utilised in the more widely utilised liquid metallurgical approach, where melting is done in an inert environment such as argon (Ar) or under vacuum. Nevertheless, there are also occasional accounts of resistance heating furnaces being used. Since the expected SM properties and transformation temperatures are largely determined by the chemical composition, the metals utilised often have high purity levels. All researchers used electrolytic grade metallic raw materials to manufacture alloy ingots, which correspond to 99.91 purity standards. (Dasgupta, 2014).

A common method for creating Cu-based SMAs with the greatest number of required characteristics is powder metallurgy, PM. Since PM offers greater control over composition and grain size, it is preferable for producing near net shape alloy products. Premixed elemental powder mixes in the ratio of the intended alloy are utilised when creating alloys via the powder metallurgy process. The particles' purity and median size are carefully chosen. To lessen surface oxides, elemental Cu and Ni powders are typically annealed for 30 minutes at 600 °C in an H<sub>2</sub> environment. Ball milling is used to turn Cu, Al, and Ni elemental powder mixtures into prealloyed powders; high energy planetary ball milling is replacing standard ball milling in order to get superior characteristics. The final particle size and location are influenced by the milling time. The mixture of elemental powders was cold-compressed in dies. Typically, the green compacts were sintered in a stepwise

fashion, ideally in an environment of hydrogen. Nonetheless, SMAs are always utilized in the wire or sheet form, which is produced from cast alloys using either liquid metallurgy or powder metallurgy, as was previously mentioned. The following techniques are applied to create these shapes.

The sheet form Homogenized alloys are formed into thin plates by hot forging and then cold rolling. After that, heat was applied to the plates to reduce the stress caused by rolling, drawing, and forging. They differ because researchers optimized the heat treatment procedures based on the actual alloy composition. The majority of researchers, however, recommend 850 °C for up to 24 hours for early homogenization and stress relief, but 6–8 hours is a far shorter time frame. A certain reduction ratio, which changes depending on the machine and the researcher's needs, is achieved by cold rolling in phases down to the necessary thickness; the range was discovered to be between 30 and 88 pct. between the several rolling processes, the material undergoes 900 seconds of solution treatment at 1173 K.

#### **Preparation of the CuAlNi and CuAlNiC Shape Memory Alloy**

The weight of each sample was determined separately with a mettler weighing balance of 0.02 g precision for accuracy. The alloy was created using the casting method of metal formation. Sand casting is employed due to its ease of usage, inexpensive tooling costs, and the ability to cast nearly any material with no restrictions on size, shape, or weight. (Callister, & Rethwisch, 2018). The sand casting process's fundamental steps are: (Ganesh, 2020).

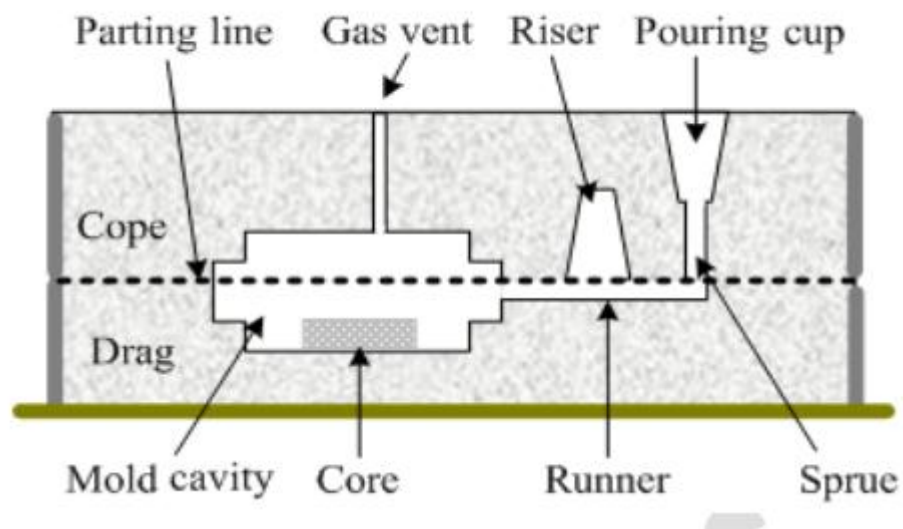
1. Choose the right sand to make a sand mold and manage the casting quality.
2. To create a mold cavity, place a metal or wood pattern in the sand.
3. To make the pattern more stable, lightly pound the sand.
4. Take the pattern out.
5. Pour molten metal into the mold cavity.
6. Let the molten material cool.
7. Remove the casting product by breaking the sand mold.

Sand casting is typically a cost-effective method for producing small batches, but it has a few drawbacks, including a small coarse finish, wide tolerances, and the need for some polishing.

The grade of the green sand used to make the mold and its consistency determine the quality of the sand casting. Figure 22 schematically depicts two sand mold components, often known as cope and drag sand molds. Once the molten metal has passed through the down sprue, runner, and gate, it is poured via the pouring cup and fills the mold cavity. The term "core" describes the loose parts that are inserted into the mold cavity to produce internal holes or an exposed area. In order to compensate for volumetric shrinkage during solidification, the riser serves as a reservoir or container for surplus molten metal, allowing for extra filling of the mold cavity. The process of sand casting offers a number of benefits. It can be used on any kind of metal. Very intricate shapes can be cast using this inexpensive equipment. Sand castings, however, have subpar surface polish and dimensional accuracy. (Callister, & Rethwisch, 2018; Ganesh, 2020).

Figure 22.

*Schematic of sand molding*



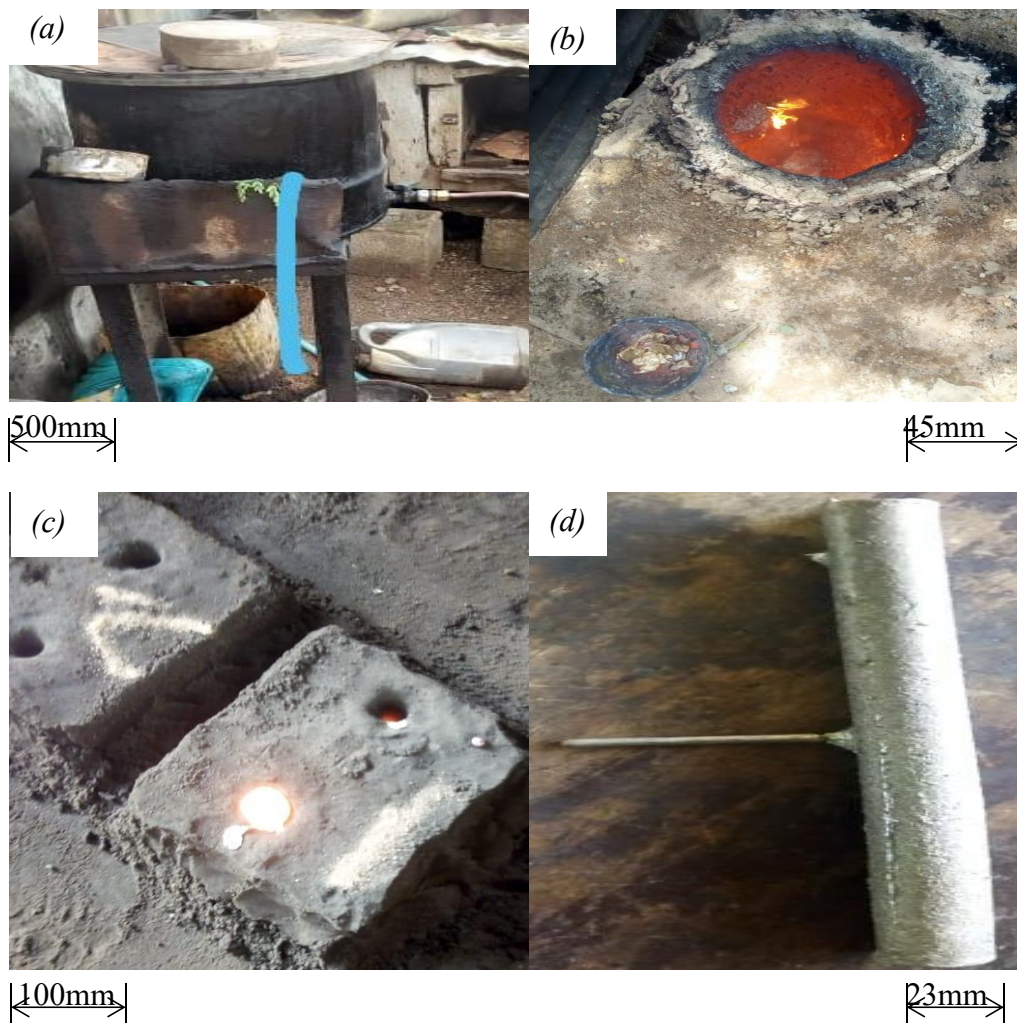
Nickel with the highest melting point was charged first into the furnace at about 1400°C followed by aluminium. The ingot was stirred for homogeneity. Oxidation was prevented through the use of argon gas to shield the surrounding atmospheric air.

After that, air was used to chill the ingot. There are four distinct specimens (A, B, C, and D). where then produced from it. Sample A has no graphene (control sample). Graphene content of samples B, sample C and sample D are 0.15%, 0.3%, 0.45%

respectively. These percentages of graphene were added to the ingot in the furnace at 1400°C. Consequently, samples A (100 wt.%, SMA, 0% C), B (99.5 wt.%, SMA, 0.5% C), C (99.7 wt.%, SMA, 0.3% C), and D (99.55 wt.%, SMA, 0.45% C) were developed, where C represents graphene (an allotrope of carbon) other than diamond. The molten alloys were then poured into a 1 cm diameter mould, see Figure 23, with a cooling at room temperature. Produced alloy in rod form were removed from the mould and then heated to about 500°C followed by air cooling.

Figure 23.

*Alloy casting (a) Pit Furnace (b) Crucible Pot containing metal to be melted (c) Mould (d) Casted Alloy*



***Mechanical Testing of Samples.*** (HR150 Manual).

An HR-150A Rockwell Apparatus with a diamond indenter Kgf 150 was used for the hardness test for samples A, sample B, sample C, and sample D.

Rockwell hardness tester of Model HR-150A the state superior product, silver award, for three time in succession. The tester has wide usage for testing the Rockwell hardness quenched steels, hard alloy, and unquenched steels in institutions of researches, factories, mines and universities.

**Principle of Test**

The Rockwell hardness test is to use diamond cone indenter dent the surface of the specimen in two steps as described in figure 24. This indentation will also be return for some time. After the applied test force is removed, the depth helps to measure the preliminary test force. The value of the Rockwell hardness is then estimated through the formula (1) . The values for h, S and constant, N can be found in Table 5.

Rockwell hardness value =  $N - h/S$  ..... (1)

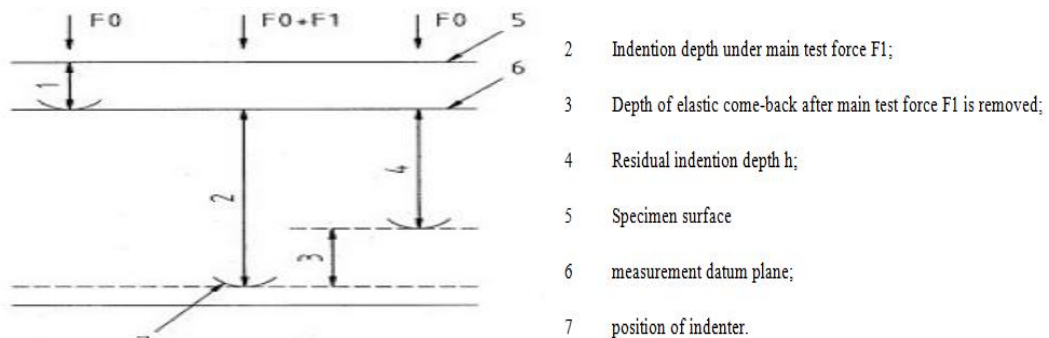
Table 5.

*Rockwell test descriptions with symbols.*

Symbols	Descriptions	Units
F0	Preliminary test force	N
F1	Main test force	N
F	Total test force	N
S	Unit of given scale	mm
N	Hardness value of given scale	
h	Residual indentation depth under preliminary test force after main test force is removed	mm
HRA	Rockwell hardness = $100 - h/0.002$	
HRC		
HRB	Rockwell hardness = $130 - h/0.002$	

Figure 24.

*Rockwell hardness Test Principle.*



In Figure 24, the depth of indentation under preliminary investigation or test force  $F_0$ ;

- 2 Indentation depth under main test force  $F_1$ ;
- 3 Depth of elastic come-back after main test force  $F_1$  is removed;
- 4 Residual indentation depth  $h$ ;
- 5 Specimen surface
- 6 measurement datum plane;
- 7 position of indenter.

Example: 59 HRC means that Rockwell hardness determined by scale C is 59.

### ***Application range***

For Rockwell hardness, the values of hardness can be represented scales like A, B and C, as for hardness range and specimen size, different loads and indenters can be chosen. The indenters, K values, indenters, with the different applications are shown in Table 6.

Table 6.

*Rockwell Hardness C scale.*

Scale	Indenter (mm)	Test force (kg)			Constant	Application examples
		$F_0$	$F_1$	F	N	
A	Diamond cone indenter	10	50	60	100	Hard metal and alloy
B	Steel ball ( $\phi$ 1.588) indenter	10	90	100	130	Non-ferrous and soft metal
C	Diamond cone indenter	10	140	150	100	Structural and tool steel

Table 7.

*Schematic Diagram of Overall Dimensions used in .Rockwell test.*

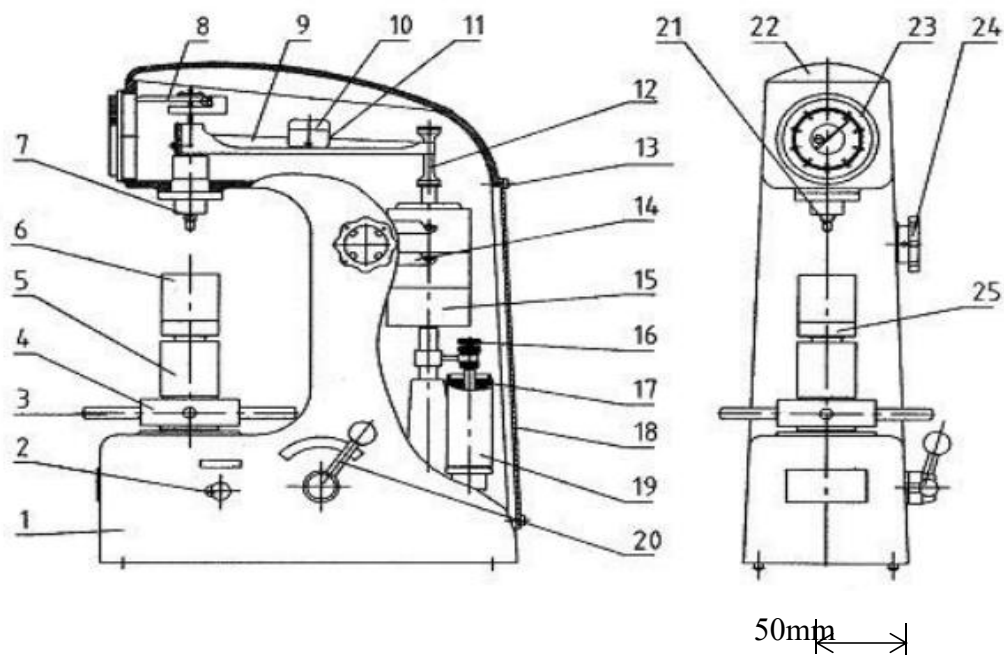
Scale	Range of hardness	Readings allowance
A	20HRA < ~ <= 75HRA	$\pm 2$ HRA
	75HRA < ~ <= 88HRA	$\pm 1.5$ HRA
B	20HRB < ~ <= 45HRB	$\pm 4$ HRB
	45HRB < ~ <= 80HRB	$\pm 3$ HRB
	80HRB < ~ <= 100HRB	$\pm 2$ HRB
C	20HRC < ~ <= 70HRC	$\pm 1.5$ HRC

### Descriptions of Mechanism Parts

The tester is composed of the following as seen in Figure 25.

Figure 25.

Schematic parts diagram.



1. machine body
2. loading handle
3. elevation handle
4. hand wheel
5. elevating screw rod sleeve (elevating screw rod inside)
6. specimen to be tested
7. main shaft
8. smaller lever
9. larger lever
10. adjustment block
11. position mark
12. hoist ring
13. screw
14. weight changeover support bracket
15. weight
16. oil needle
17. oil carpet
18. rear cover
19. buffer
20. unloading handle
21. indenter
22. top cover
23. indication dial gauge
24. load changeover handle
25. Worktable.

The weight and lever applied the test force applied to the main shaft. i.e.the buffer helps the indenter to penetrates deep the surface of the specimen with the larger level applying the load. The main shafts generates the vertical displacement, at exact time the indenter presses upon the specimen. This is transmitted to part number 6 i.e. the reading device, from which the result of hardness is shown with the measurement lever.

### Normal Operation

#### Prior to test:

Choose scale type based on the specimen. The current test operation uses scale C to test with indenter with a diamond cone. The test force is up to 150kgf.

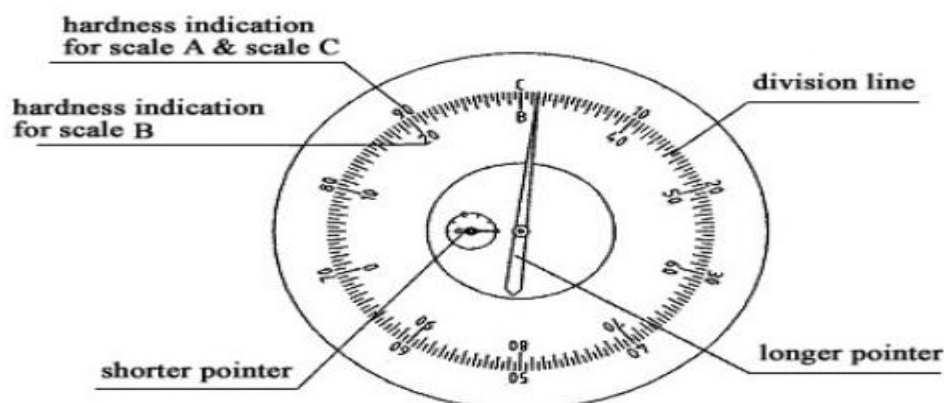
1. Preparation before the normal operation: Firstly, study each parts of the dial gauge indicator functions; This includes the division lines, longer pointer, hardness readings, shorter pointer, among others. (see Figure 26).

- Hardness indications are the black division. The inner ring red digits are used for scale B while scale A and C uses the outer ring black digits. Changing weights and indenter helps to compose different scales. (see Table 6).
- The preliminary test force is indicated by the shorter pointer.
- The tested specimen harness result is read from the longer pointer.

B and C are scale symbols. The zero point of scale C or A is letter C position. For scale B, the position of B (letter) refer to the division value 30. See Figure 26.

Figure 26.

*Indication dial gauge schematic diagram*



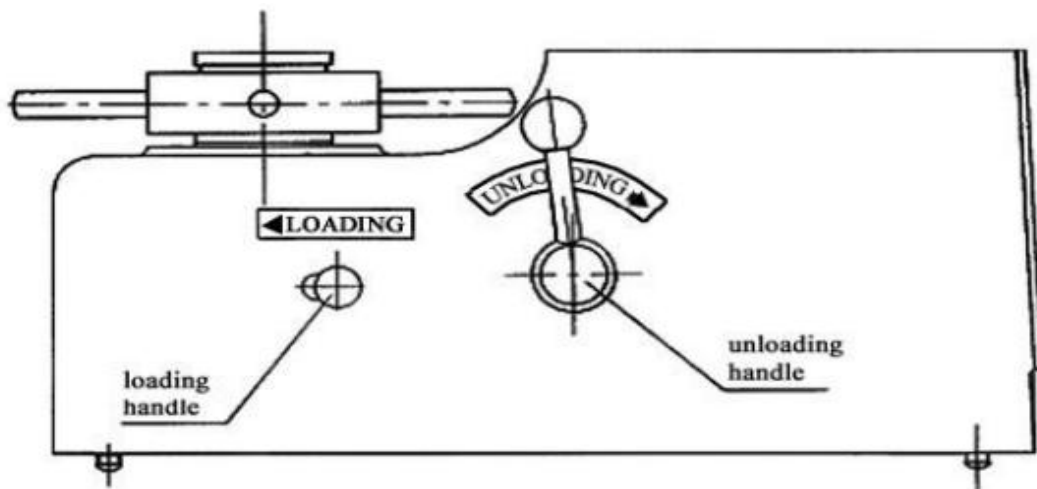
23mm

1) Main test force loading ratio should be regulated.

a. Ensure the unloading handle (part 20) is positioned at the unloading point. Else, slowly turn it there, for few seconds. The unloading direction is displayed on the label of unloading. (see Figure 27).

Figure 27.

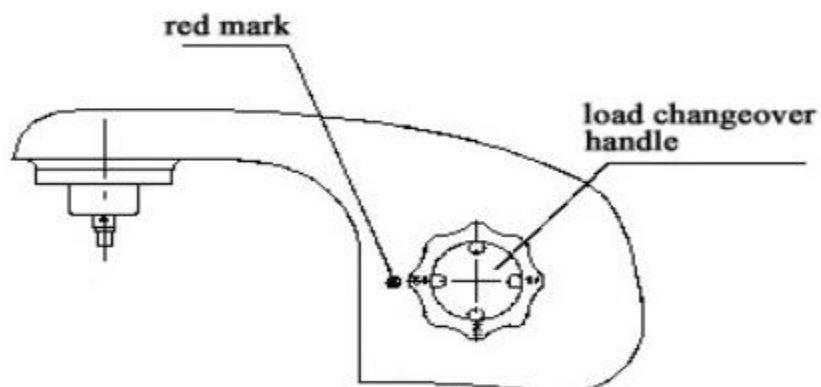
*Handles of Loading and unloading.*



b. load changeover handle should be turned (part 24) to 150kgf position and also ensure that the red mark aligns with 150 (number). (see figure 28).

Figure 28.

*Selection of test force.*

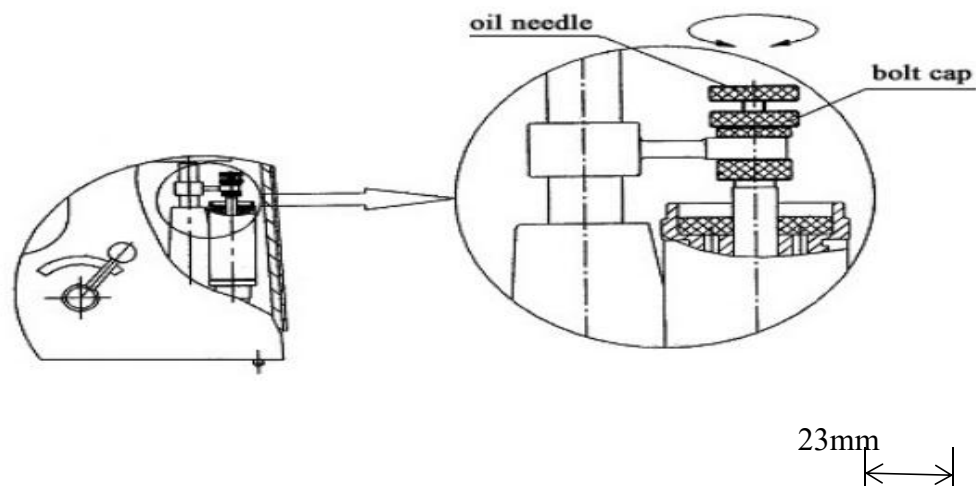


50mm

- c. 40~50HRC standard hardness block should be placed on the worktable.
- d. The hand wheel (part 4) should be turned so as the indenter be lift by the hardness block till the red mark is being pointer by the shorter pointer. Thus, application of the preliminary test force has been done.
- e. The loading handle (2) should be pulled regarding loading label, loading direction. This should be done slowly to the limit position, along the machine body front (say for 4 seconds) and the main test force has been then applied (Figure 27).
- f. Eyes should be maintained on the dial guage of the longer pointer. Ensure it runs for about 4 to 8 seconds before stopping. Else, it should be regulated through the use of oil needle, by: Firstly, loosening the buffer bolt cap (Figure 29), then slightly turn oil needle. These steps should be repeated till everything is normal, then bolt cap should be tighten.

Figure 29.

*Oil needle Regulation.*



### **Test force selection**

The selected test force number should points to the red mark by turning the changeover load (see Figure 28).

### **Indenter installation (Figure 30)**

- a. Put the indenter on, slowly tighten it so not to fall down.

- b. The standard block should be placed on the worktable.
- c. Apply the preliminary test force by turning the hand wheel.
- d. Apply to the indenter the load test force by pulling the loading handle towards the left. (see Figure 27).
- e. By tightening the screw, the installation is complete.

Figure 30.

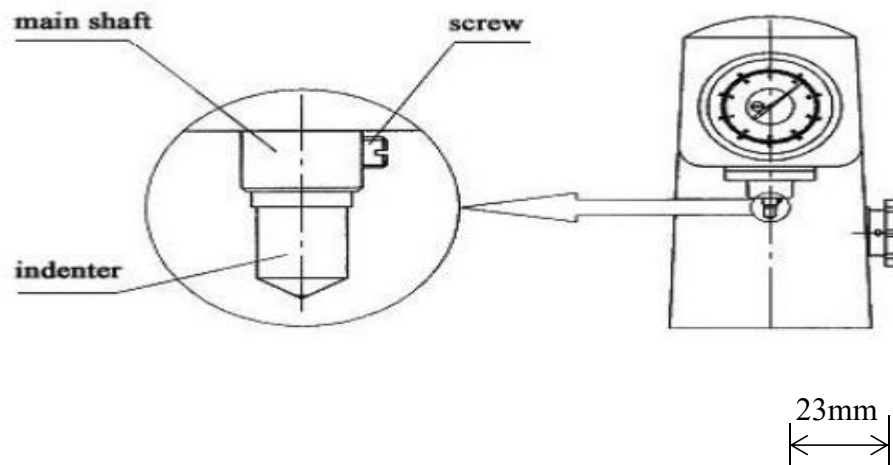
*Indenter Installation*

Figure 31.

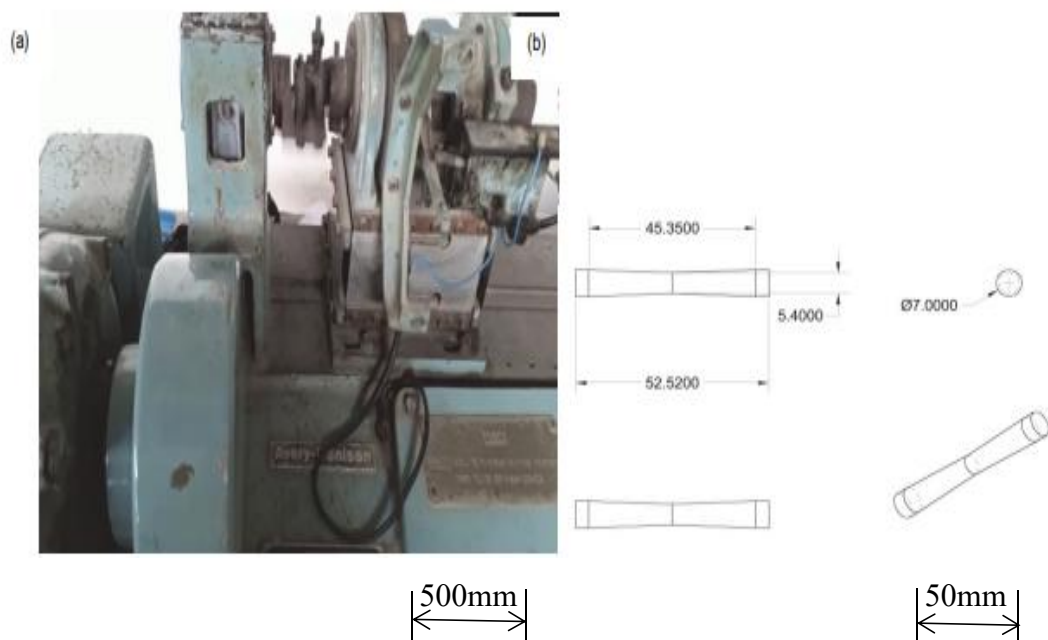
*Rockwell Hardness Testing*

### *Fatigue Testing of Samples*

The reduction in resistance offered by a material to a fluctuating stress is a phenomenon referred to as fatigue failure (Bhandari, 2016; Ugural & Fenster, 2012). Fatigue test is determined with the application of reversal stresses of known value to a material (Obiukwu, et al., 2015). The applied reversed stresses may have the same stress value in both directions. This is useful as it gives the stress amount a test piece can sustain before eventual failure in service (Callister, & Rethwisch, 2018). The Fatigue Testing Machine used to perform the fatigue test is the Avery Dennison 7305 (Figure 32 (a)). The machine specification (Figure 32 (b)). was used to further produce the specimens to four samples each i.e. four for specimen A, B, C and D of the standards specimens of the used fatigue testing machine. Thus a total of sixteen samples was subjected to fatigue test. The load was applied as bending moment. This was applied at the tail of the specimen with the aid of an oscillating spindle through the use of a crank, eccentrics and connecting rod. Number of cycles. The specimen could sustained before failure was read from the revolution counter. The fracture of the specimen stops the machine operation.

Figure 32.

*(a) Machine Specimen specifications (b) Avery Denison Fatigue Testing Machine,*



The measured bending moments aids in calculating the applied stress using the following relationships. (Obiukwu, et al., 2015).

To apply the bending moment, the stair case method was used (Obiukwu et al., 2015). Using this procedure, a fixed amount of bending moment was applied and subsequently raised. This is the value of the bending moment test for the next sample.

***Calculation of the applied stress from the measured bending moments***

$$\sigma = \frac{M_{max}}{W} ; \quad (5)$$

$$\text{From the relations: } \sigma = \text{Stress} = \frac{M_{max}}{W} \quad (6)$$

$M_{max}$  = Bending Moment Value Measured by Machine (kgfcm)

$$\text{Modulus} = W = \frac{\pi d^3}{32} = \frac{\pi(0.0054)^3}{32} = 1.545899 \times 10^{-8} \text{m}^3$$

Where: Diameter (d) = 5.4 mm = 0.0054m; Gauge Length (G) = 45.35mm

**SAMPLE A (Control Sample).**

$M_{max} = 65 \text{kgfcm}$

$$\sigma = \frac{M_{max}}{W} = \text{Stress} = 412.31 \text{ MPa}$$

$M_{max} = 130 \text{kgfcm}$

$$\sigma = \frac{M_{max}}{W} = \text{Stress} = 824.62 \text{ MPa}$$

$M_{max} = 195 \text{kgfcm}$

$$\sigma = \frac{M_{max}}{W} = \text{Stress} = 1236.94 \text{ MPa}$$

$M_{max} = 260 \text{kgfcm}$

$$\sigma = \frac{M_{max}}{W} = \text{Stress} = 1649.25 \text{ MPa}$$

**SAMPLE B**

$M_{max} = 65 \text{kgfcm}$

$$\sigma = \frac{M_{max}}{W} = \text{Stress} = 412.31 \text{ MPa}$$

$M_{max} = 130 \text{kgfcm}$

$$\sigma = \frac{M_{max}}{W} = \text{Stress} = 824.62 \text{ MPa}$$

$$M_{max} = 195\text{kgfcm}$$

$$\sigma = \frac{M_{max}}{W} = \text{Stress} = 1236.94 \text{ MPa}$$

$$M_{max} = 260\text{kgfcm}$$

$$\sigma = \frac{M_{max}}{W} = \text{Stress} = 1649.25 \text{ MPa}$$

### **SAMPLE C**

$$M_{max} = 65\text{kgfcm}$$

$$\sigma = \frac{M_{max}}{W} = \text{Stress} = 412.31 \text{ MPa}$$

$$M_{max} = 130\text{kgfcm}$$

$$\sigma = \frac{M_{max}}{W} = \text{Stress} = 824.62 \text{ MPa}$$

$$M_{max} = 195\text{kgfcm}$$

$$\sigma = \frac{M_{max}}{W} = \text{Stress} = 1236.94 \text{ MP}$$

$$M_{max} = 260\text{kgfcm}$$

$$\sigma = \frac{M_{max}}{W} = \text{Stress} = 1649.25 \text{ MPa}$$

### **SAMPLE D**

$$M_{max} = 65\text{kgfcm}$$

$$\sigma = \frac{M_{max}}{W} = \text{Stress} = 412.31 \text{ MPa}$$

$$M_{max} = 130\text{kgfcm}$$

$$\sigma = \frac{M_{max}}{W} = \text{Stress} = 824.62 \text{ MPa}$$

$$M_{max} = 195\text{kgfcm}$$

$$\sigma = \frac{M_{max}}{W} = \text{Stress} = 1236.94 \text{ MPa}$$

$$M_{max} = 260\text{kgfcm}$$

$$\sigma = \frac{M_{max}}{W} = \text{Stress} = 1649.25 \text{ MPa}$$

### **Microstructural Investigation**

Specimen A, B, C and D were prepared for microscopic examination through appropriate polishing and etching. The different phases present can be identified or distinguished through their appearance.

The characterization techniques were conducted on the samples includes the samples structures being examined using X-ray diffractometer developed in Japan by Rigaku Int. Corporation called Rigaku D/Max-IIIc. The data analysis was carried out and the peaks obtained were matched with the phases of the samples. The surface morphologies of the samples were examined using a scanning electron microscope (SEM), and their elemental compositions were examined using an energy dispersive X-ray spectroscope (EDS). The scanning electron microscope and energy dispersive X-ray spectroscope (SEM, EDS) were carried out using JOEL JSM 7600F scanning electron microscope. To investigate the alloy, an X-Ray Diffraction (XRD) equipment was utilized in crystalline phase by identifying the diffraction peaks.

### **Use of Computer Software to Analyse Fatigue of SMA**

#### **Method used to Analyse Result**

The procedure for analysing the data will be through the use of Multiple Linear Regression Model (MLR) and Analysis of Variance (ANOVA).

Multiple linear regressions MLR is described as the relationship dependent (y) and independent variables (x). It can be expressed as:

$$y_i = \beta_0 + \beta_1 x_{1i} + \beta_2 x_{2i} + \dots + \beta_n x_{ni} + e_i \dots \dots \dots (7)$$

where  $y_i$  denotes the dependent variable (Fatigue Life) and  $x_i$  where  $i = 1, 2, \dots, n$  denotes the explanatory or independent variables,  $\beta$  is called the intercept and  $\varepsilon_i$  (errors, or noise) are i.i.d.  $N(0, \sigma^2)$ . In order to evaluate the relationship between the dependent and independent variables, the Pearson correlation test is examined. SPSS was used for the regression and testing of the data.

## CHAPTER IV

### Findings and Comments

The results and findings derived from the samples and data gathered are presented in this chapter.

#### Findings for Crystal Orientation of the Samples

The results for each samples structure of material used (copper, aluminium, Nickel and graphene) after examining them using X-ray diffractometer developed in Japan by Rigaku Int. Corporation called Rigaku D/Max-IIIc, is as presented in Figure 33-36. The data analysis was carried out and the peaks obtained were matched with the phases of the samples.

Figure 33.

*Pattern obtained for copper via use of XRD (X-Ray Diffraction)*

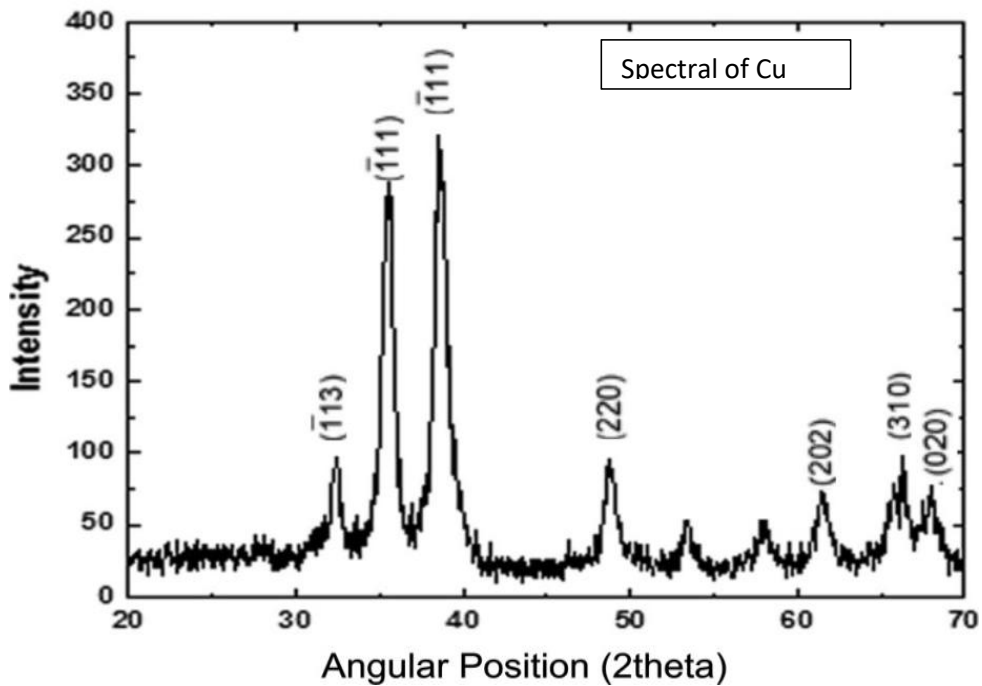


Figure 34.

*Pattern obtained for Aluminium via use of XRD (X-Ray Diffraction)*

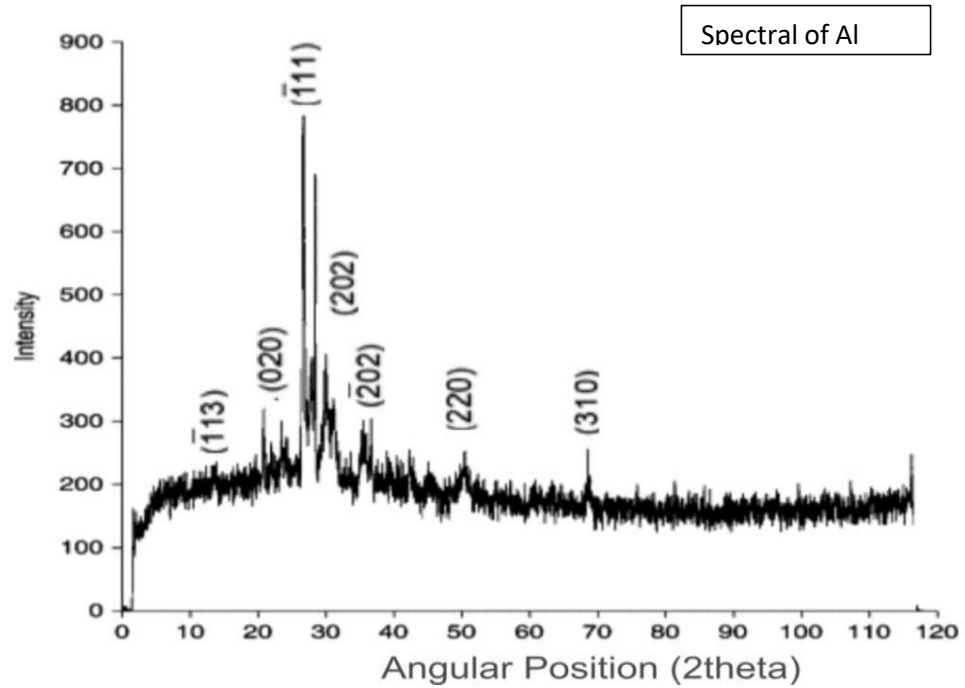
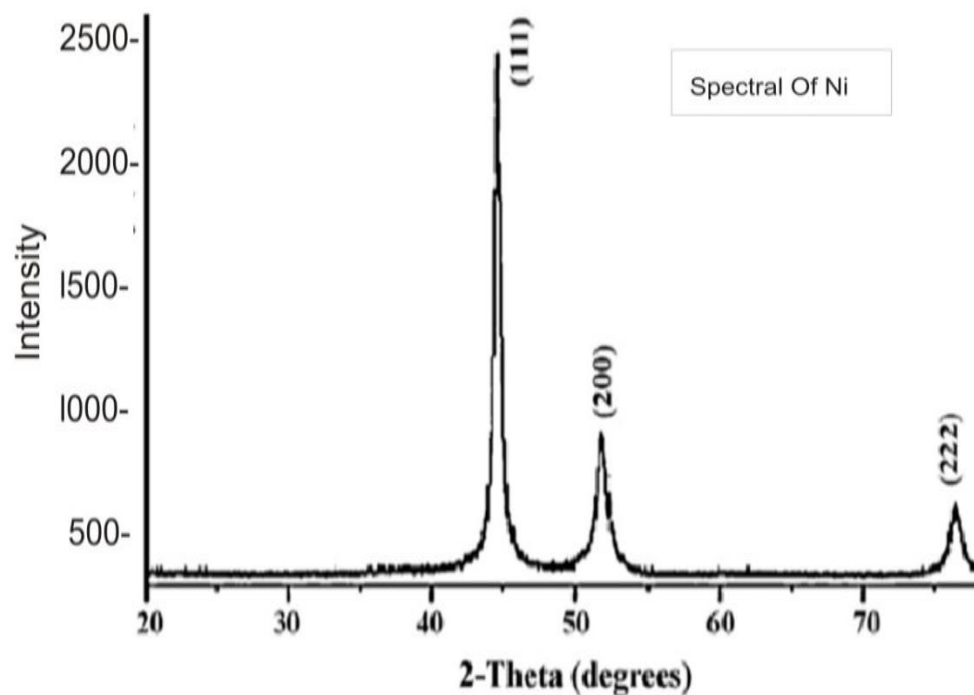


Figure 35.

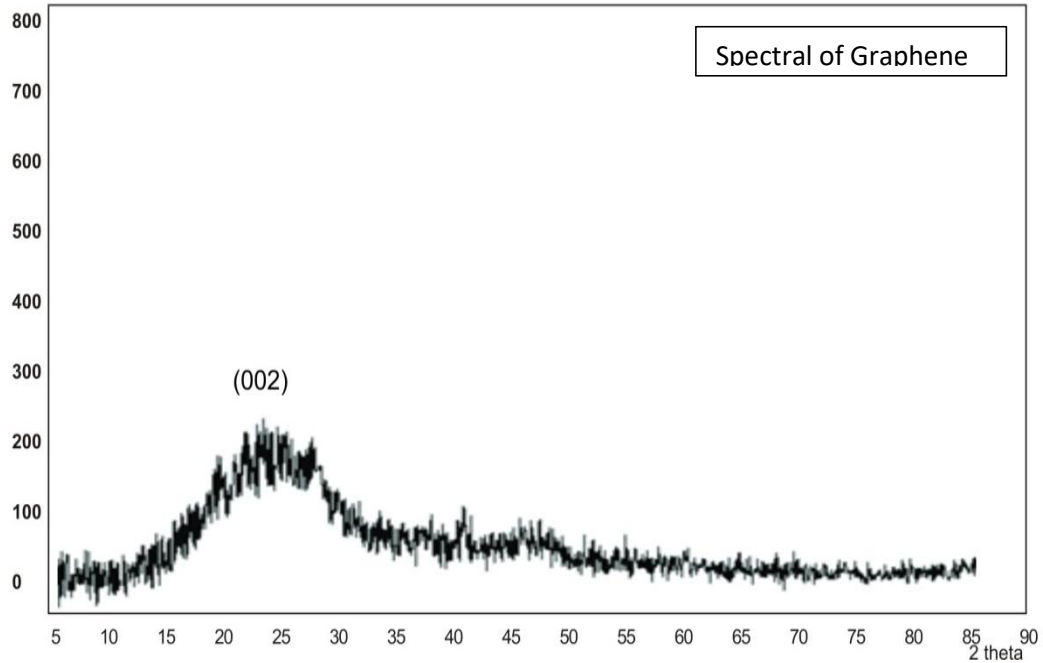
*Pattern obtained for Nickel using X-Ray Diffraction (XRD)*



The peaks obtained are similar to those Copper, Aluminium, and Nickel. They are Face Centre Cubic (FCC) metals. Their planes are closed planes. Therefore, strongest diffraction peak were observed from them.

Figure 36.

*Pattern obtained for Graphene via use of XRD (X-Ray Diffraction)*



### **Findings for Samples' Elemental Composition and Surface Structure/ Morphology**

The surface morphologies of the samples were examined using a scanning electron microscope (SEM), and their elemental compositions were examined using an energy dispersive X-ray spectroscopy (EDS). Results showing surface morphology and elemental compositions are as presented in Figure 37-40.

Figure 37.

*Surface morphology and elemental compositions of Copper (Cu) sample*

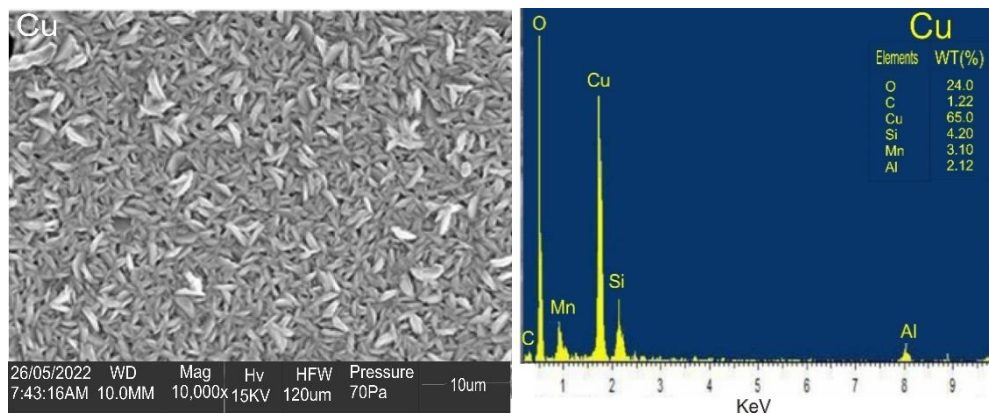


Figure 37 is the SEM micrograph of copper which is the matrix or parent metal in developing the SMA. It is observed from the micrograph that the structure appeared needle like having different colours. It is evidence from the structure that the copper is fine grained which is likely to justify its high mechanical properties.

Figure 38.

*Surface morphology and elemental compositions of Aluminium (Al) sample*

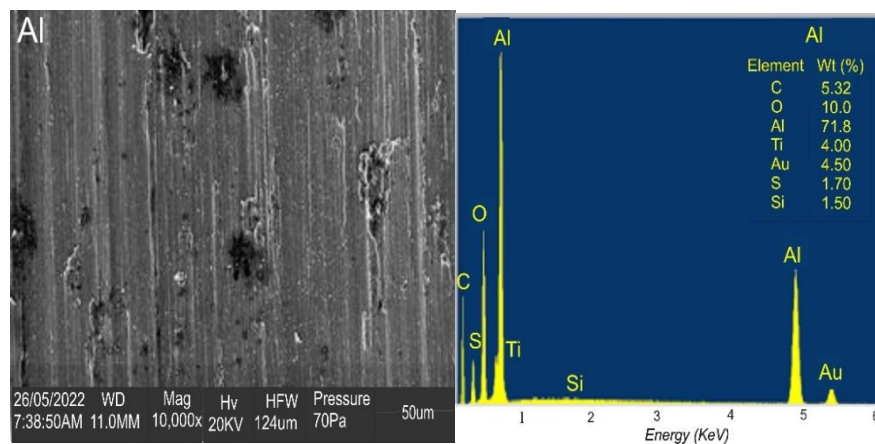
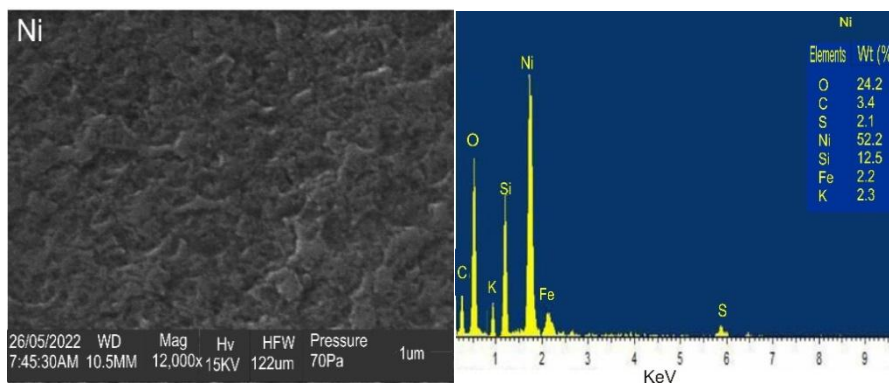


Figure 38 is the SEM micrograph of the aluminium surfaces used as one of the alloying elements in developing the SMA. It is observed from the surfaces of the micrograph that the surface has undulating layers, abhorring some particles which are proposed to be the compound or second phases produced from the alloying element in aluminium.

Figure 39.

*Surface morphology and elemental compositions of Nickel (Ni) sample*



Microstructure in Figure 39 presents surface of the nickel used as alloying element in copper for developing the SMA. It is clear from the microstructure that the surface appears in form of strata lined over another.

Figure 40.

*Surface morphology and specification of Graphene used.*

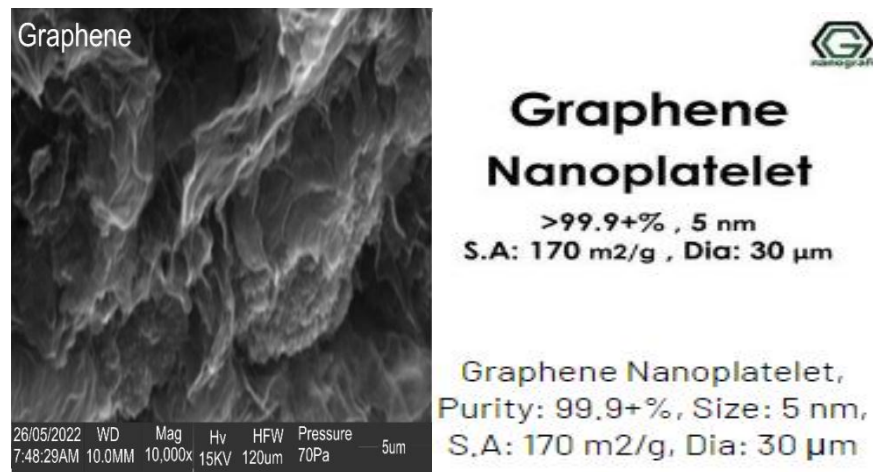


Figure 40 is the micrograph of graphene used as alloying element in copper for developing the SMA. It is evident from the micrograph that the structure has many networks of hexagonal structure connected with a layer over another abhorring many pores.

### **Findings for Mass Composition of Samples**

Table 8 show results for the mass of Graphene, Copper, Aluminium and Nickel used as obtained using the principle of rule of mixtures.

Table 8.

*Mass Composition of Specimen*

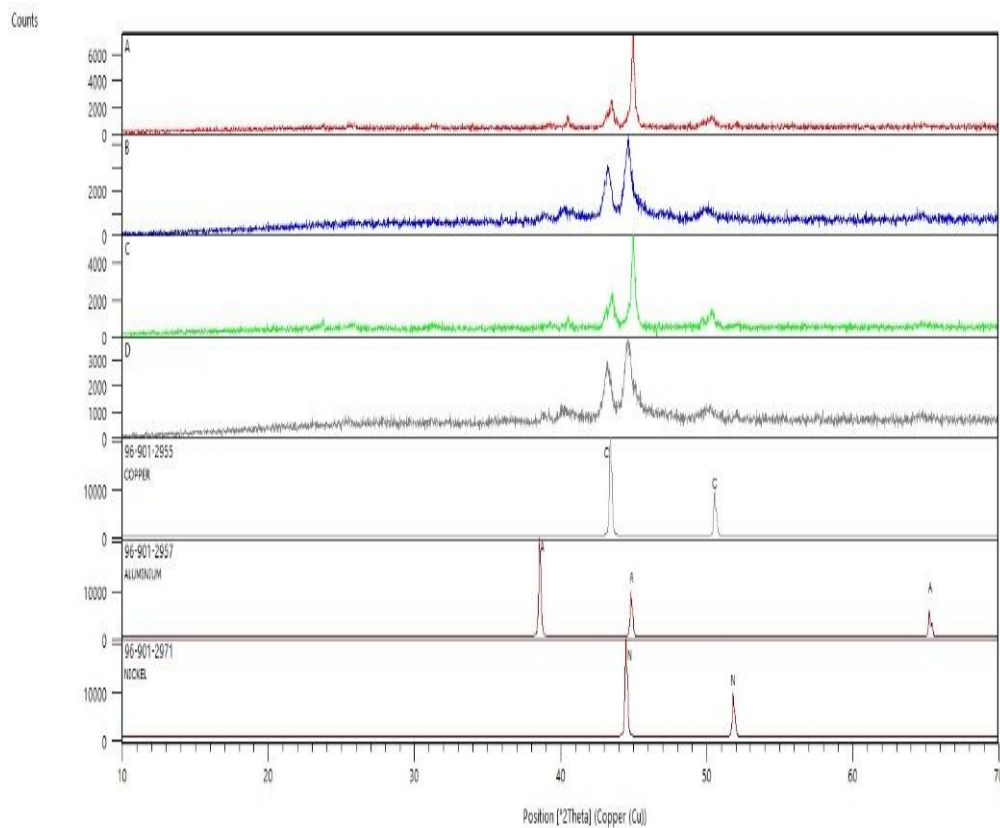
Specimen	Graphene (%)	Copper (%)	Aluminium (%)	Nickel (%)
A	-	464.92	65.63	20.957
B	0.8359	469.0897	62.218	21.147
C	1.644	460.629	65.023	20.764
D	2.46	458.5	64.720	20.69

### Findings for Characterization of SMA

XRD (X-Ray Diffraction) result for alloy produced is presented in Figure 41. Specimen A, B, C and D were four samples produced.

Figure 41.

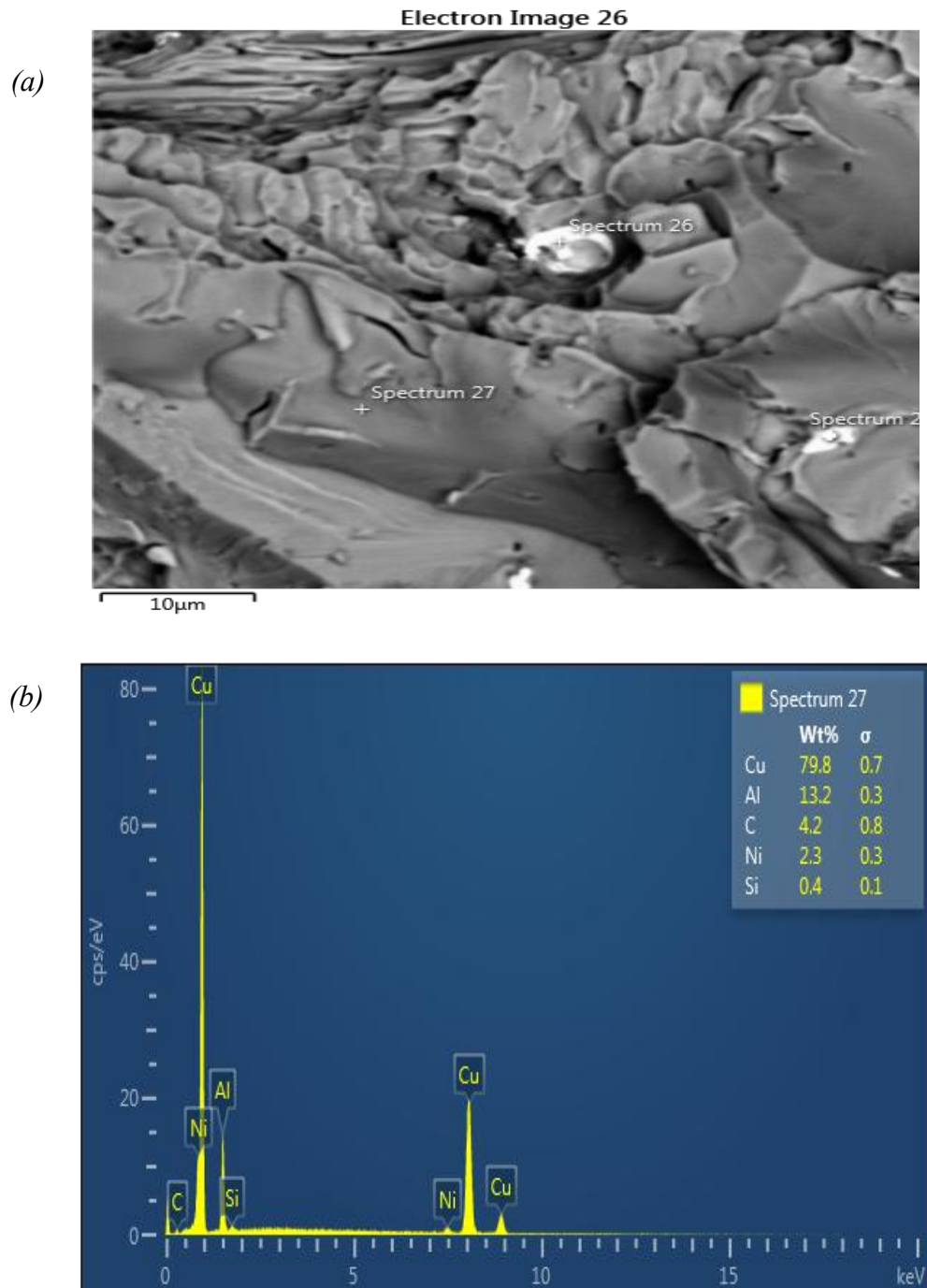
*Pattern obtained for Sample A, B, C and D via use of XRD (X-Ray Diffraction)*



Results obtained have peak akin to those of sample A, B, C and D where C represents graphene. Sample A (control sample) without graphene added is shown in the Scanning Electron Microscope (SEM) micrograph in Figure 42(a). The alloy's structure, which appears as several rock fragments arranged one on top of the other to form undulating layers, is evident from the micrograph.

Figure 42.

The composition of elements and surface morphology of Alloy specimen A (a) SEM micrograph (b) EDX result.



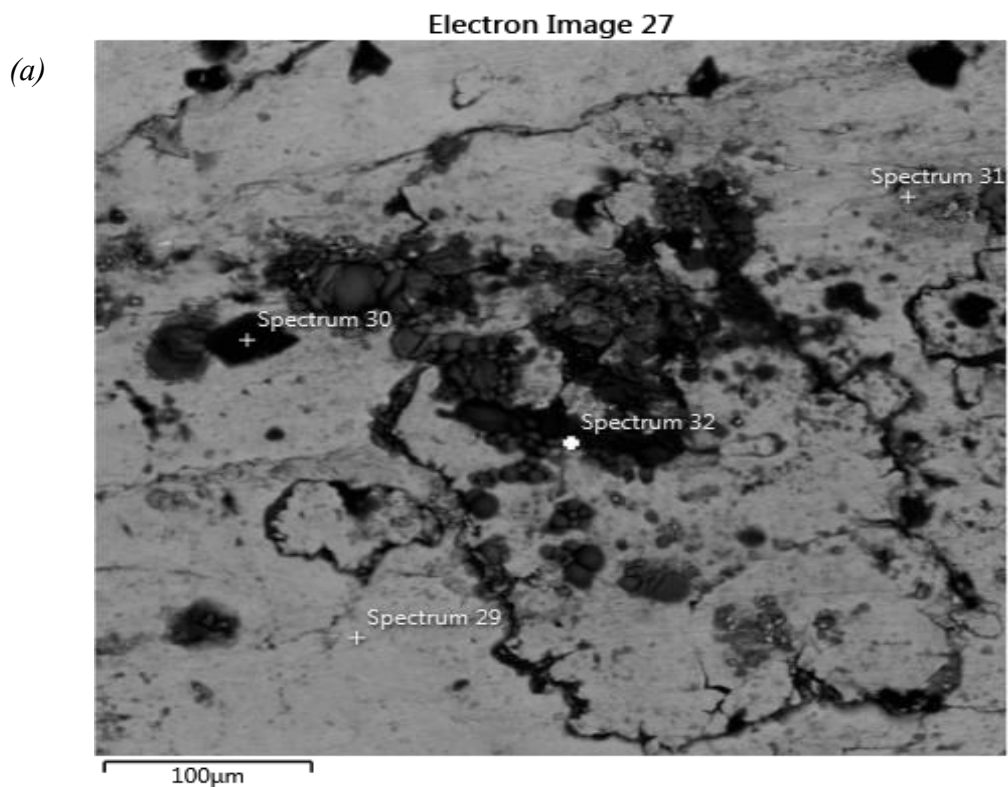
The various shapes and sizes of the debris found in Figure 42(a) suggest that the alloy hardened from melt to form dendritic grains, which expanded at varying rates until they intersected and interlocked to form the structures that were seen.

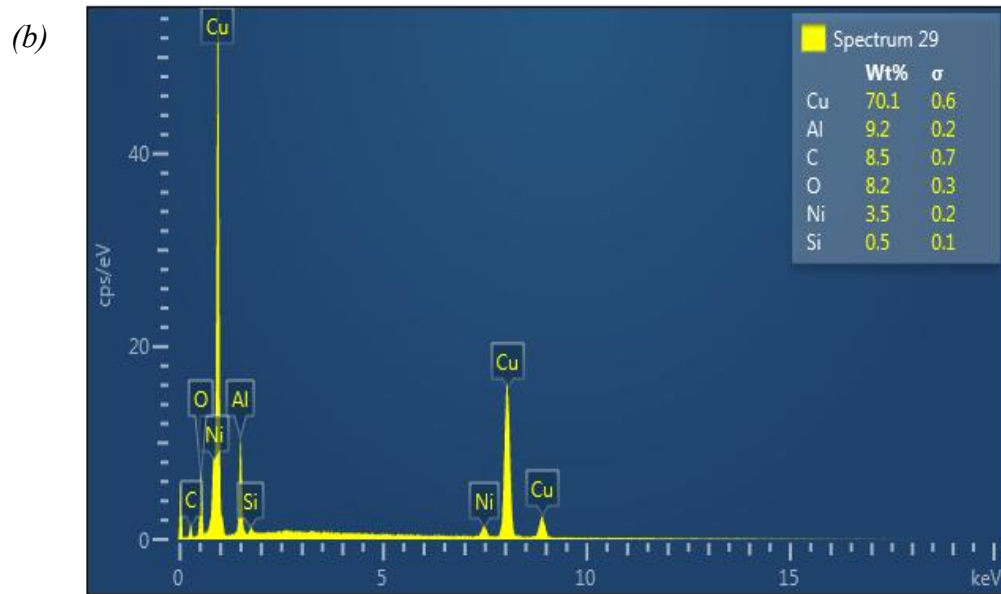
The EDS (Energy Dispersive X-ray Spectroscopy) result that was obtained to show the elemental analysis of the structure is shown in Figure 42(b). It shown that microsegregation takes place inside the alloy as a result of variations in the content of each element found in the alloy from one location to another. The main elements found at spectrum 27 are nickel, copper, aluminium, and graphene (carbon). The silica sand used to make the mould may have contributed to the silicon detection.

The microstructure characteristics of the graphene-reinforced CuAlNi SMA are displayed in the micrographs in Figures: 43, 44, and 45.

Figure 43.

The composition of elements and surface morphology of *Alloy specimen B* (a) SEM micrograph (b) EDX result

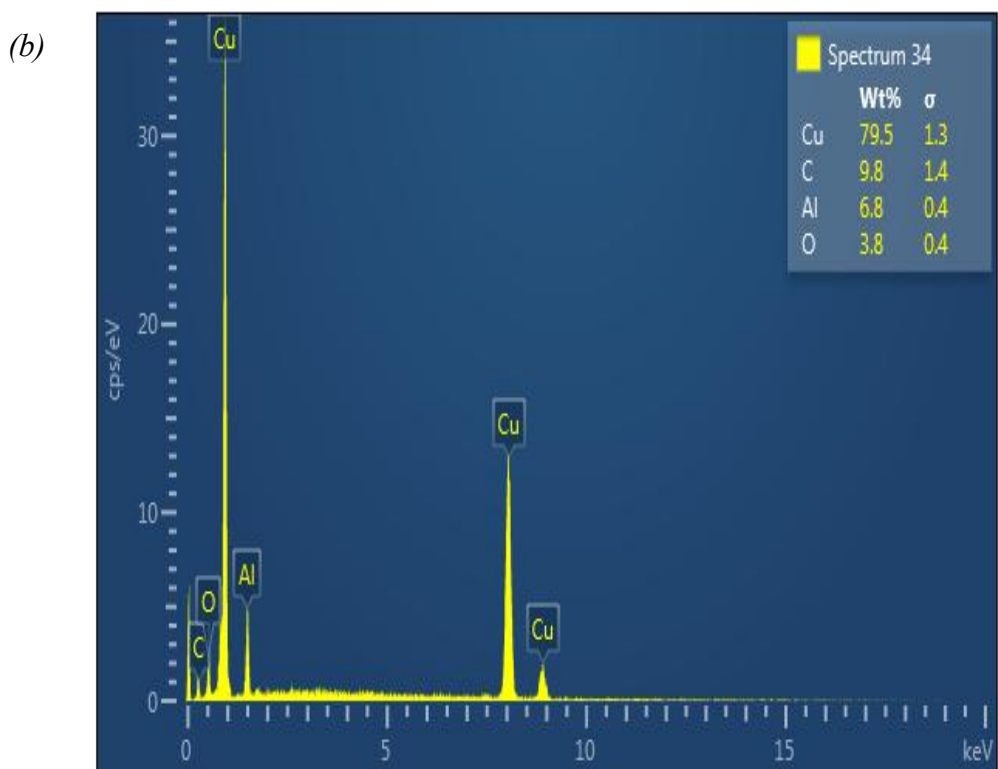
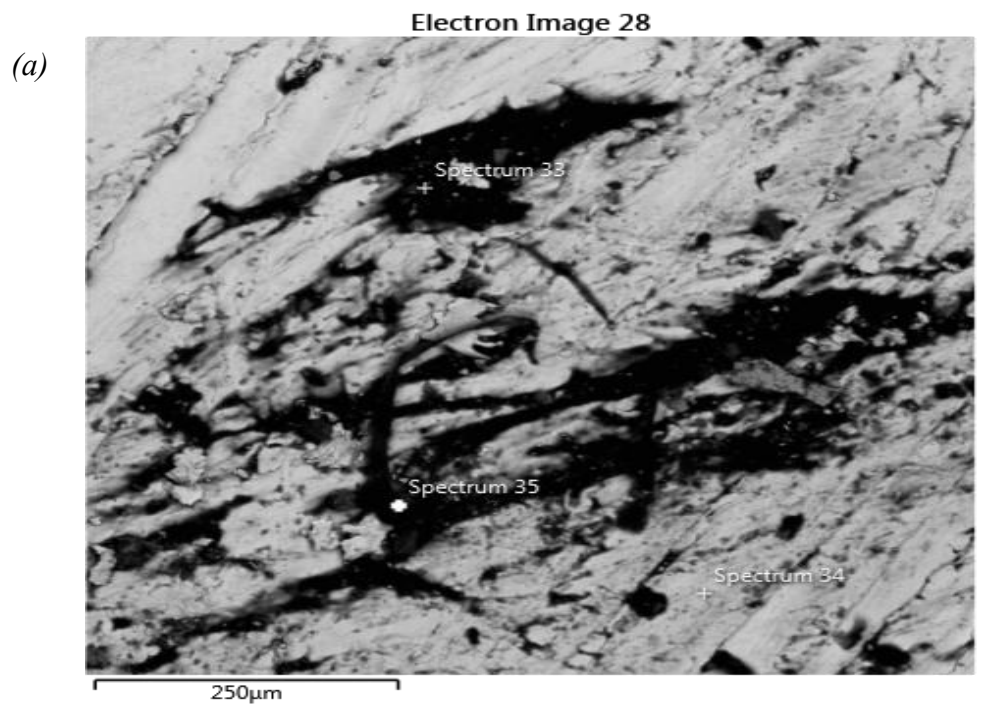




Every microstructure displays an ash-like structure that detests phases that resemble darkness or blackness. Figure 43(a), which depicts CuAlNi SMA with 0.15% graphene, shows that the black phase is sparsely distributed inside the host, which resembles ash. The centre of the structure, which has dense particle agglomerate, is where evidence of particle agglomeration is proven. Certain chemicals that are created when graphene interacts with any element in the matrix or based alloy are responsible for the black phase. This is clear from the results of the Energy Dispersive X-ray Spectroscopy (EDS), which indicate the alloy's constituent compositions in Figure 43(b).

Figure 44.

The composition of elements and surface morphology of Alloy specimen C (a) SEM micrograph (b) EDX result

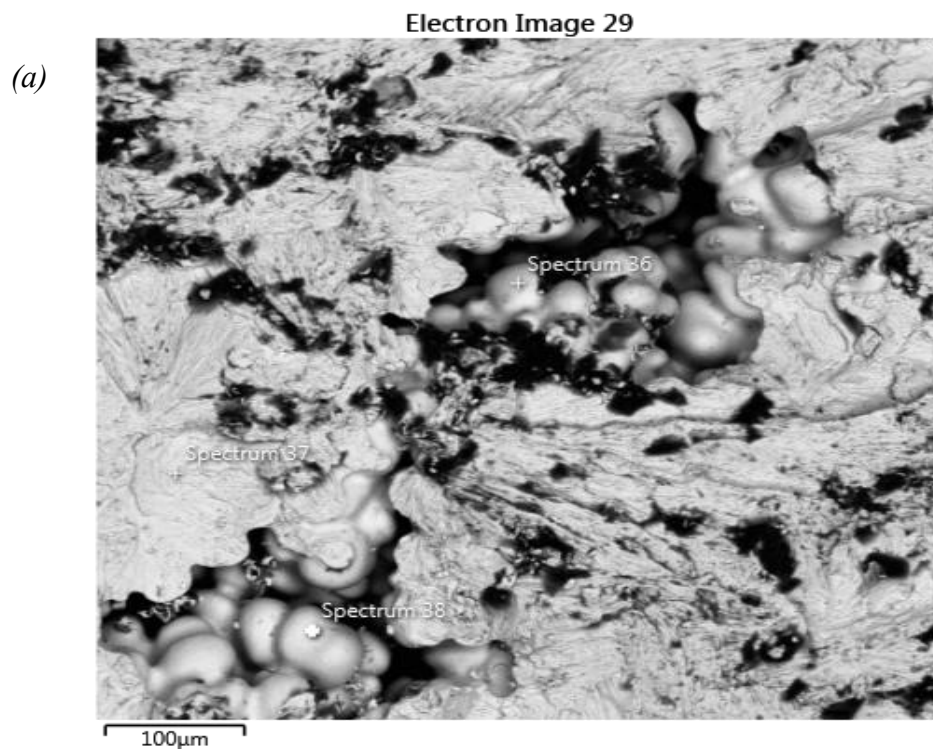


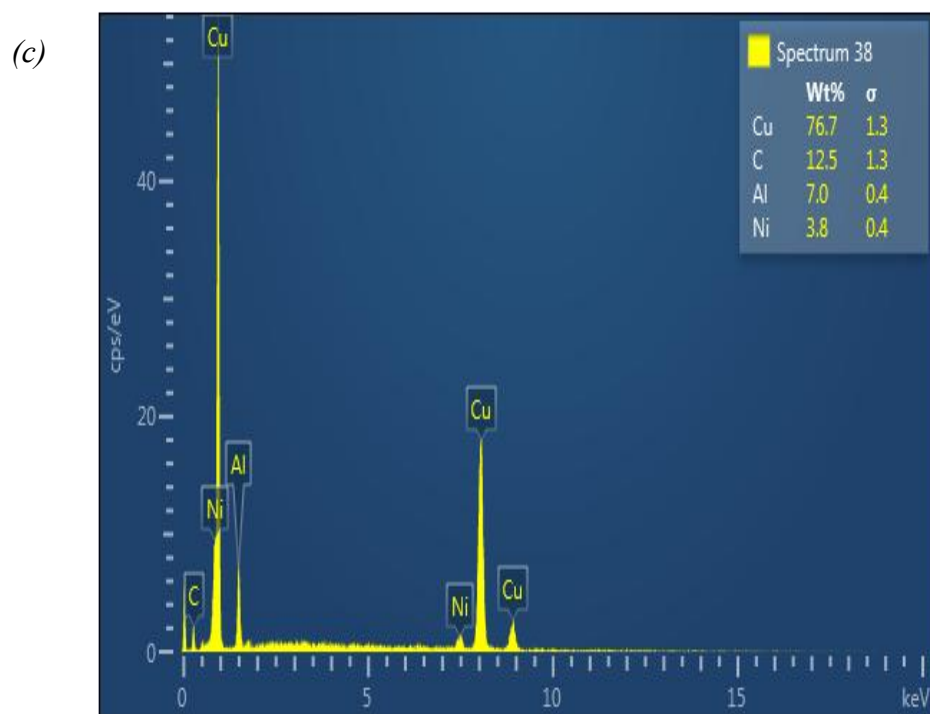
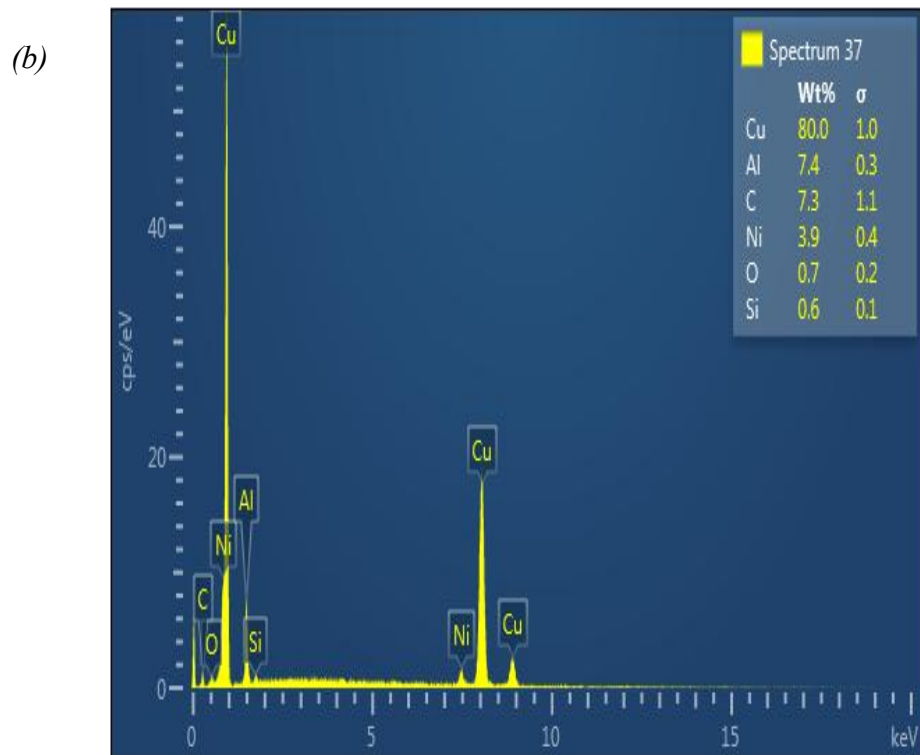
The SEM result acquired for SMA involving 0.3% graphene is shown in Figure 44(a) above. The microstructure exhibits secondary black phase clustering in several structural locations. Additionally, the structure of the host resembles striations that are connected to create an undulating layer structure.

In Figure 44(b), the elemental compositions at spectrum 34 are revealed by the EDS (Energy Dispersive X-ray Spectroscopy) result. This verified that the alloy was based on copper. It is likely that nickel is not discovered in this area because its concentration is too low to be detected at this time or because other elements that have been detected have blocked or marked the nickel's reflected x-ray.

Figure 45.

The composition of elements and surface morphology of *Alloy specimen D* (a) SEM micrograph (b) EDX result





A micrograph of CuAlNi SMA with 0.45% graphene is shown in Figure 45(a). The finding shows that the host plain structure detests black particles that are grouped together and rounded grains. The simple structures resemble strengthened

egg threads. Because of the second phase particles' rather equal dispersions, a reasonably homogeneous structure is seen here.

The elemental compositions at spectra 37 and 38 are revealed by the EDS (Energy Dispersive X-ray Spectroscopy) data, which are displayed in Figures: 45 (b) and 45 (c). The elemental compositions at various locations confirmed that copper, which acts as the host for every other component found in the alloy, is abundant in various alloy parts. The silica sand used to make the mould may have contributed to the silicon detection.

### **Findings for Mechanical Testing of SMA**

Table 9 below is the results of the Rockwell hardness test (RH) using a diamond indenter of Kgf 150 using Scale C.

Table 9.

Rockwell Hardness (RH) test, C-scale, results with diamond indenter of Kgf 150.

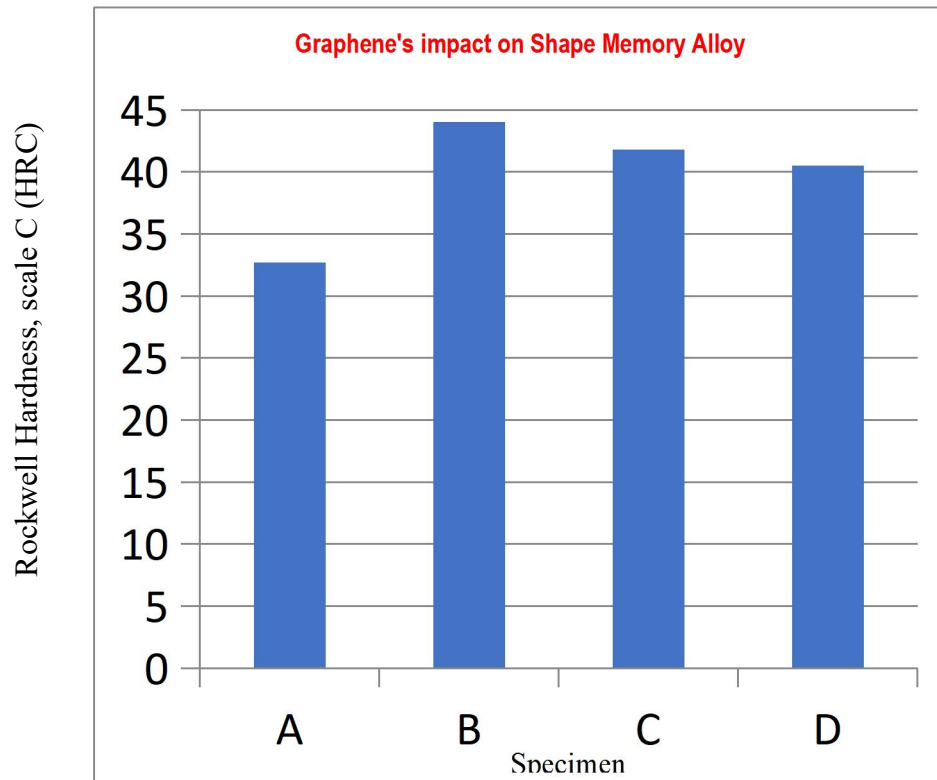
Specimen	Trial 1	Trial 2	Trial 3	RH
A	26.0	43.0	29.0	32.7HRC
B	42.0	43.5	46.5	44.0HRC
C	38.5	44.5	42.0	41.8HRC
D	40.0	40.0	41.0	40.5HRC

The results show an increased in hardness value for sample B, sample C and sample D.

The graph in Figure 46, shows that Sample B has the highest hardness value as compared with A, C and D. It can be inferred from the graph that graphene addition to the alloy actually increased the mechanical property i.e. hardness value.

Figure 46.

*Impact of graphene on SMA as determined by the hardness test findings*



### **Findings for Fatigue Testing of SMA**

A study of how much stress or amount of cycles a component can endure before failure of the component of a specific kind is referred to as the fatigue life for that component/material. The result presented in Table 10, show the value of the applied moments to each component and the equivalent stress values. The number of stress cycles each component sustained before failure by fatigue occurred is also presented. This referred to as the fatigue life for that stress value. The fatigue life is shown on the S-N (Stress-Number of Cycles) curve. This graphs illustrate the relationship between the number of cycles (N) before fatigue failure and stress (S), see Figure 47-51.

Table 10 shows the fatigue test results obtained for specimen A, B, C and D.

Table 10.

*Results of Fatigue testing of specimen A, B, C and D.*

MOMENT (Kgfcm)	GUAGE LENGTH (m)	FINAL LENGTH (m)	INITIAL REVOLUTION	FINAL REVOLUTION	DIAMETER (mm)	STRESS (MPa)	NO OF CYCLES (10 <sup>3</sup> )
Sample A							
65	45.35	52.52	5052	5053.7	5.4	412.31	1.7
130	45.35	52.52	5054	5055.2	5.4	824.62	1.2
195	45.35	52.52	5056	5056.7	5.4	1236.94	0.7
260	45.35	52.52	5057	5057.5	5.4	1649.25	0.5
Sample B							
65	45.35	52.52	5058	5059.5	5.4	412.31	1.5
130	45.35	52.52	5060	5061.1	5.4	824.62	1.1
195	45.35	52.52	5061.1	5061.7	5.4	1236.94	0.6
260	45.35	52.52	5061.7	5062	5.4	1649.25	0.3
Sample C							
65	45.35	52.52	5062	5063.8	5.4	412.31	1.8
130	45.35	52.52	5064	5065	5.4	824.62	1.0
195	45.35	52.52	5065	5065.7	5.4	1236.94	0.7
260	45.35	52.52	5066	5066.5	5.4	1649.25	0.5
Sample D							
65	45.35	52.52	5067	5067.9	5.4	412.31	0.9
130	45.35	52.52	5068	5068.7	5.4	824.62	0.7
195	45.35	52.52	5069	5069.4	5.4	1236.94	0.4
260	45.35	52.52	5069.4	5069.2	5.4	1649.25	0.2

Figure 47.

*Fatigue Life (S-N) graph for specimens A.*

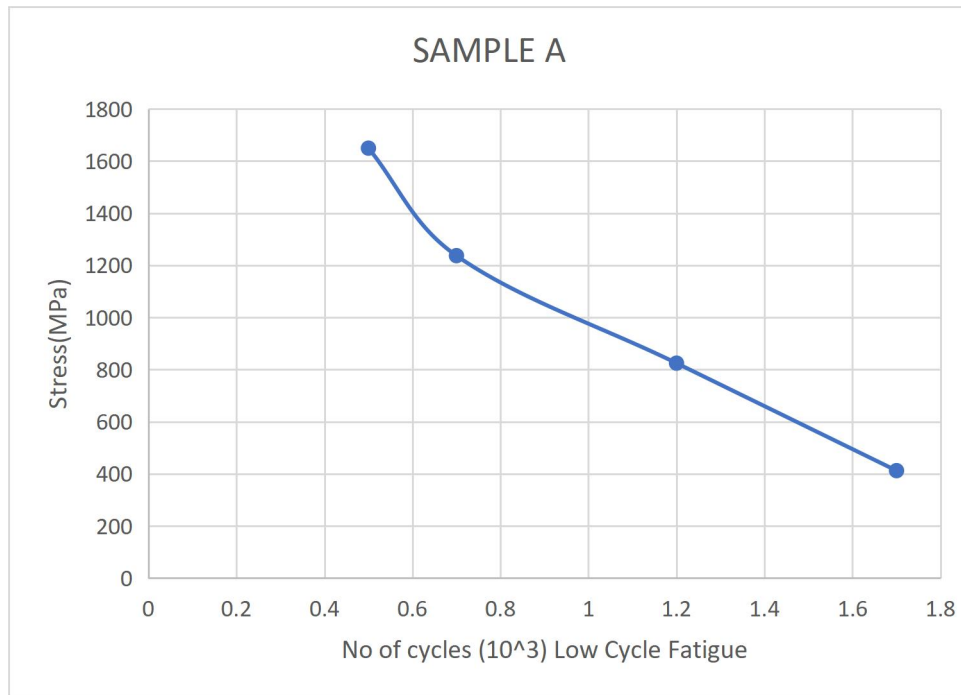


Figure 48.

*Fatigue Life (S-N) graph for specimens B.*

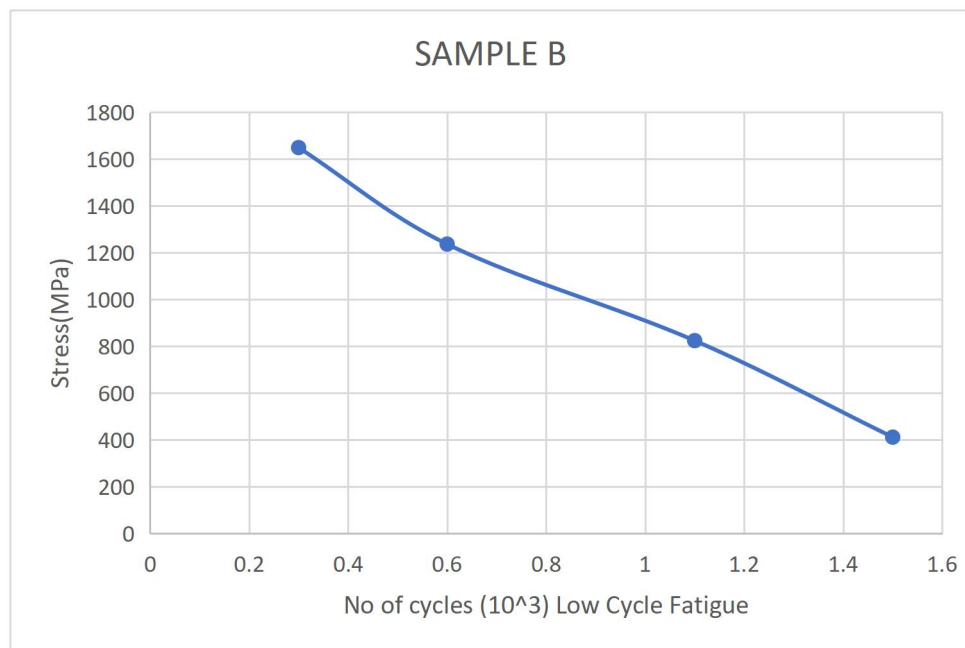


Figure 49.

*Fatigue Life (S-N) graph for specimens C.*

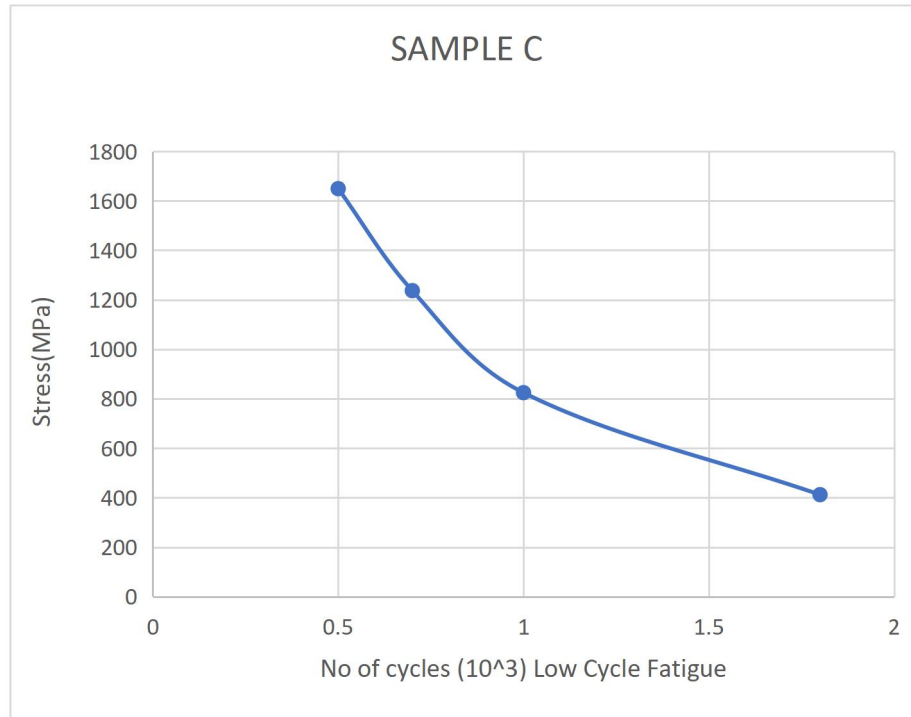


Figure 50.

*Fatigue Life (S-N) graph for specimens D.*

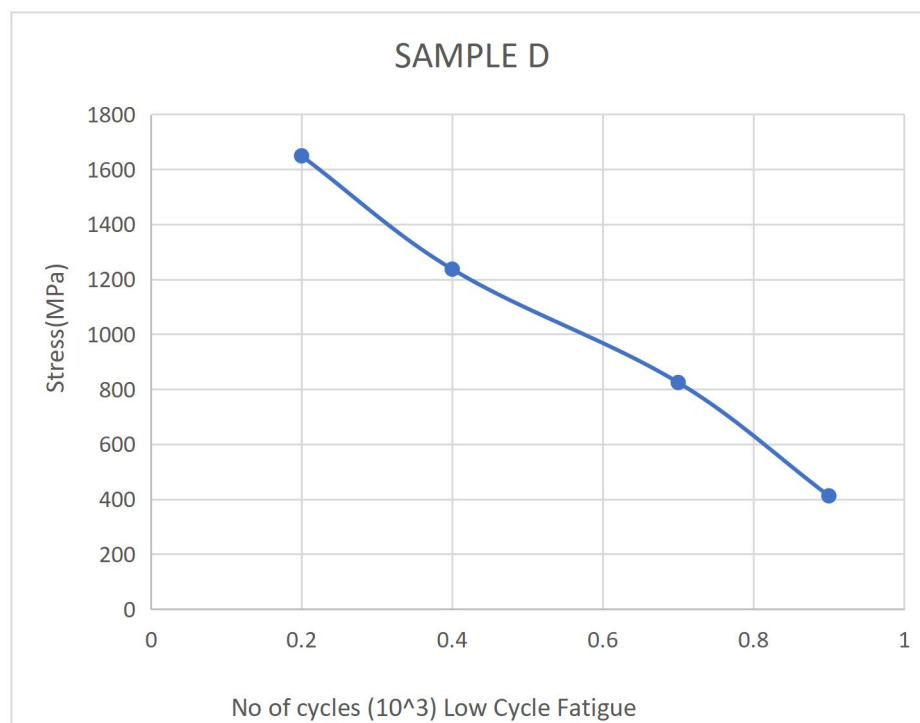
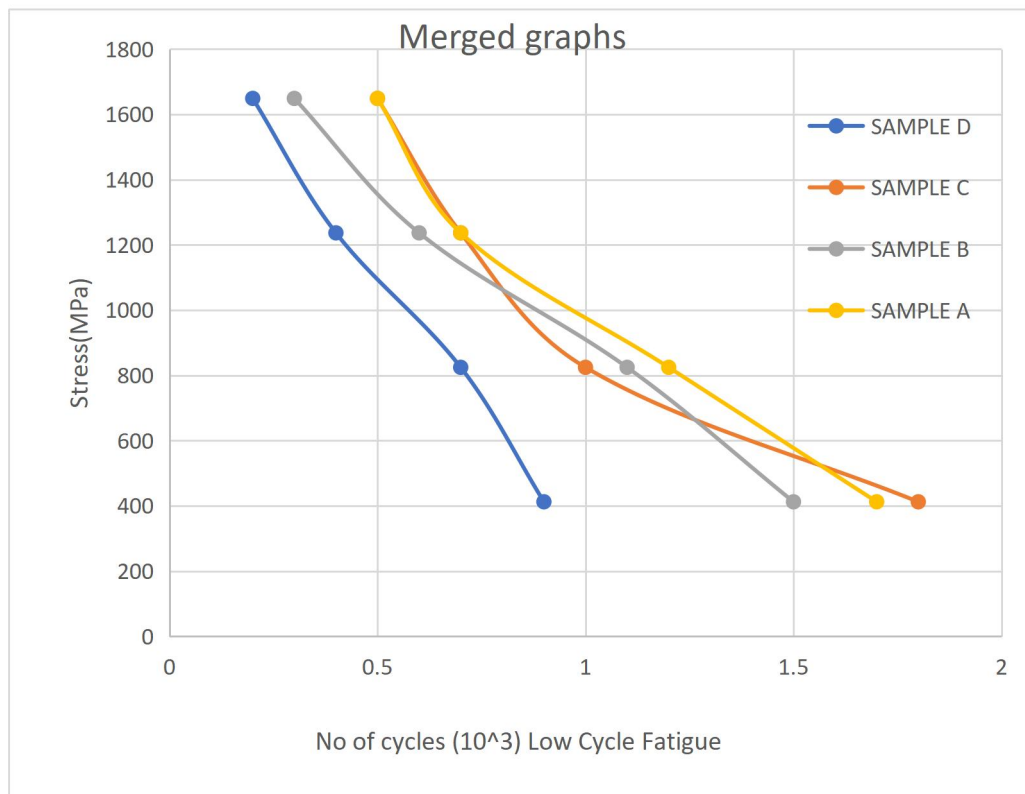


Figure 51.

*Fatigue Life (S-N) graph for the combined graph*



From the graphs in Figure 47-50 showing the S-N curves obtained, the fatigue type is a low cycle fatigue, as the fatigue failure occurs at high stress and low cycles, less than  $10^4$  (George, 1988). Additional observation made was that as the value of applied stress reduces, the resulting number of stress cycles yielding fatigue failure reduces. The graph combined (Figure 51) helps to compare the fatigue life of specimen A, B, C and D. Specimen A and C at a particular value of stress on the combine graph, falls towards the right of specimen B and C, which indicates higher value of stress cycle or fatigue life. Increasing the stress value to 1649.25MPa, sample C containing 0.3% graphene display an optimum value of fatigue when in comparison with specimen/sample A, B and C. Sample D containing the highest amount of graphene of 0.45% gives the least fatigue life at a stress value of 149.25MPa, when compared with samples A, B and C. This is as a result of increased in graphene content above optimum amount.

Figure 52.

*Further Comparison of the Fatigue Life of the four specimens A, B, C and D*

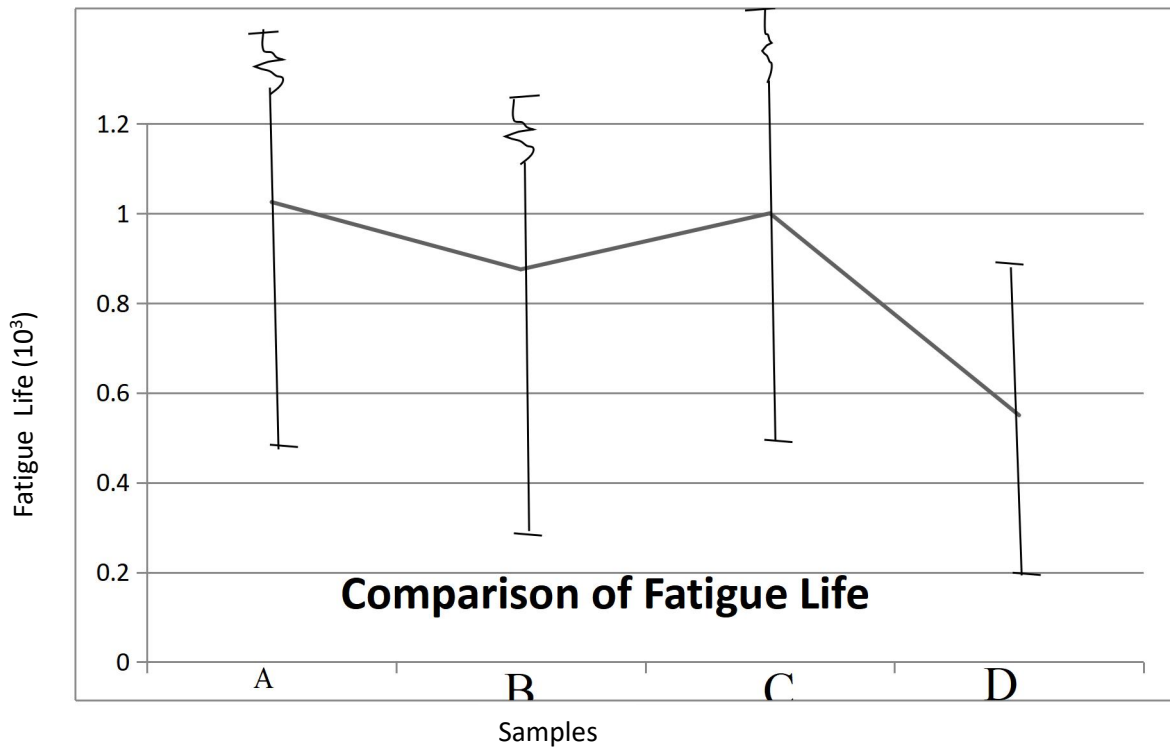


Figure 52 further compares the fatigue life of samples A, B, C and D by taking average value obtained from the four samples.

For Sample A

$$\begin{aligned} \text{Difference in Fatigue Life (Highest Value - Lowest Value)} \\ = (1.7 - 0.5)(1000) = 1.2(1000) \end{aligned}$$

For Sample B

$$\begin{aligned} \text{Difference in Fatigue Life (Highest Value - Lowest Value)} \\ = (1.5 - 0.3)(1000) = 1.2(1000) \end{aligned}$$

For Sample C

$$\begin{aligned} \text{Difference in Fatigue Life (Highest Value - Lowest Value)} \\ = (1.8 - 0.5) = 1.3(1000) \end{aligned}$$

For Sample D

$$\text{Difference in Fatigue Life (Highest Value - Lowest Value)}$$

$$= (0.9 - 0.2) = 0.7(1000)$$

From the comparison above, we can further confirm that sample C has the optimum Fatigue Life.

### Findings for the use of Computer Software for the Fatigue of SMA

#### D-Optimal Model Formulation

Based on D-Optimal design which is a sub-division of combined methodology of the Design Expert Software version 13.0, the model obtained for the accurate prediction of the fatigue life in terms of the coded factors is shown in Table 12.

Table 11.

*Experimental runs (input) and responses (output)*

Input		Output		
Graphene (%)	Cu (%)	Al	Ni	Fatigue Life cycles to failure (x10 <sup>3</sup> )
0	84.3	11.9	3.8	1.7
0	84.78	11.25	3.8	1.2
0	84.05	11.32	3.79	0.7
0	83.92	11.85	3.78	0.5
0.15	84.3	11.9	3.8	1.5
0.15	84.78	11.25	3.8	1.1
0.15	84.05	11.32	3.79	0.6
0.15	83.92	11.85	3.78	0.3
0.3	84.3	11.9	3.8	1.8
0.3	84.78	11.25	3.8	1.0
0.3	84.05	11.32	3.79	0.7
0.3	83.92	11.85	3.78	0.5
0.45	84.3	11.9	3.8	0.9
0.45	84.78	11.25	3.8	0.7
0.45	84.05	11.32	3.79	0.4
0.45	83.92	11.85	3.78	0.2

A total of sixteen runs were carried out as part of the experiment (See Table 11). The linear model (see equation. 8) for forecasting fatigue life in terms of coded factors was created using the Design Expert Software version 13.0.

Table 12.

*Fatigue life in terms of coded factors*

Source	Sum of Squares	Df	Mean square	F-value	P-value
<b>Model</b>	3.22	9	0.3580	6.41	0.0174
<sup>(1)</sup> Linear Mixture	2.38	3	0.7933	14.20	
AE	0.0277	1	0.0277	0.4961	
BE	0.0349	1	0.0349	0.6249	
CE	0.0243	1	0.0243	0.4343	
DE	0.0295	1	0.0295	0.5277	
AE <sup>2</sup>	0.0009	1	0.0009	0.0165	
BE <sup>2</sup>	0.0000	0			
CE <sup>2</sup>	0.0429	1	0.0429	0.7685	
DE <sup>2</sup>	0.0000	0			
Residual	0.3353	6	0.0559		
Lack of Fit	0.3086	4	0.0772	5.79	
Pure Error	0.0267	2	0.0133		
Cor Total	3.56	15			

Where FL is Fatigue Life. A, B, C, D represents the composition (%) of Graphene (C), Cu, Al, Nickel, respectively and E is Stress.

$$FL = -1.04A+2.35B-2.30C-28.87D-1.17AE-8.37BE-3.51CE+381.67DE-0.2827AE^2 + 0.0000BE+ 8.04CE^2 +0.0000DE^2.....(8)$$

The significance of each coefficient was obtained from the probability (p) values and residual least square error. According to table 12, the linear models were adequate in fitting the experimental result. The model F-Value of 14.85 was obtained with a chance of 0.02% occurrence due to noise. This indicates that the model is significant at 99% confidence interval. The stress and moment are significant model terms, thus they have significant effect on the fatigue life.

#### **Analysis of Fatigue life using ANOVA (Analysis of Variance)**

As indicated in Table 8 for the analysis, as inputs for the experiment, two parameters were chosen: the percentages of Cu and Graphene (C). The output parameter in this case was the number of cycles to failure, which determines the fatigue life.

From the Analysis of Variance result shown in Table 13, and by considering graphene and copper being dominant elements. The importance/significance of each coefficient is obtained from the residual least square error values and probability (p). It was observed that the linear model fits the results of the experiment at probability value of  $p < 0.05$  adequately according to Table 13.

Table 13.

#### *ANOVA (Analysis of Variance) for Fatigue Life*

Source	DF	Seq SS	Contribution	Adj SS	Adj MS	F-Value	P-Value
Graphene (%)	3	0.5725	16.09%	0.5725	0.19083	9.41	0.004
Cu (%)	3	2.8025	78.78%	2.8025	0.93417	46.07	0.000
Error	9	0.1825	5.13%	0.1825	0.02028		
Total	15	3.5575	100.00%				

Table 13 is the ANOVA results and it signifies that Cu (%) with p-value far less than 0.05 is the most important factor affecting the fatigue life.

Table 14.

*Summary of the model*

---

S	R-sq	R-sq(adj)	PRESS	R-sq(pred)
0.142400	0.9487	0.9145	0.576790.	83.79%

---

According to the model summary in Table 14 above, the fatigue life mathematical model indicates a satisfactory fit. The model's ability to forecast fatigue life is demonstrated by its R-squared result of 0.9487 and adjusted R-squared result of 0.9145.

Similarly, a 3D response surface plot is used to study the mutual interaction between input and output parameters (see Figure 53-55). These plots were generated using the Design Expert Software version 13.0. They show the relationships that exist among different parameters at a time in three dimensions.

Figure 53.

*For fatigue life, a three-dimensional response surface plot A*

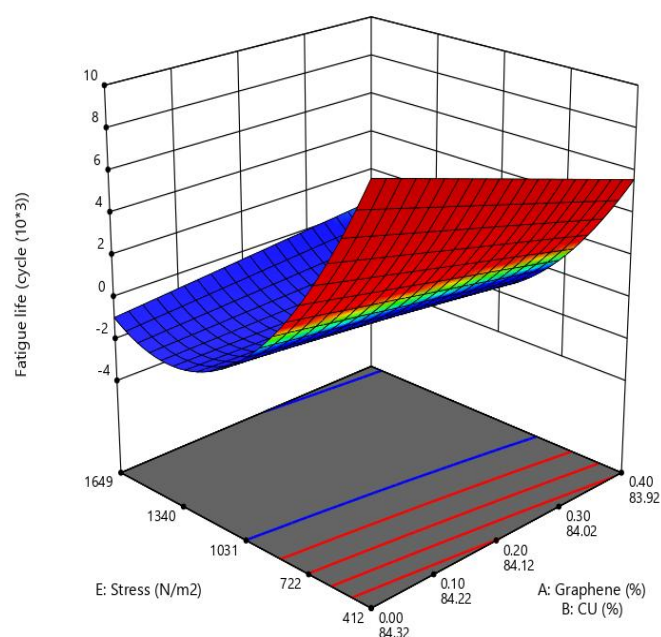


Figure 53 shows that by increasing percentage of graphene with a decrease in the percentage of copper, fatigue life increases with a decrease in stress value.

Figure 54.

*For fatigue life, a three-dimensional response surface plot B*

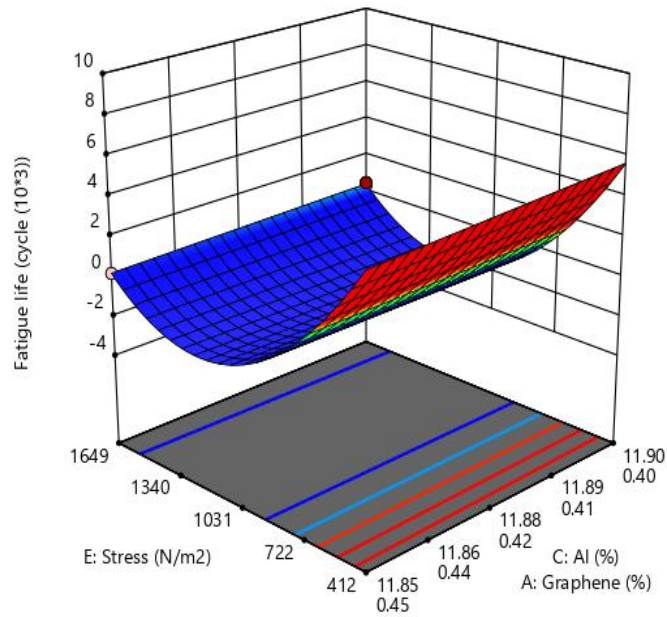


Figure 54 shows that by decreasing the percentage of graphene with an increment in the percentage of Aluminium, fatigue life increases with a decrease in stress value.

Figure 55.

*For fatigue life, a three-dimensional response surface plot C*

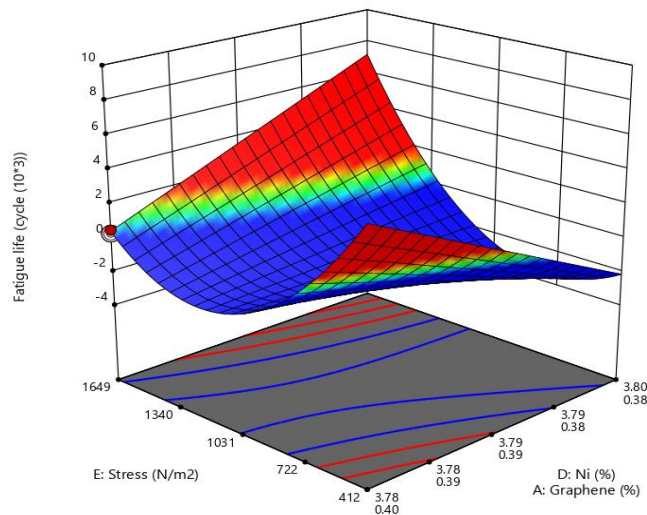


Figure 55 shows that by decreasing percentage of graphene with an increase in the percentage of Nickel, fatigue life increases with a decrease in stress value.

Lastly, from the 3 D plots showing the mutual interaction of number of cycles and percentage content of copper (Cu), aluminium (Al), and graphene (C), Ni (nickel) and stress value, it is also observed that a higher fatigue life is attained at lower stress value. Thus increasing the applied stress on a component result to a reduction in its fatigue life.

## CHAPTER V

### Discussion

The findings from this research show an improvement in frontier of knowledge in the study of alloys having shape memory effect.

#### *Crystal Orientation of the Samples*

The peaks obtained are similar to those of Copper, Aluminium, and Nickel. They are Face Centre Cubic (FCC) metals. Their planes are closed planes. Therefore, strongest diffraction peak were observed from them.

A scanning electron microscope (SEM) was used to analyze the samples' surface morphologies, and an energy dispersive X-ray spectroscopy (EDS) was used to analyze their elemental compositions. Figures 33–36 display the results, which include surface morphology and elemental compositions.

The SEM micrograph of copper, the matrix or parent metal used to form the SMA, is shown in Figure 33. The micrograph shows that the structure looked like a needle with many colors. The structure provides proof that the copper is finely grained, which probably explains its excellent mechanical qualities.

The SEM micrograph of the aluminum surfaces utilized as one of the alloying materials in the creation of the SMA is shown in Figure 34. The surface of the micrograph exhibits undulating layers, and certain particles that are thought to represent the compound or second phases formed from the alloying element in aluminum are repelled.

The surface of the nickel employed as an alloying element in copper to develop the SMA is shown in the microstructure in Figure 35. The microstructure makes it evident that the surface is composed of strata arranged one above the other.

The graphene micrograph utilized as an alloying element in copper to develop the SMA is shown in Figure 36. The microscope clearly shows that the structure is made up of numerous interconnected networks of hexagonal structures with a layer over another abhorring many pores.

***SMA Composition/Production***

The Shape Memory Alloy developed through this study contains the following composition: Sample A (100 wt.%, SMA, 0% C), Sample B (99.5 wt.%, SMA, 0.5% C), Sample C (99.7 wt.%, SMA, 0.3% C), and Sample D (99.55 wt.%, SMA, 0.45% C) as in Table 15 and the alloy was continuously stirred to achieve a mixture which is homogeneous in the course of production.

Table 15.

*SMA Percentage Composition of Samples*

Sample	C (%)	Copper (%)	Aluminium (%)	Nickel (%)
A	-	84.3	11.9	3.8
B	0.15	84.78	11.25	3.8
C	0.3	84.05	11.32	3.79
D	0.45	83.92	11.85	3.78

The results from literature that include a quaternary, Table 16, are consistent with this. The quaternary element was introduced to CuAlNi SMA in traceable amounts. Continuous stirring was used to blend the mixture until it was homogeneous (Saud, et al., 2015; Karaduman & Canbay, 2021).

Table 16.

*SMA Percentage Composition derived from literary works*

(%) C	(%) Co	(%)Ti	(%) Mn	Copper (%)	Aluminium (%)	Nickel (%)
-	-	-	-	84	11.9	4.10
-	-	-	0.97	82.94	11.93	4.16
-	-	0.99	-	82.92	11.94	4.15
-	1.14	-	-	82.96	11.9	4
0.55	-	-	-	84.78	11.25	3.8

### ***Effect of graphene on the Alloy Characterization***

Comparing the micrographs in Figure 31-34, show that Figure 32, 33 and 34 have black particles that may be connected to compound precipitations as a result of graphene contact, which creates new compounds with black hues. This is not present in figure 31, which is the control sample and does not contain graphene.

The alloy with 0.45% graphene (sample D) had the largest quantities of carbon, which were related to the secondary black component found in each of the graphene-reinforced alloys (Figures: 43, 44, and 45). More resistance to dislocation movement is provided by the host's secondary phase particles which are black, increasing dislocation obstruction or impingement. For the sample to get indentations during the hardness measurement, dislocation movement necessitates additional force. When compared to sample A (control sample) without secondary black substance, this is the reason why each of the Shape Memory Alloy having quaternary (graphene), i.e. specimen B, C, and D, had higher hardness values (Figure 42).

The alloy's rather homogenous microstructure, as seen in Figure 42, may be the reason why sample C, which included 0.3% graphene, was able to withstand the most cycles during the fatigue test. The likelihood of local deformations that can result in failure by fatigue at fewer numbers of cycles is decreased by evenly distributed carbon. This is seen in Figure 45 i.e. quaternary with 0.45% graphene (specimen D), which exhibits rounded grain presence and other discontinuities in the structure.

### ***Effect of graphene on the Hardness of CuAlNi SMA***

Cu–Al–Ni shape memory alloys (SMA) have been identified as materials with great potential for use at high temperatures. Their great thermal stability at temperatures exceeding 100°C is the reason for this (lojen, 2005). However, these alloys have drawbacks, including significant brittleness due to the emergence of brittle phase at grain boundaries and a large increase in grain size that is mirrored by a high elastic variation (wayman, 1986). As a result, these alloys' commercial use has been limited due to their drawbacks. Grain refinement is one method to address this issue; by changing the compositions of Ni or Al or by adding alloying elements such Ti, Mn, V, Nb, B, and others, the mechanical characteristics of the traditionally Cu–Al–Ni SMAs showed some improvement (vajpai, 2011). This enhancement is

ascribed to the presence of alloying elements, which purify the grains and limit their expansion. However, because of their development as a second phase structure in the microstructure, these alloying elements significantly impact the mechanical properties of Cu-Al-Ni SMAs (Zhu, 2009).

Table 9 shows the results of an investigation using a Rockwell hardness testing machine, using the C scale. This reveals how graphene affected the mechanical properties of CuAlNi SMA. According to the test results, samples A (SMA 100%), B (SMA 99.85%, C 0.15%), C (SMA 99.70%, C 0.3%), and D (SMA 99.55%, C 0.45%) all had higher hardness values, which is indicative of improved alloy mechanical properties. The CuAlNi SMA was subjected to Vicker's microhardness test by other researchers after quaternary elements like Mn, Co, and Ti were added to the alloy. The hardness value increased with the addition, according to the microhardness value they acquired, and they credit the precipitates of the alloy for this improvement in microstructure of CuAlNi SMA mechanical properties (Saud, et al., 2015).

### ***Effect of graphene on the Fatigue Property***

The findings in Table 5 and Figure 46 explained how graphene affected the fatigue behaviour of CuAlNi SMA. They demonstrate that the alloy's fatigue life is increased by adding graphene to CuAlNi SMA.

Based on the S-N curves produced from the graphs in Figure 47-50, the fatigue type is low cycle fatigue because fatigue failure happens at high stress and low cycles, less than  $10^4$  (George, 1988). The number of stress cycles that result in fatigue failure also decreased as the applied stress value decreased. The combined graph (Figure 51) facilitates comparison of specimens A, B, C, and D's fatigue lives. At a given stress value, specimens A and C fall to the right of specimens B and D on the composite graph, indicating a higher fatigue life or stress cycle value. Comparing sample C, which contains 0.3% graphene, to specimens A, B, and D, the fatigue value is at its peak when the stress value is increased to 1649.25 MPa. When sample D is compared to samples A, B, and C, it has the lowest fatigue life at a stress value of 149.25 MPa due to its maximum graphene content of 0.45%. This is because the amount of graphene has gone beyond what is ideal.

A 0.3% addition of graphene was found to be the ideal amount for the best fatigue life. Other researchers that looked into the impact of adding a fourth element to CuAlNi SMA added beryllium (Be), and they found that doing so actually lengthened the fatigue life of the Cu-Al-Ni Shape Memory Alloy (XU, et al. 2008; Xu, Song & Mao, 2011).

### **D-Optimal Model Formulation**

The model derived for the precise prediction of the fatigue life in terms of the coded factors is displayed in Table 12 and is based on D-Optimal design, a subset of the combined methodology of the Design Expert Software version 13.0. As part of the experiment, sixteen runs were conducted in total (see Table 11). Using Design Expert Software version 13.0, a linear model (see equation 8) was developed to forecast fatigue life in terms of coded factors. The residual least square error and probability (p) values were used to determine each coefficient's significance. Table 12 shows that the experimental result may be adequately fitted by the linear models. The model's F-Value was 14.85, and noise had a 0.02% chance of occurring. At a 99% confidence interval, this suggests that the model is significant. The fatigue life is significantly impacted by the stress and moment, which are important model terms.

The linear mathematical model and 3D plots developed for fatigue life from this research is a novel addition to knowledge in researches involving shape memory alloy.

## CHAPTER VI

### Conclusion and Recommendations

Alloys showing the shape memory property possess wide range of applications, such as their use in, greenhouse window openers, eyeglass frames, antennas which are collapsible, tooth-straightening braces, showers antiscald control valves, fire sprinkler valves, weldless shrink-to-fit pipe couplers which is used in aircraft hydraulic lines in aircrafts, for submarines, and subsea pipelines, and foundation garments for women. Copper–zinc–silicon (Cu–Zn–Si), iron–palladium (Fe–Pd), Copper–aluminum–nickel (Cu–Al–Ni), indium–titanium (In–Ti), copper–zinc–aluminum (Cu–Zn–Al), nickel–aluminum (Ni–Al), copper–zinc–gallium (Cu–Zn–Ga), nickel–titanium (Ni–Ti), copper–aluminum–manganese (Cu–Al–Mn), iron–platinum (Fe–Pt), copper–tin (Cu–Sn), copper–zinc–tin (Cu–Zn–Sn), etc., are among twenty elements in the actual periodic table region that exhibit shape memory (dagusta, 2014). (dagusta, 2014).

Because they are less expensive, Cu-based SMAs is preferable to Ni-Ti ones in other applications. Cu-based SMAs have been at the forefront of research and development for many years, although they are not widely available commercially (Callister, & Rethwisch, 2018, Rupa, 2014). These material undergo a cyclic operation and are subjected to failures. Fatigue failure is a major problem associated with these alloys. This thesis investigates' graphene addition to the mechanical and fatigue behaviour of a copper based Shape Memory Alloy.

#### Conclusion

This experimental research involving Shape Memory Alloy helps to investigate the relevance of quaternary to CuAlNi SMA hardness and fatigue properties. The weight of each sample was determined separately with a mettler weighing balance of 0.02 g precision for accuracy. Errors due to parallax were avoided in taking reading on weighing balance for casting and Rockwell scales for hardness test. Trace amount of graphene (0.15%, 0.3%, 0.45%) were added to Copper, Aluminium and Nickel through the method of mixture to produce CuAlNiC SMA and CuAlNi (control sample) through the method of casting.

A close study of the microstructure of the alloy produced utilizing EDS (Energy Dispersive X-ray Spectroscopy) and SEM (Scanning Electron Microscope)

show that Secondary black compounds seen in all graphene-reinforced alloys are associated with higher quantities of carbon, which are found in the alloy with 0.45% graphene. This poses more dislocation impediment due to increased resistance to dislocation movement which is responsible for the increase hardness values and mechanical properties of SMA reinforced with graphene (CuAlNiC) as compared with the control sample without graphene (CuAlNi). Similarly, CuAlNiC containing 0.3% graphene display optimum fatigue properties during the test carried out on fatigue. This possibly is explained by the alloy's rather uniform structures from the micrograph. The likelihood of local deformations that can result in fatigue failure at fewer cycles is decreased by evenly distributed carbon. CuAlNiC containing 0.45% graphene display least fatigue properties and this could be that because of the spherical grains, there are discontinuities in the structure.

To investigate the relationship between fatigue life, stress, and the percentage composition of Cu, Al, Ni, and graphene (C), Design Expert Software version 13.0 was used. One advantage is that the modelling equation is easily accessible; making it simple to see how each input parameter affects the result. As a result, a new mathematical model for fatigue life is created. This model's  $R^2$  of 0.9058 suggests a good fit. Therefore, this model can be used to calculate the fatigue life in SMA studies that include a quaternary element, such as graphene.

### **Recommendations**

To improve study in this area and for further research, the following recommendations are suggested.

#### ***Recommendations According to Findings***

- 1....Silicon is detected in the energy dispersive x-ray result of the produce alloy which is possibly as a result of silica sand used to create the mould. Metal mould may be used for further studies.
- 2....This research utilized the rockwell hardness test. To have a wide area for comparison, other mechanical test show the carried out to further determined how graphene affected the mechanical characteristics of CuAlNi SMA.

### ***Recommendations for Further Research***

1. Using Design expert software (version 13.0), a novel linear model for fatigue life of CuAlNiC was developed. Further research should utilize other simulation softwares to predict relationship among input parameters.
2. Thermal fatigue experiments is needed to be carried out to complete the full fatigue characteristics.

## References

- Al-Humairi, S. N. S. (2022). Cu-based shape memory alloys: modified structures and their related properties. *Recent Advancements in the Metallurgical Engineering and Electrodeposition*, 25, <http://dx.doi.org/10.5772/intechopen.86193>.
- Amrit, K. (2021). Stress and Strain: Definition, Formula, Types, Curve Diagram. <https://themechanicalengineering.com/stress-and-strain/>
- Ashby, M. F., & Jones, D. R. H. (2005). *Engineering Materials 1, An Introduction to Their Properties and Applications*, 3rd edition, Butterworth Heinemann, Woburn, UK.
- Ashby, M. F., & Jones, D. R. H. (2005). *Engineering Materials 2, An Introduction to Microstructures, Processing and Design*, 3rd edition, Butterworth-Heinemann, Woburn, UK, 2005.
- Askeland, D. R., & Phulé, P. P. (2006). *The Science and Engineering of Materials*, 5th edition, Nelson, Toronto..
- Ataalla, T., Leary, M., & Subic, A. (2012). Functional Fatigue of Shape Memory Alloys. In: Subic, A., Wellnitz, J., Leary, M., Koopmans, L. (eds) *Sustainable Automotive Technologies 2012*. Springer, Berlin. [https://doi.org/10.1007/978-3-642-24145-1\\_6](https://doi.org/10.1007/978-3-642-24145-1_6).
- Baillie, C., and L. Vanasupa, *Navigating the Materials World*, Academic Press, San Diego, CA, 2003. Fischer, T., *Materials Science for Engineering Students*, Academic Press, San Diego, CA, 2009.
- Barbarino, S., Saavedra, F., Ajaj, E. I., Dayyani, R. M., & Friswell, I. (2014). A review on shape memory alloys with applications to morphing aircraft. *Smart Material and Structures* 23 (6), 063001. <https://doi.org/10.1088/0964-1726/23/6/063001>.
- Bhandari, V. D. (2016). *Design of machine elements*. MC GRAW HILL INDIA (3 ed.). 149-153.
- Buehler, W. J. & Wang, F. W. (1968). A summary of recent research on the nitinol alloys and their potential application in ocean engineering. *Ocean Engineering*, 1, pp. 105–120.

<https://www.sciencedirect.com/science/article/abs/pii/002980186890019X>

- Callister, W. D. & Rethwisch, D. G. (2018). *Materials Science and Engineering An Introduction*. John Wiley & Sons, Inc.
- Campbell, J. S. (1995). *Principles of Manufacturing Materials And Processes*, Tata McGraw Hill.
- Canbay, C. A., Karaduman, O., & Özkul, İ. (2020). Lagging temperature problem in DTA/DSC measurement on investigation of NiTi SMA. *Mater Sci: Mater. in Electronics*, 31(16), 13284-13291.  
<https://doi.org/10.1007/s10854-020-03881-y>.
- Cisse, Cheikh, Zaki, Wael, Zineb, & Tarak Ben. (2016). A review of modelling techniques for advanced effects in shape memory alloy behaviour. *Smart Materials and Structures* 25 (10), 103001.  
<https://doi.org/10.1088/0964-1726/25/10/103001>
- Chen, L. Y., Xu, J. Q., Choi, H., Pozuelo, M., Ma, X., Bhowmick, S. & Li, X. C. (2015). Processing and properties of magnesium containing a dense uniform dispersion of nanoparticles. *Nature*, 528(7583), 539- 543.  
<https://doi.org/10.1038/nature16445>
- Cho, J. W., Kim, J. W., Jung, Y. C. (2005). Electroactive shape-memory polyurethane composites incorporating carbon nanotubes. *Macromol Rapid Commun* 26: 412–416. <https://doi.org/10.1088/0964-1726/16/3/032>
- Dasgupta, R. (2014). A look into Cu-based shape memory alloys: Present scenario and future prospects. *Mater Res.*, 29(16), 1681-1698.  
<https://doi.org/10.1557/jmr.2014.189>.
- Delaey, L. et al. (1978). Martensite and equilibrium phases in Cu-Zn and Cu-Zn-Al alloys. *Scripta Metall.*, 12, pp. 373–376.  
<https://www.sciencedirect.com/science/article/abs/pii/0079642586900071>
- Edwards, T., Gioacchino, F., Goodfellow, A. J., & JohnClegg, W. (2019). Slip bands in lamellar TiAl during high cycle fatigue microcompression by correlative total strain mapping, diffraction orientation mapping and

- transmission electron imaging. *International Journal of Fatigue*. 124:520-527. <https://doi.org/10.1016/j.ijfatigue.2019.03.016>
- Ganesh, R. N. ME 222, Manufacturing Technology lecture note.  
Indian Institute of Technology Guwahati
- George E. D. (1988). Mechanical Metallurgy.  
*McGraw-Hill Book Company*.
- Gomes, R. M., Veloso, A. R., Buono, V.T.L., Guedes de Limam S. J., Azevedo Groover, M.P. (2010). Fundamental of modern manufacturing Materials, Processes a And systems, 4ed, *John Wiley & Sons*.
- Ghosh, A & Mallik, A. K. (1986). Manufacturing Science. *Wiley Eastern*.
- Melo, T. A. (2008). Pseudoelasticity of Cu-13.8Al-Ni Alloys Containing V and Nb. *Advances in Science and Technology*. 59, 101-107. <https://doi.org/10.4028/www.scientific.net/AST.59.101>
- Groover, M. P. (2012). Introduction to manufacturing processes. *John Wiley & Sons*.
- Guniputi, B. N., & Murigendrappa, S. (2018). Influence of Gd on the microstructure, mechanical and shape memory properties of Cu-Al-Be polycrystalline shape memory alloy. *Materials Science and Engineering: A*. 737:245-252. <https://doi.org/10.1016/j.msea.2018.09.064>
- Hartl, D. J. & Lagoudas, D. C. (2007). Aerospace applications of shape memory alloys. *Journal of Aerospace Engineering*. 221, 535-552.
- Hussain, S., Pandey, A., & Dasgupta, R. (2019). Designed polycrystalline ultra-high ductile boron doped Cu–Al–Ni based shape memory alloy. *Materials Letters*. 240:157-160. <https://doi.org/10.1016/j.matlet.2018.12.142>
- Issa, W. A., Camur, H., & Savas, M. (2021). A brief review of characteristics and applications of shape memory alloys in engineering and related fields. *IJMET.*, 12 (9), 34-43. <https://doi.org/10.34218/IJMET.12.9.2021.004>.
- Jacobs, J.A., & Kilduff, T. F. (2005). Engineering Materials Technology, 5th edition, Prentice Hall PTR, Paramus, NJ.
- Janssen, J. et al.(1982). THE FATIGUE PROPERTIES OF SOME Cu-Zn-Al SHAPE MEMORY ALLOYS. *Journal de Physique IV*, C4, pp. 809–812.

- <https://jphyscol.journaldephysique.org/articles/jphyscol/abs/1982/04/jphyscol198243C4132/jphyscol198243C4132.html>
- Ji, F., Zhu, Y., Hu, J. (2006). Smart polymer fibers with shape memory effect. *Smart Materials and Structures* 15: 1547. <https://doi.org/10.1088/0964-1726/15/6/006>
- Jani, J. M., Leary, M., Subic, A., & Gibson, M. A. (2014). A review of shape memory alloy research, applications and opportunities. *Mater. Des.*, 56, 1078-1113. <https://doi.org/10.1016/j.matdes.2013.11.084>.
- Jiang, Z., Zhang, Z., & Friedrich, K. (2007). Prediction on wear properties of polymer composites with artificial neural networks. *Composites Science and Technology*, 67(2), 168–176. <https://doi.org/10.1016/j.compscitech.2006.07.026>
- Karaduman, O., & Canbay, C. A. (2021). Investigation of CuAlNi Shape Memory Alloy Doped with Graphene. *Mater. & Elect. Dev.* 3, 8-14.
- Kalpakjian, K & Schmid, S. R. (2009). *Manufacturing Processes for Engineering Materials*, Pearson education.
- Kaya, E., & Kaya, İ. (2019). A review on machining of NiTi shape memory alloys: The process and post process perspective. *The International Journal of Advanced Manufacturing Technology*. 100 (5-8):2045-208. <https://doi.org/10.1007/s00170-018-2818-8>
- Kumar, P.K. & Lagoudas, D.C. (2008). Introduction to Shape Memory Alloys. Shape Memory Alloys Modeling and Engineering Applications. *Springer Science*. DOI:10.1007/978-0-387-47685-8\_1
- Leal, P. B., & Savi, M. A. (2018). Shape memory alloy-based mechanism for aeronautical application: Theory, optimization and experiment. *Aerospace Science and Technology*.76:155-163. <https://doi.org/10.1016/j.ast.2018.02.010>
- Lendlein, A., Jiang, H., & Junger, O. (2005). Light-induced shape-memory polymers. *Nature* 434: 879–882. <https://doi.org/10.1038/nature03496>
- Lendlein, A., Schmidt, A. M., & Schroeter, M. (2005). Shape-memory polymer networks from oligo ( $\epsilon$ -caprolactone) dimethacrylates. *J Polym Sci, Part A: Polym Chem* 43: 1369–1381. <https://doi.org/10.1002/pola.20598>

- Lester, B. T., Baxevanis, T., Chemisky, Y., & Lagoudas, D. C. (2015). Review and perspectives: shape memory alloy composite systems. *Acta Mechanica*, 226(12), 3907-3960. <https://doi.org/10.1007/s00707-015-1433-0>
- Lojen G et al. (2005). Microstructure of rapidly solidified Cu–Al–Ni shape memory alloy ribbons. *Journal of Materials Processing Technology*. 162-163:220-229. <https://doi.org/10.1016/j.jmatprotec.2005.02.196>
- Lokesh, N, Mallikarjun, U. S., & Shivasiddaramaiah, A. G. (2020). Synthesis and evaluation of shape memory effect of Cu-Al-Ni shape memory alloys. *AIP Conference proceedings*. <https://doi.org/10.1063/5.0022458>
- López-Ferreño, I., Gómez-Cortés, J. F., Breczewski, T., Ruiz-Larrea, I., Nó, M. L., & San Juan, J. M. (2020). High-temperature shape memory alloys based on the Cu-Al-Ni system: design and thermomechanical characterization. *J. Mater. Res. & Tech.*, 9(5), 9972- 9984. <https://doi.org/10.1016/j.jmrt.2020.07.00>
- Ma, J., Karaman, I., & Noebe, R. D. (2010). High temperature shape memory alloys. *International Materials Reviews* 55: 257–315. <https://doi.org/10.1179/095066010X12646898728363>
- MAaSG M. (1992). Effect of heat treatment and thermal cycling on transformation temperatures of ductile Cu-Al-Ni-Mn-B alloys. *Scripta Metallurgica et Materiala*. 26(11):1663-1668. <https://doi.org/10.5772/intechopen.86193>
- McNichols, J. L. Jr., Brookes, P. C. & Cory, J. S. (1981). Ni-Ti Fatigue behaviour. *J. Appl. Phys.*, 52, pp. 7442–7444. <https://doi.org/10.1063/1.328738>
- Melton, K. N. & Mercier. O. (1979). The mechanical properties of NiTi-based SMA. *Mater. Sci. and Eng.*, 40, pp. 81–87. <https://www.sciencedirect.com/science/article/abs/pii/0001616081901656>
- Miyazaki, S., Kawai, T., & Otsuka, K. (1982). Study of fracture in Cu-Al-Ni shape memory bicrystals. *Le Journal de Physique Colloques*. 43:C4, C4-813-C4-818. <https://doi.org/10.5772/intechopen.86193>
- Miyazaki, S. et al.(1999). Fatigue life of Ti–50 at.% Ni and Ti–40Ni–10Cu (at.%)

- shape memory alloy wires. *Mater. Sci. and Eng.*, A273-275 (1999), pp. 658–663. [https://doi.org/10.1016/S0921-5093\(99\)00344-5](https://doi.org/10.1016/S0921-5093(99)00344-5)
- Morris, M. A. (1991). Microstructural influence on ductility and shape memory effect of some modified Cu.Ni.Ai alloys. *Scripta Metallurgica*. 25:1409-1414
- Murray, G.T., White, C. V., & Weise, W (2007). *Introduction to Engineering Materials*, 2nd edition, CRC Press, Boca Raton, FL.
- Obiukwu, O., Nwafor, M., & Grema, L. (2015). The effect of surface finish on the low cycle fatigue of low and medium carbon steel. *International Conference on Mechanical and Industrial Engineering (ICMIE 15)* Harare, Zimbabwe July 14-15.
- Oliveira, J. et al. (2019). Microstructure and mechanical properties of gas tungsten arc welded Cu-Al-Mn shape memory alloy rods. *Journal of Materials Processing Technology*. 217:93-100. <https://doi.org/10.1016/j.jmatprotec.2019.03.020>
- Oshima, R. & Yoshida, N. (1982). MARTENSITE TRANSFORMATIONS IN Fe-Pd ALLOYS. *Journal de Physique IV*, C4, pp. 803–808. <https://jphyscol.journaldephysique.org/articles/jphyscol/abs/1982/04/jphyscol198243C456/jphyscol198243C456.html>
- Pandey, P. C. & Singh, C. K. (2003). *Production Engineering Sciences*, Standard Publishers Ltd.
- Petrini, L., Migliavacca, F. (2011). Biomedical applications of shape memory alloys. *Journal of Metallurgy*: 1–14. <https://doi.org/10.1155/2011/501483>
- Prasad, K., Bazaka, O., Chua, M., Rochford, M., Fedrick, L., Spoor, J., Symes, R., Tieppo, M., Collins, C., Cao, A., Markwell, D., Ostrikov, K., Bazaka, K. (2017). Metallic biomaterials: Current challenges and opportunities. *Materials*. 10 (8), 884. <https://doi.org/10.3390/ma10080884>
- Prashant P. (2010). *Introduction to manufacturing technologies Principles and technologies*, Jaico publications.
- Prendota, W., Goc, K., Miyazawa, S., Takasaki, A., Rybicki, D., & Kapusta, C. (2018). Influence of carbon addition to Fe-Mn-Si type alloy on the structure and shape memory effect. *Advances in Materials Science*

- and Engineering, Vol. 2018, Article ID 6950876, 9 pages.  
<https://doi.org/10.1155/2018/6950876>
- Rachinger, W. A. (1957). A "super-elastic" single crystal calibration bar. *Brit. J. of Appl Phys.*, 9, pp. 250–252. DOI 10.1088/0508-3443/9/6/308
- Rao, P. (2008). *Manufacturing Technology: Foundry, Forming And Welding. Tata McGraw Hill.*
- Razooqi, R. N., Razej, K. H., Abdulhameed, A. T., & Irhayyim, S. S. (2018). The physical and mechanical properties of a shape memory alloy reinforced with carbon nanotubes (CNTs). *Tikrit J. Pure Sci.*, 23 (9), 80-88. <http://tjps.tu.edu.iq/index.php/j/article/view/596>.
- Sade, M. & Ahlers, M. (1985). Cyclic mechanical properties of copper-based shape memory alloys: The effect of strain accommodation at grain boundaries. *Scripta Metall.*, 19 (1985), pp. 425– 430.
- Sattar.casting [https://www.uobabylon.edu.iq/eprints/publication\\_11\\_21839\\_1710.pdf](https://www.uobabylon.edu.iq/eprints/publication_11_21839_1710.pdf)
- Saud, S. N. (2019). Cu-Based Shape Memory Alloys: Modified Structures and Their Related Properties. DOI: <https://doi.org/10.5772/intechopen.86193>.
- Saud, S. N., Hamzah, E., Bakhsheshi-Rad, H. R., & Abubakar, T. (2007). Effect of Ta Additions on the Microstructure, Damping, and Shape Memory Behaviour of Prealloyed Cu-Al-Ni Shape Memory Alloys. <https://doi.org/10.1155/2017/1789454>.
- Saud, S. N., Hamzah, E., Abubakar, T., & Bakhsheshi-Rad, H. R. (2015). Microstructure and corrosion behaviour of Cu–Al–Ni shape memory alloys with Ag nanoparticles. *Materials and Corrosion*, 66(6), 527-534. <https://doi.org/10.1002/maco.201407658>
- Saud, S.N., Hamzah, E., Abubakar, T. *et al.* (2014). Effects of Mn Additions on the Structure, Mechanical Properties, and Corrosion Behavior of Cu-Al-Ni Shape Memory Alloys. *J. of Materials Engineering and Performance* 23, 3620–3629. <https://doi.org/10.1007/s11665-014-1134-1>
- Saud, S. N., Hamzah, E., Abubakar, T., Zamri, M., & Tanemura, M. (2014).

- Influence of Ti additions on the martensitic phase transformation and mechanical properties of Cu–Al–Ni shape memory alloys. *J Therm Anal Calorim.* 118,111–122.
- Saud, S. N., Hamzah, E., Abu Bakar, T. A., & Abdolahi, A. (2014). Influence of addition of carbon nanotubes on structure–properties of Cu–Al–Ni shape memory alloys. *Mater Sci & Tech.*, 30 (4), 458-464.  
<https://doi.org/10.1179/1743284713Y.0000000379>.
- Saud, S. N., Hamzah, E., Abubakar, T., Bakhsheshi-Rad, H. R., Farahany, S., Abdolahi, A., & Taheri, M. M. (2014). Influence of Silver nanoparticles addition on the phase transformation, mechanical properties and corrosion behaviour of Cu–Al–Ni shape memory alloys. *Journal of Alloys and Compounds.* 612, 235-247.  
<https://doi.org/10.1016/j.jallcom.2014.05.173>
- Saud, S. N., Hamzah, E., Abubakar, T. A., & Hosseinian, (2013). R. A Review on Influence of Alloying Elements on the Microstructure and Mechanical Properties of Cu-Al-Ni Shape Memory Alloys. *Jurnal Teknologi* 64, 1.  
<https://journals.utm.my/jurnalteknologi/article/view/1338/1525>.
- Schaffer, J. P., Saxena, A., Antolovich, S. D., Sanders, Jr., T. H., & Warner, S. B. (1999). *The Science and Design of Engineering Materials*, 2nd edition, McGraw-Hill, New York.
- Sellitto, A., & Riccio, A. (2019). Overview and future advanced engineering Applications for morphing surfaces by shape memory alloy materials. *Materials.* 12(5):708. <https://doi.org/10.3390/ma12050708>
- Shackelford, J.F. (2009). *Introduction to Materials Science for Engineers*, 7th edition, Prentice Hall PTR, Paramus, NJ.
- Shalabh. *Regression Analysis; Chapter 3 ; Multiple Linear Regression Model*. IIT Kanpur. <https://home.iitk.ac.in/~shalab/regression/Chapter3-Regression-MultipleLinearRegressionModel.pdf>
- Shebani, A., & Iwnicki, S. (2018). Prediction of wheel and rail wear under different contact conditions using artificial neural networks. *Wear*, 406–407.  
<https://doi.org/10.1016/j.wear.2018.01.007>
- Smith, W.F., & Hashemi, J. (2010). *Foundations of Materials Science and Engineering*, 5th edition, McGraw-Hill, New York.

- Strittmatter, J., Hieffer, M., & Gümpel, P. (2019). Intelligent materials in modern production-current trends for thermal shape memory alloys. *Procedia Manufacturing*. 30:347-356.  
<https://doi.org/10.1016/j.promfg.2019.02.049>
- Tablani, R.M., Simha, N. K. & Berg, B. T. (1999). Mean strain effect on fatigue properties of superelastic NiTi. *Mater. Sci. and Eng.*, A273-275, pp. 644–648.
- Tian, J., Zhu, W., Wei, Q, Wen, S., Li, S., Song, B., Shi, Y. (2019). Process optimization, microstructures and mechanical properties of a Cubased shape memory alloy fabricated by selective laser melting. *Alloys & Comp.* 785, 754-764. <https://doi.org/10.1016/j.jallcom.2019.01.153>.
- Tobushi, H. et al. (1998). Cyclic Deformation and Fatigue of a TiNi Shape-Memory Alloy Wire Subjected to Rotating Bending. *Tran ASME, J. Eng. Mater. and Technol.*, 120, pp. 64–70.
- Tsuchiya, K. (2011). Mechanisms and properties of shape memory effect and superelasticity in alloys and other materials: *A practical guide, In: Shape Memory and Superelastic Alloys, Woodhead Publishing*, 3–14.  
<https://doi.org/10.1533/9780857092625.1.3>
- Thumann, M. & Hornbogen, E. (1988). Thermal and Mechanical Fatigue in Cu-base Shape Memory Alloys. *Zeit. für Metallk.*, 29, pp. 119–126.  
<https://doi.org/10.1002/crat.2170231218>
- Ugural, A. C., & Fenster, S. K. (2012). *Advanced Mechanics of Materials and Applied Elasticity*. Pearson Education, Inc. (5 ed.). 188-190.
- Vajpai, S. K., Dube, R. K., & Sangal, S. (2011). Microstructure and properties of Cu-Al-Ni shape memory alloy strips prepared via hot densification rolling of argon atomized powder preforms. *Materials Science and Engineering A*. 529(1):378-387.
- Van Vlack, L.H. (1989). *Elements of Materials Science and Engineering*, 6th edition, Addison-Wesley Longman, Boston.
- Vanderson, M. D., Sergio, A. O., Marcelo, A. S., Pedro Manuel, C. P., & Luis Felipe, G. (2020). Fatigue on shape memory alloys: Experimental observations and constitutive modeling. *International Journal of*

- Solids and Structures* 213, 1-24.  
<https://doi.org/10.1016/j.ijsolstr.2020.11.023>
- Van Humbeeck, J. (1991). Cycling effects, fatigue and degradation of shape memory alloys. *Journal de Physique IV*, pp. 189–197.  
<https://jp4.journaldephysique.org/articles/jp4/pdf/1991/04/jp4199101C429.pdf>
- White, M. A., (1999). *Properties of Materials, Oxford University Press, New York.*
- XU, H., et al. (2008). A study on shape memory performance of single crystal Cu-Al-Ni-Be alloy. *Materials Review*. 4:036
- Xu, H. P., Song, G. F., & Mao, X., M. (2011). Influence of Be and Ni to Cu-Al alloy shape memory performance. *Advanced Materials Research*. 197:1258-1262. <https://doi.org/10.4028/www.scientific.net/AMR.197-198.1258>
- Wayman, C. M., & Lee, J. S. (1986). Grain refinement of a Cu-Al-Ni shape memory alloys by Ti and Zr additions. *Transactions of Japan Institute of Metals*. 27(8):584-91. <https://doi.org/10.2320/matertrans1960.27.584>
- Williams, T., Meador, M., Miller, s., Scheiman, D., (2011). Effect of graphene addition on shape memory behavior of epoxy resins. [https://www.researchgate.net/publication/288234270\\_Effect\\_of\\_graphene\\_addition\\_on\\_shape\\_memory\\_behavior\\_of\\_epoxy\\_resins](https://www.researchgate.net/publication/288234270_Effect_of_graphene_addition_on_shape_memory_behavior_of_epoxy_resins)
- Yang, S. et al. (2019). Excellent superelasticity and fatigue resistance of Cu-Al-Mn-W shape memory single crystal obtained only through annealing polycrystalline cast alloy. *Materials Science and Engineering: A*. 749:249-254. <https://doi.org/10.1016/j.msea.2019.02.033>
- Yih-Chang Chen (2001). *Empirical Modelling for Participative Business Process Reengineering. The university of warwick.*  
<http://webcat.warwick.ac.uk/record=b1380228~S15>
- Ying Ci, E, Tuty Asma Abu Bakar, Esah Hamzahand, Safaa Najah Saud. (2017). Study of X-phase formation on Cu-Al-Ni shape memory alloys with Ti addition. *Journal of Mechanical Engineering and Sciences*, 11, 2, 2770. DOI:10.15282/jmes.11.2.2017.17.0251
- Zare, M & Ketabchi, M. (2017). Effect of chromium element on transformation,

mechanical and corrosion behavior of thermomechanically induced Cu–Al–Ni shape-memory alloys. *J Therm Anal Calorim* 127, 2113–2123. DOI 10.1007/s10973-016-5839-2.

Zhu, M., Xiaosu Ye, Chonghe Li, Gaofeng Song, Qijie Zhai. (2009). Preparation of Single Crystal CuAlNiBe SMA and Its Performances. *ChemInform*. 478, (1-2), 404-410. <https://doi.org/10.1002/chin.200934004>

**Appendix X**  
**Turnitin Similarity Report**

1734344239651\_Thesis Similarity Report.pdf

ORIGINALITY REPORT

<b>14%</b>	<b>9%</b>	<b>8%</b>	<b>4%</b>
SIMILARITY INDEX	INTERNET SOURCES	PUBLICATIONS	STUDENT PAPERS

PRIMARY SOURCES

<b>1</b>	<b>www.coursehero.com</b> Internet Source	<b>2%</b>
<b>2</b>	<b>Kenneth E. Wilkes. "The fatigue behavior of shape-memory alloys", JOM, 10/2000</b> Publication	<b>2%</b>
<b>3</b>	<b>hrcak.srce.hr</b> Internet Source	<b>1%</b>
<b>4</b>	<b>Rupa Dasgupta. "A look into Cu-based shape memory alloys: Present scenario and future prospects", Journal of Materials Research, 2014</b> Publication	<b>1%</b>
<b>5</b>	<b>www.researchgate.net</b> Internet Source	<b>&lt;1%</b>
<b>6</b>	<b>pdfs.semanticscholar.org</b> Internet Source	<b>&lt;1%</b>
<b>7</b>	<b>Submitted to Australian College of Kuwait</b> Student Paper	<b>&lt;1%</b>
<b>8</b>	<b>baixardoc.com</b> Internet Source	<b>&lt;1%</b>

## **CURRICULUM VITAE**

### **WASIU AYINDE ISSA**

Address: 23, Block 5, OCDA, Ilorin, Kwara State, Nigeria  
Telephone: +2347069440642  
Email: 20195806@std.neu.edu.tr

#### PERSONAL INFORMATION

Place of birth: Lagos, Nigeria  
Date of birth: 30th June, 1986  
Marital Status: Married

#### EDUCATIONAL INFORMATION

2020 – 2024. Near East University, Nicosia, Cyprus  
Ph.D. Mechanical Engineering  
2012 – 2014 University of Ibadan, Ibadan, Nigeria  
M.Sc. Mechanical Engineering  
2005 – 2010 University of Ilorin, Ilorin, Nigeria  
B.Eng. Mechanical Engineering  
2000 – 2004 Agboju Secondary School Agboju, Lagos, Nigeria  
West Africa Examination Certificate  
1995 – 1999 Command Children School, Mile II, Lagos, Nigeria  
Primary School Leaving Certificate

#### WORK EXPERIENCE

<b>S/no</b>	<b>Status</b>	<b>Employer</b>	<b>Period</b>
1	Lecturer	KWASU	Nov 2015- till date
2	Lecturer	Federal POLY Ilaro, Nigeria	Dec 2010- Oct 2011
3	Trainee Engineer	Rahamanniyya Oil & Gas	June 2018 – Jan. 2019

#### JOURNAL PUBLICATIONS

1. **W. A. Issa**, H. Camur, M. Savas, (2024). A study of the effect of graphene on the fatigue life of CuAlNi Shape Memory Alloy. Technical gazette. <https://doi.org/10.17559/TV-20240212001324>
2. **Issa, Wasiu Ayinde**, Dare, Ademola, Oladosu, Kamoru & Kareem, Morakinyo. (2024). Performance Characteristics of Nanofluid Pump. Saudi Journal of Engineering and Technology. 9. 442-450. <https://doi.org/10.36348/sjet.2024.v09i09.003>.
3. K.O. Oladosu, S.A. Babalola, M.W. Kareem, H.A. Ajimotokan, M.Y. Kolawole, **W.A. Issa**, A.S. Olawore, E.A. Ponle, (2023). Optimization of fuel briquette made from bi-composite biomass for domestic heating applications, Scientific African, 21 (01824), ISSN 2468-2276, <https://doi.org/10.1016/j.sciaf.2023.e01824>.  
(<https://www.sciencedirect.com/science/article/pii/S2468227623002806>)
4. **W. A. Issa**, H. Camur, M. Savas, (2021). A brief review of characteristics and applications of shape memory alloys in engineering and related fields. International Journal of Mechanical Engineering and Technology, 12(9), pp. 34-43.
5. D. H., Oladebeye, E. R., Adefidipe, **W. A., Issa**. (2021). Microstructural Investigation of Cast 6063 Aluminium Rods Produced from Sand and Permanent Cast Moulds. International Journal of Software & Hardware Research in Engineering (IJSHRE), 9(11), pp. 1-6.
6. **Issa, W.A.**, Fatile, O.E., Abdulmumuni B., Ologunye, O.B., & Okpara, I.N. (2020). Design and Fabrication of a Charcoal Fish Smoking KILN. International Journal of Recent Technology and Engineering (IJRTE), 9(1). <https://www.ijrte.org/wp-content/uploads/papers/v9i1/A1271059120.pdf>
7. **Issa, W.A.**, Abdulmumuni, B., Azeez, R.O., Okpara I.N., Fanifosi, J.O. & Ologunye O.B. (2020). Design, Fabrication, and Testing of a Movable Solar Operated Sprayer for Farming Operation. International Journal of Mechanical Engineering and Technology, 11(3), pp. 6-14.  
[http://www.iaeme.com/MasterAdmin/Journal\\_uploads/IJMET/VOLUME\\_11\\_ISSUE\\_3/IJMET\\_11\\_03\\_002.pdf](http://www.iaeme.com/MasterAdmin/Journal_uploads/IJMET/VOLUME_11_ISSUE_3/IJMET_11_03_002.pdf)